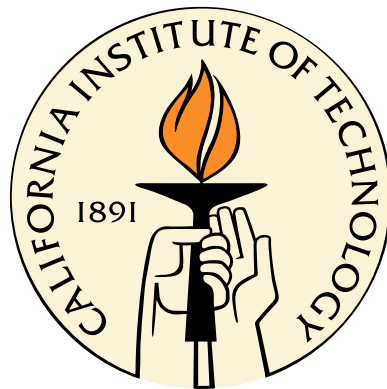


Neutrino Mass Constraints on Electroweak Parameters

Thesis by
Rebecca Joan Erwin

In Partial Fulfillment of the Requirements
for the Degree of
Doctor of Philosophy



California Institute of Technology
Pasadena, California

2007
(Defended May 24, 2007)

© 2007

Rebecca Joan Erwin

All Rights Reserved

Acknowledgments

I would like to thank my advisor, Michael Ramsey-Musolf, for giving me an interesting thesis project, and for letting me switch to electroweak physics halfway through my graduate career. I would also like to thank my collaborators and fellow graduate students, Peng Wang and Jennifer Kile, for their insights into countless physics issues. I have had many helpful discussions with Brad Filippone, Mark Wise, and Petr Vogel. I also acknowledge the support of a Forris Jewett Moore Fellowship from Amherst College.

Few people have influenced me as much as my undergraduate advisor, Professor Robert Hilborn, whose example as a researcher and as a person I do my best to follow every day.

Most of all I must thank Matt, whose support and patience were constant and boundless.

Abstract

We use the scale of neutrino mass and naturalness considerations to obtain model-independent expectations for the magnitude of possible contributions to muon decay Michel parameters from new physics above the electroweak symmetry-breaking scale. Focusing on Dirac neutrinos, we obtain a complete basis of effective dimension four and dimension six operators that are invariant under the gauge symmetry of the Standard Model and that contribute to both muon decay and neutrino mass. We show that—in the absence of fine tuning—the most stringent neutrino mass naturalness bounds on chirality-changing vector operators relevant to muon decay arise from one-loop operator mixing. The bounds we obtain on their contributions to the Michel parameters are two orders of magnitude stronger than bounds previously obtained in the literature. In addition, we analyze the implications of one-loop matching considerations and find that the expectations for the size of various scalar and tensor contributions to the Michel parameters are considerably smaller than those derived from previous estimates of two-loop operator mixing. We also show, however, that there exist gauge-invariant operators that generate scalar and tensor contributions to muon decay but whose flavor structure allows them to evade neutrino mass naturalness bounds. We discuss the implications of our analysis for the interpretation of muon decay experiments.

We then repeat the analysis with Majorana neutrinos. Since the lowest dimension mass operator in this case is a five-dimensional operator, we start with a new basis of effective dimension five and dimension seven operators that contribute to muon decay and neutrino mass through radiative corrections. In contrast to similar studies of magnetic moments and masses using Dirac and Majorana neutrinos, which found substantially weaker bounds for Majorana magnetic moments, we find that the limits on muon decay Michel parameters from Majorana neutrinos are similar in magnitude to the limits from Dirac neutrinos. We also find, similar to the Dirac case, that there are operators in our basis whose coefficients are not bound by neutrino mass.

Finally, we calculate one-loop renormalization factors of twist-two operators in massless QCD with domain-wall fermions. The Shamir type domain-wall fermion, with an infinitely large extra dimension to describe the massless fermion, is used.

Contents

Acknowledgments	iii
Abstract	iv
1 Introduction	1
1.1 Notation and Conventions	3
2 Muon Decay	4
2.1 Purpose	4
2.2 Muon Decay and the Michel Parameters	4
2.3 Experimental Details and Results	6
3 Dirac Neutrinos and μ-decay	10
3.1 Introduction	10
3.2 Operator Basis	15
3.3 Operator Renormalization: Mixing and Matching Considerations	19
3.3.1 Matching with $\mathcal{O}_{M,AD}^{(4)}$	19
3.3.2 Mixing among $n = 6$ operators	23
3.4 Neutrino Mass Constraints	29
3.5 Conclusions	33
4 Majorana Neutrinos and μ-decay	35
4.1 Introduction	35
4.1.1 Majorana neutrinos	36
4.2 Operator Basis	38
4.2.1 $n = 7$ operators contributing to neutrino mass	38
4.2.2 Flavor structure	40

4.3	Operator Renormalization: Matching and Mixing	43
4.3.1	$7D \rightarrow 5D$ matching	43
4.3.2	Mixing among the 7D operators	46
4.4	Neutrino Mass Constraints	48
4.5	Conclusions	51
A	Perturbative Renormalization for Domain-Wall Fermions	52
A.1	Introduction	52
A.2	Domain-Wall Action and Propagators	57
A.2.1	Physical quarks	60
A.3	Renormalization	61
A.3.1	Wavefunction renormalization	66
A.3.1.1	Sunset diagram	67
A.3.1.2	Numerical evaluation of the sunset diagram	70
A.3.1.3	IR singularities	72
A.3.1.4	Tadpole diagram	74
A.3.1.5	Renormalization constants: Z_2 , Z_w , and Z_m	76
A.3.2	Vertex renormalization	80
A.3.2.1	Scalar and pseudoscalar currents	82
A.3.2.2	Vector and axial vector currents	85
A.3.2.3	Tensor current	87
A.4	Twist-Two Operators	89
A.4.1	Vertex diagram	92
A.4.2	Sails diagrams	93
A.4.3	Tadpole diagram	96
A.5	Conclusions	97
B	Domain-Wall Propagators	99
	Bibliography	104

List of Figures

2.1	<i>A conceptual drawing of the TWIST spectrometer. The superconducting solenoid is inside the steel yoke (the yoke itself is required to produce the highly uniform 2 Tesla field for the drift chamber). The drift chambers and proportional chambers (measuring the energies of the particles) are symmetrically placed from the central target. Picture taken from [6].</i>	8
3.1	<i>Contributions from the operators (a) $\mathcal{O}_{\tilde{V},AD}^{(6)}$ and (b) $\mathcal{O}_{W,AD}^{(6)}$ (denoted by the shaded box) to the amplitude for μ-decay. Solid, dashed, and wavy lines denote fermions, Higgs scalars, and gauge bosons, respectively. After SSB, the neutral Higgs field is replaced by its vev, yielding a four-fermion μ-decay amplitude. .</i>	19
3.2	<i>One-loop graphs for the matching contributions of the $n = 6$ operators (denoted by the shaded box) to the $n = 4$ mass operator $\mathcal{O}_{M,AD}^{(4)}$. Solid, dashed, and wavy lines denote fermions, Higgs scalars, and gauge bosons, respectively. Panels (a, b, c) illustrate contributions from $\mathcal{O}_{B,W}^{(6)}$, $\mathcal{O}_{\tilde{V}}^{(6)}$, and $\mathcal{O}_F^{(6)}$, respectively, to $\mathcal{O}_{M,AD}^{(4)}$.</i>	20
3.3	<i>One-loop graphs for the mixing among $n = 6$ operators. Notation is as in previous figures. Various types of mixing (a–g) and self-renormalization (h–j) are as discussed in the text.</i>	26
3.4	<i>Two-loop graphs for the mixing of the $n = 6$ operators. Only representative graphs for the mixing of the four-fermion operators $\mathcal{O}_{F,ABCD}^{(6)}$ into $\mathcal{O}_{M,AD}^{(6)}$ are shown.</i>	27
4.1	<i>Contributions of the operators $\mathcal{O}_{\tilde{V},AE}^{(7)}$ and $\mathcal{O}_{\tilde{V},EA}^{(7)}$ (denoted by the solid box) to muon decay. Solid, dashed, and wavy lines denote fermions, Higgs scalars, and gauge bosons, respectively. After SSB, the neutral Higgs field is replaced by its vev, yielding a four-fermion μ-decay amplitude.</i>	43

4.2	One-loop graphs for the matching of the $n = 7$ operators (denoted by the box) into the $n = 5$ mass operator $\mathcal{O}_{M,AE}^{(5)}$. Solid, dashed, and wavy lines denote fermions, Higgs scalars, and gauge bosons, respectively. Panels (a, b) illustrate mixing of $\mathcal{O}_F^{(7)}$ and $\mathcal{O}_4^{(7)}$, respectively, into $\mathcal{O}_{M,AE}^{(5)}$	45
4.3	One-loop graphs for the mixing of the $n = 7$ operator $\mathcal{O}_{\tilde{V}}^{(7)}$ (denoted by the box) into the $n = 7$ mass operator $\mathcal{O}_{M,AE}^{(7)}$. Solid, dashed, and wavy lines denote fermions, Higgs scalars, and gauge bosons, respectively.	46
A.1	Sunset diagram for physical quarks. Solid and curly lines represent fermions and gluons, respectively.	69
A.2	Tadpole diagram for physical quarks. Solid and curly lines represent fermions and gluons, respectively.	74
A.3	Vertex diagram for quark bilinear operators (denoted by the box). Solid and curly lines represent fermions and gluons, respectively.	81
A.4	Momentum conventions for the twist-two operator $\bar{q}(x)\Gamma D_\nu \bar{q}$ (denoted by the box). Solid and curly lines represent fermions and gluons, respectively.	90
A.5	Vertex diagram for twist-two operators (denoted by the box). Solid and curly lines represent fermions and gluons, respectively.	92
A.6	Sails diagram for twist-two operators (denoted by the box). Solid and curly lines represent fermions and gluons, respectively.	93
A.7	Tadpole diagram for twist-two operators (denoted by the box). Solid and curly lines represent fermions and gluons, respectively.	97

Chapter 1

Introduction

This thesis is a collection of three phenomenological projects I have worked on as a graduate student. Two of the three fall under the somewhat small but interesting umbrella of “neutrino-matter interactions”; these two projects are the focus of this dissertation and I have attempted to reflect this focus with the title. The third project is in a very different area — namely, the lattice — and is an excerpt from a longer paper I worked on before moving to electroweak physics.

Since it would be neither interesting nor insightful to construct this thesis as simply a collection of papers, I have endeavored to make it more than the sum of its parts by adding material to provide background and context. The brief review of muon decay theory and experiment in the next chapter is an example. Muon decay, a purely leptonic process, is important because it provides a direct test of the spin structure of the charged weak current and as a result is one of the best methods available to test the structure of physics beyond the Standard Model (SM). With this in mind, the chapter is intended to make the results of the two subsequent chapters, on the theoretical connection between Dirac and Majorana neutrinos and muon decay, more illuminating by contrasting them with experimental findings and describing how these findings are obtained.

With the discovery of neutrino oscillations, neutrino mass has become the focus of much theoretical and experimental work since it provides a unique window onto beyond the SM physics. Much of this work has focused on crucial areas such as finding the number of neutrino species, the values of the mass eigenstates and mixing angles, whether or not neutrinos violate charge and parity (CP), are neutrinos “Dirac” or “Majorana” particles, and if neutrinos have (measurable) effects on other particle physics processes. It is the last question that this thesis explores. As I will show, neutrino mass can be related to

muon decay in a *model-independent way*: our phenomenological analysis will not make any assumptions about the dynamical origin of neutrino mass. At the same time, I will assume a very generous limit for the neutrino mass — based on experimental and cosmological data — that still gives interesting results. Since the number of candidates for physics beyond the SM is large, model-independent studies of neutrino-matter interactions and neutrino mass are a valuable tool in the search for new physics.

Chapter 3 discusses how Dirac neutrino mass limits can be used to put interesting constraints on muon decay parameters. The first step is constructing the operator basis, which means looking for chirality-changing operators that contribute to both processes. This is, in fact, a specific example of a general connection between neutrino mass and certain neutrino-matter interactions: under minimal assumptions, we will see that these chirality-changing interactions generate contributions to neutrino mass through loop effects. After constructing the basis we will proceed with the operator analysis, calculating matching contributions from higher-dimensional operators to lower-dimensional operators, and mixing between operators. In the end, we will see that neutrino mass does put strong constraints on some contributions to muon decay parameters.

The work described in Chapter 4 is similar in outline and scope and is intended to complement the material in Chapter 3. I will first discuss the reasons why a separate analysis for Majorana neutrinos is necessary. The rest of the chapter will then closely follow the previous chapter: we will construct the operator basis using five-dimensional and seven-dimensional operators and perform the operator analysis with matching and mixing calculations. As it turns out, the limits on muon decay parameters from Majorana neutrinos will not be much different than those obtained from Dirac neutrinos, and we will explore some of the implications of this result.

The two appendices address the very different area of the lattice, which is the only way at present to study quantum chromodynamics (QCD) in a non-perturbative way. I will be looking at a specific type of fermion implemented on the lattice, called the “domain-wall fermion,” giving a pedagogical introduction to how it is constructed and using it to calculate the matching coefficients for various twist-two operators. I first introduce the domain-wall action and then move into a review of lattice perturbation theory, with a few illustrative examples. The remainder is devoted to presenting results for specific operators, including quark self-energies and bilinears and twist-two operators. The last results, on twist-two

operators, are new and have not appeared in the literature.

1.1 Notation and Conventions

We work throughout in units in which $\hbar = c = 1$.

We use the Weyl or chiral basis for the Dirac matrices

$$\gamma^\mu = \begin{pmatrix} 0 & \sigma^\mu \\ \bar{\sigma}^\mu & 0 \end{pmatrix}, \quad \gamma^5 = \begin{pmatrix} -1 & 0 \\ 0 & 1 \end{pmatrix},$$

where $\sigma^\mu = (1, \vec{\sigma})$, $\bar{\sigma}^\mu = (1, -\vec{\sigma})$, and the σ^i s are the Pauli matrices

$$\sigma^1 = \begin{pmatrix} 0 & 1 \\ 1 & 0 \end{pmatrix}, \quad \sigma^2 = \begin{pmatrix} 0 & -i \\ i & 0 \end{pmatrix}, \quad \sigma^3 = \begin{pmatrix} 1 & 0 \\ 0 & -1 \end{pmatrix}.$$

In Chapter 4 we will need a new way of writing fermion mass terms using the charge-conjugation matrix C . In the chiral representation of the Dirac matrices,

$$C = \begin{pmatrix} -\epsilon & 0 \\ 0 & \epsilon \end{pmatrix},$$

where ϵ is the antisymmetric matrix. So for a Dirac spinor ψ , the conjugate spinor is [1]

$$\psi^c \equiv C\gamma^0\psi^*$$

and

$$\bar{\psi}^c = \psi^T C.$$

The Majorana mass is then written

$$\mathcal{L} = -\frac{1}{2}m(\psi_L^T C\psi_L + \text{h.c.}) . \tag{1.1}$$

All other conventions are the standard ones in the literature.

Chapter 2

Muon Decay

2.1 Purpose

The study of neutrino-matter interactions has the potential to set bounds on beyond-the-Standard Model parameters that may soon be accessible by experiment. For muon decay, these bounds are on some of the so-called *Michel parameters* that contain information about contributions to muon decay from unknown physics. In the Standard Model, there are well-known predictions for what these parameters should be. In order to analyze the effect of neutrino masses on the Michel parameters (MPs), we will need to cover some background material.

I will first review what should be the familiar process of muon decay by looking at the muon decay spectrum and its use. I will then examine the Michel parameters — essentially a way of parameterizing contributions to muon decay from beyond the Standard Model — by explaining how they are constructed. Lastly, I will roughly sketch how muon decay experiments work and give some recent results for a particular experiment.

2.2 Muon Decay and the Michel Parameters

Muon decay ($\mu^- \rightarrow e^- \bar{\nu}_e \nu_\mu$) is an ideal laboratory for testing electroweak interactions in the Standard Model because it provides a direct test of the spin structure of the charged weak current. Since this process only involves leptons, there is no need to consider more complicated and unknown strong interaction contributions. This means that we have a clean way to probe the electroweak $V - A$ structure, and a careful analysis of the muon decay spectral shape parameters can illuminate potential physics beyond the Standard Model.

Muon decay is typically described with the following effective interaction:

$$\mathcal{L}_{\mu\text{-decay}} = -\frac{4G_\mu}{\sqrt{2}} \sum_{\gamma, \alpha, \beta} g_{\alpha\beta}^\gamma \bar{e}_\alpha \Gamma^\gamma \nu^e \bar{\nu}^\mu \Gamma_{\gamma\mu\beta}, \quad (2.1)$$

where $\gamma = S, V, T$ indicate scalar, vector, and tensor interactions, and $\alpha, \beta = R, L$ indicate the chiralities of the charged leptons. The chiralities of the neutrinos are determined by the values of γ, α , and β . The coupling constants g parameterize the strength of the corresponding phenomenological interactions. In the SM, we can easily see that $g_{LL}^V = 1$, while all other g s are expected to be zero. In many extensions of the SM, however, some of the other coupling constants besides $g_{LL}^V = 1$ can be nonzero. In the left-right symmetric model, for instance, g_{RR}^V , g_{LR}^V , and g_{RL}^V are no longer zero, although the details of that will not be discussed here.

The Michel parameters, of which there are many, describe the energy of the decay electron or positron, its angular distribution of the electrons if the muons are polarized, and its spin polarization. In extensions of the SM, any new interactions of the muon would affect these observables, so they are highly sensitive to deviations caused by physics beyond the SM. The Michel parameters themselves are bilinear combinations of the coupling constants g . For example, one of the parameters, called ρ , can be written as [2]

$$\rho = \frac{3}{4} - \frac{3}{4} [|g_{LR}^V|^2 + |g_{RL}^V|^2 + 2|g_{LR}^T|^2 + 2|g_{RL}^T|^2 + \text{Re}(g_{RL}^S g_{RL}^{T*} + g_{LR}^S g_{LR}^{T*})]. \quad (2.2)$$

The four most commonly used parameters, ρ , η , ξ , and δ , describe the momentum dependence of the isotropic part (ρ) of the electron energy spectrum plus an additional small term proportional to another parameter (η), while the asymmetry is proportional to a third parameter (ξ) multiplied by the muon polarization P_μ , and a fourth parameter (δ) describes the momentum dependence. In the Standard Model, these parameters are expected to be $\rho = 3/4$, $\eta = 0$, $\xi = 1$, and $\delta = 3/4$.

We will now examine the muon decay spectrum in some detail to see where the Michel parameters fit in. For the four-fermion interaction, the differential decay rate at tree-level for a polarized muon, after doing the neutrino phase space integrals and before integrating

over the electron phase space (and where the final state spin is not detected), is [3]

$$\frac{d^2\Gamma_{\mu\rightarrow e\nu\mu\bar{\nu}_e}}{dx d\cos\theta} = \frac{G_F^2 m_\mu^5}{192\pi^3} x^2 \left[\overbrace{6(1-x) + 4\rho\left(\frac{4x}{3} - 1\right)}^{F_{IS}(x)} \pm P_\mu \cos\theta \overbrace{2\xi\left(1-x + 2\delta\left(\frac{4x}{3} - 1\right)\right)}^{F_{AS}(x)} \right]. \quad (2.3)$$

Here we have assumed that the e^\pm and neutrino masses are zero, θ is the angle between the longitudinal muon polarization P_μ and the e^\pm momentum, the plus/minus sign corresponds to μ^\pm decay, and x is a reduced electron energy (notice that $\mu/2$ is the maximum e^\pm energy in the $m_e \rightarrow 0$ limit. The isotropic ($F_{IS}(x)$) and anisotropic ($F_{AS}(x)$) parts of the e^\pm energy spectrum are labeled.

All of the previously mentioned Michel parameters, aside from η , are visible in Eq. (2.3). The parameter η occurs when the e^\pm mass in the rate formula is not neglected, and so does not enter into this simplified formula. There are also less-commonly used MPs that arise from taking e^\pm polarization into account, such as ξ' , ξ'' , η'' , α , and β , but they do not enter into this analysis. In the SM with massless neutrinos, the muon polarization magnitude P_μ is one; in actual experiments, only the product $P_\mu\xi$ is measured. When comparing experimental values for the Michel parameters with the rate formula, corrections due to radiative effects should first be subtracted from the data.

2.3 Experimental Details and Results

In order to elucidate the practical considerations behind measuring muon decay parameters, we will briefly look at the experiment at TRIUMF responsible for some of the most recent spectral shape parameter measurements, TWIST (TRIUMF Weak Interaction Symmetry Test). The goal of TWIST is to measure the entire differential spectrum of positrons from the decay of polarized muons. It recently improved on the accepted Particle Data Group values of two Michel parameters by factors of 2.5 (for ρ [7]) and 2.9 (for δ [8]). In the past, each of the Michel parameters was determined in dedicated experiments, so TWIST is the first muon decay experiment to measure more than one MP with the same apparatus [4].

The experiment requires an high-intensity beam of spin-polarized muons from π^+ decay. The charged pions are produced by the collisions of energetic protons in a proton beam with the nuclei of a heavy metal target. Ideally, the pions, with mass $m_{\pi^\pm} = 139.5669$ MeV, then simply decay at the surface of a production target to produce a muon and a muon

neutrino. Not surprisingly, however, these charged pions and muon decay products behave differently in the target depending on whether they are positively or negatively charged. Negative pions that stop in the target behave like heavy e^- , rapidly cascading down to tightly bound orbitals where they are almost always captured by the nucleus instead of decaying to negative muons. In contrast, the positive pions that come to rest in the target take up positions between atoms and are usually too far from any nuclei to be captured. For these reasons, TWIST uses a polarized μ^+ beam.

The μ^+ resulting from π^+ decay are completely spin polarized and decay anisotropically via the weak interaction to a positron (and neutrinos) whose momentum is correlated with the muon angular momentum at the instant of decay. The pions that happen to come to rest just within the surface of the pion production target decay to low momentum (up to 29.6 MeV) “surface” muons that only need to travel a short distance out of the target and into the beamline vacuum. Unfortunately, the surface muon beam is not monoenergetic — the muons come from pions decaying at various depths in the pion production target, and those travelling from deeper in lose more of their energy — and the muon spectrum rises with momentum and drops sharply at the “surface muon edge.” It is desirable to use those muons with lower energy so that they can be stopped in the thinnest targets possible. As a result, the muon beam must be fine-tuned into a narrow momentum range, typically just below the surface muon edge, in order to obtain the greatest beam density.

After being tuned or “degraded,” the beam enters a 2 Tesla superconducting solenoid and is stopped in a thin target at the center of a symmetric array of 56 low-mass, high-precision planar drift chambers, which are used to track the paths and energies of the particles (see [5] for a more complete description of muon beamlines). The drift chambers were constructed to minimize the effects of multiple scattering and energy loss of both the incoming μ^+ and the outgoing e^+ from the target. The final errors are primarily limited by systematic effects, since the statistical precision in this experiment is very high. See Fig. 2.3 for a schematic cutaway diagram of the TWIST spectrometer.

By accumulating 10^9 muon decays, TWIST’s goal is to achieve precisions that are 3–10

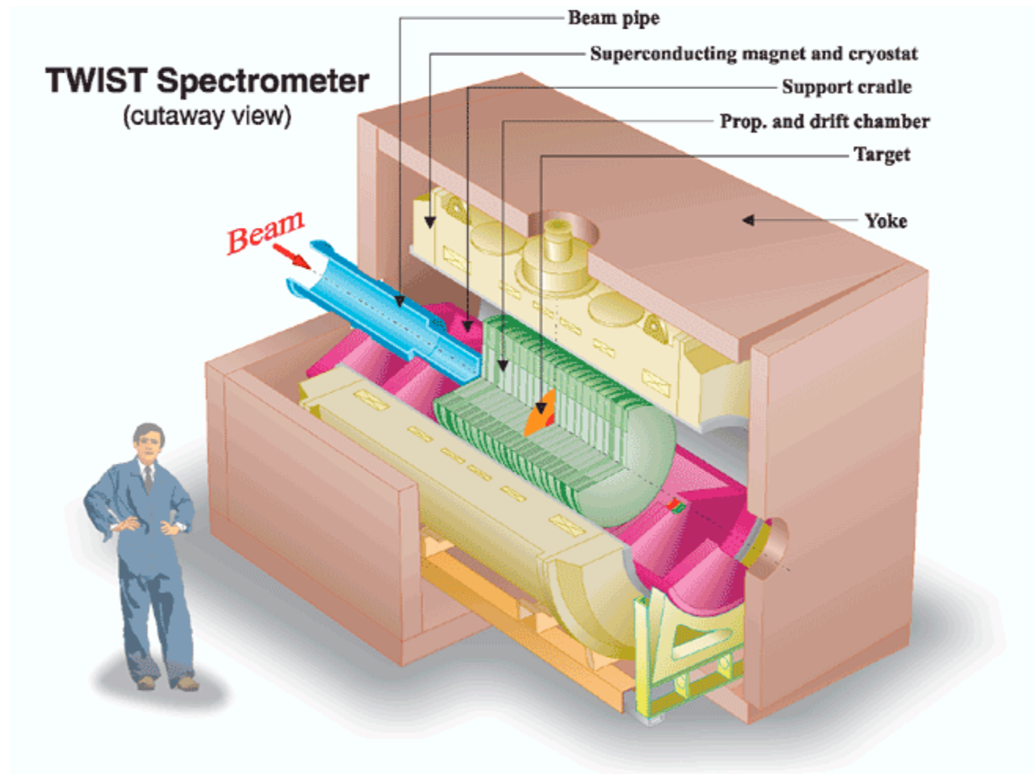


Figure 2.1: A conceptual drawing of the TWIST spectrometer. The superconducting solenoid is inside the steel yoke (the yoke itself is required to produce the highly uniform 2 Tesla field for the drift chamber). The drift chambers and proportional chambers (measuring the energies of the particles) are symmetrically placed from the central target. Picture taken from [6].

times better than previous experiments; this means

$$\begin{aligned}\Delta\rho &< 1 \times 10^{-4} \\ \Delta\delta &< 3 \times 10^{-4} \\ \Delta(P_\mu\xi) &< 2 \times 10^{-4}.\end{aligned}$$

The most recent results from TWIST are for the Michel parameters ρ , δ , and $P_\mu\xi$ [7, 8, 9]:

$$\begin{aligned}\rho &= 0.75080 \pm 0.00032(\text{stat.}) \pm 0.000097(\text{syst.}) \pm 0.00023 \\ \delta &= 0.74964 \pm 0.00066(\text{stat.}) \pm 0.00112(\text{syst.}) \\ P_\mu\xi &= 1.0003 \pm 0.0006(\text{stat.}) \pm 0.0038(\text{syst.}).\end{aligned}$$

Deviations from the SM value of $\rho = 3/4$ imply mixing of left- and right-handed muon and electron couplings so that the muon decay Lagrangian would include scalar, vector, or tensor couplings between left-handed muons and right-handed electrons, or vice versa. (Such deviations can occur, for example, in left-right symmetric models.) The last uncertainty in ρ represents the dependence of ρ on the MP η , and is the change in ρ when η changes within its uncertainty. In the SM, δ is also $3/4$; it is in the anisotropic part of the Michel decay spectrum and parameterizes the momentum dependence of the outgoing electron. Finally, $P_\mu\xi = 1$ in the SM. The parameter ξ expresses the level of parity violation in μ -decay. All of these quantities agree with previous measurements and the SM values.

With the context for muon decay now set by this chapter, we may now examine the particular details of the connection between neutrino mass and muon decay.

Chapter 3

Dirac Neutrinos and μ -decay

3.1 Introduction

Precision studies of muon decay continue to play an important role in testing the Standard Model (SM) and searching for physics beyond it. In the gauge sector of the SM, the Fermi constant G_μ that characterizes the strength of the low-energy, four-lepton μ -decay operator is determined from the μ lifetime and gives one of the three most precisely known inputs into the theory. Analyses of the spectral shape, angular distribution, and polarization of the decay electrons (or positrons) probe for contributions from operators that deviate from the $(V - A) \otimes (V - A)$ structure of the SM decay operator. In the absence of time-reversal (T) violating interactions, there exist seven independent parameters — the so-called Michel parameters [10, 11] — that characterize the final state charged leptons: two (ρ, η) that describe the spatially isotropic component of the lepton spectrum; two (ξ, δ) that characterize the spatially anisotropic distribution; and three additional quantities (ξ', ξ'', η'') that are needed to describe the lepton's transverse and longitudinal polarization¹. Two additional parameters $(\alpha'/A, \beta'/A)$ characterize a T-odd correlation between the final state lepton spin and momenta with the muon polarization: $\hat{S}_e \cdot \hat{k}_e \times \hat{S}_\mu$.

Recently, new experimental efforts have been devoted to more precise determinations of these parameters. The TWIST Collaboration has measured ρ and δ at TRIUMF [7, 8], improving the uncertainty over previously reported values by factors of ~ 2.5 and ~ 3 , respectively. An experiment to measure the transverse positron polarization has been carried out at the Paul Scherrer Institute (PSI), leading to similar improvements in sensitivity over the results of earlier measurements [12]. A new determination of $P_\mu \xi$ with a similar de-

¹The parameters η and η'' are alternately written in terms of the independent parameters α/A and β/A .

gree of improved precision is expected from the TWIST Collaboration, and one anticipates additional reductions in the uncertainties in ρ and δ [13].

At present, there exists no evidence for deviations from SM predictions for the Michel parameters (MPs). It is interesting, nevertheless, to ask what constraints these new measurements can provide on possible contributions from physics beyond the SM. It has been conventional to characterize these contributions in terms of a set of ten four-fermion operators

$$\mathcal{L}^{\mu\text{-decay}} = -\frac{4G_\mu}{\sqrt{2}} \sum_{\gamma, \epsilon, \mu} g_{\epsilon\mu}^\gamma \bar{e}_\epsilon \Gamma^\gamma \nu \bar{\nu} \Gamma_{\gamma\mu\mu} \quad (3.1)$$

where the sum runs over Dirac matrices $\Gamma^\gamma = 1$ (S), γ^α (V), and $\sigma^{\alpha\beta}/\sqrt{2}$ (T), and the subscripts μ and ϵ denote the chirality (R, L) of the muon and final state lepton, respectively². In the SM, one has $g_{LL}^V = 1$ and all other $g_{\epsilon\mu}^\gamma = 0$. A recent, global analysis by Gagliardi, Tribble, and Williams [15] give the present experimental bounds on the $g_{\epsilon\mu}^\gamma$ that include the impact of the latest TRIUMF and PSI measurements.

Theoretically, the $g_{\epsilon\mu}^\gamma$ can be generated in different scenarios for physics beyond the SM. The most commonly cited illustration is the minimal left-right symmetric model that gives rise to non-zero g_{RR}^V , g_{RL}^V , and g_{LR}^V . From a model-independent standpoint, the authors of [16] recently observed that the operators in Eq. (3.1) having different chiralities for the muon and final state charged lepton will also contribute to the neutrino mass matrix m_ν^{AB} through radiative corrections. Consequently, one expects that the present upper bounds on m_ν should imply bounds on the magnitudes of the $g_{\epsilon\mu}^\gamma$. The authors of [16] argued that the most stringent limits arise from two-loop contributions, because the one-loop contributions are suppressed by three powers of the tiny, charged lepton Yukawa couplings. The two-loop constraints are nonetheless stronger than the present bounds given in [15] and could become even more so with the advent of future terrestrial and cosmological probes of the neutrino mass scale.

In this chapter, we present the results of a follow-up analysis of m_ν constraints on the μ -decay parameters, motivated by the observations of [16] and the new experimental developments in the field. Our study follows the approach of [17, 18, 19], used recently in deriving model-independent naturalness bounds on neutrino magnetic moments implied by the scale of m_ν . We concentrate on the case of Dirac neutrinos, deferring a detailed

²The normalization of the tensor terms corresponds to the convention adopted in [14]. We do not specify the neutrino flavors in Eq. (3.1) since the μ -decay experiments do not observe the final state neutrinos.

consideration of Majorana neutrinos to the following chapter. Although there exists a long-standing theoretical prejudice favoring the see-saw mechanism with light Majorana neutrinos as an explanation of the small scale of m_ν , we see several reasons for studying the Dirac and Majorana cases separately:

- (i) From the standpoint of string phenomenology, obtaining models with neutrino self-couplings and a type I see-saw mechanism appears to be quite difficult. Recently, the authors of [20] performed a systematic study of 175 viable ways of embedding the Standard Model gauge group in the $E_8 \times E_8$ heterotic string with Z_3 orbifold compactification and found that only two of the twenty classes of such inequivalent models admitted neutrino self-couplings. The natural scale of m_ν in these two classes lies many orders of magnitude below the scale implied by neutrino oscillation data. Interactions leading to Dirac masses occur more abundantly in such constructions. On the other hand, a subsequent study of a specific $Z_3 \times Z_3$ orbifold string construction [21] indicated the plausibility of obtaining a type II see-saw mechanism, wherein left-handed lepton-number-violating neutrino self-couplings arise from interactions with scalar $SU(2)_L$ triplet fields. Either way, however, the appearance of Majorana mass terms is not at all a generic feature of string constructions, leaving the Dirac case as a logical possibility.
- (ii) Experimentally, there exists no conclusive evidence for or against the presence of light Majorana neutrinos. New searches for neutrinoless double β -decay ($0\nu\beta\beta$) could provide conclusive proof that the light neutrinos are Majorana, provided the neutrino mass spectrum has the “inverted” rather than “normal” hierarchy (for recent reviews, see, e.g., [22, 23]). If, on the other hand, future long-baseline oscillation experiments establish the existence of the inverted hierarchy and/or ordinary β -decay measurements indicate a mass consistent with the inverted hierarchy, a null result from the $0\nu\beta\beta$ searches would imply that neutrinos are Dirac particles³. Either way, the investment of substantial experimental resources in these difficult measurements indicates that determining the charge conjugation properties of the neutrino is both a central question for neutrino physics as well as one that is not settled. Until it is, considering the implications of Dirac neutrinos remains a valid enterprise.

³We thank S. J. Freedman for useful discussions on this point.

- (iii) The phenomenological analyses of Dirac and Majorana masses for other neutrino properties and interactions are quite distinct. As illustrated by the recent analyses of neutrino magnetic moments in [17, 18, 19], the characteristics of the operator basis and renormalization can be sufficiently different and complex for the two cases that separate studies of each are warranted. Moreover, the parameterization of the μ -decay Michel spectrum in the presence of Majorana neutrinos may require modification from the standard form, as indicated by the recent work of [24]. Rather than lose the reader in the details of differences in both the Michel parameterization and operator renormalization for Dirac and Majorana neutrinos, we prefer to concentrate on the Dirac case in the present study and consider the Majorana case in a separate chapter.

Having this focus in mind, we work with an effective theory that is valid below a scale Λ lying above the weak scale $v \approx 246$ GeV and that contains $SU(2)_L \times U(1)_Y$ -invariant operators built from Standard Model fields plus right-handed (RH) Dirac neutrinos. We consider all relevant operators up to dimension $n = 6$ that could be generated by physics above the scale Λ . For simplicity, we restrict our attention to two generations of lepton doublets and RH neutrinos. Extending the analysis to include a third generation increases the number of relevant operators but does not change the substantive conclusions. While the spirit of our work is similar to that of [16], the specifics of our analysis and conclusions differ in several respects:

- i) The effective theory that we adopt allows us to compute contributions to m_ν from scales lying between the weak scale v and the scale of new physics Λ . In contrast, the authors of [16] used a Fierz transformed version of $\mathcal{L}^{\mu\text{-decay}}$ in Eq. (3.1), which is not invariant under the SM gauge group and, therefore, should be used to analyze only contributions below the weak scale.
- ii) We show that for the two-flavor case the operators in $\mathcal{L}^{\mu\text{-decay}}$ proportional to $g_{LR}^{S,T}$ and $g_{RL}^{S,T}$ arise from twelve independent dimension $n = 6$ gauge-invariant four-fermion operators, while those containing g_{LR}^V and g_{RL}^V are generated by four independent $n = 6$ operators that contain two fermions and two Higgs scalars.
- iii) While the operators that contribute to μ -decay have dimension $n = 6$ or higher, the lowest dimension neutrino mass operator occurs at $n = 4$. The authors of [16] used

dimensional regularization (DR) to estimate the mixing between the $n = 6$ μ -decay and neutrino mass operators⁴ but did not consider matching with the $n = 4$ operator at the scale Λ that cannot be determined with DR. We derive order-of-magnitude expectations for the $n = 6$ operator coefficients implied by this matching, which depends only linearly on the lepton Yukawa couplings and which gives the dominant constraints for $\Lambda \gg v$.

- iv) For Λ not too different from v , constraints associated with mixing among the $n = 6$ operators can, in principle, be comparable to expectations arising from contributions to the $n = 4$ mass operator. We carry out a complete, one-loop analysis of this mixing and show that only the neutrino magnetic moment and two-fermion/two-Higgs operators mix with the $n = 6$ neutrino mass operator to linear order in the lepton Yukawa couplings. We derive the resulting bounds on the $g_{LR,RL}^V$ that follow from this mixing and find that they are comparable to expectations based on one-loop matching with the $n = 4$ mass operator for $\Lambda \gtrsim v$.
- v) From the mixing with the $n = 6$ mass operator, we find that the bounds on the $|g_{LR,RL}^V|$ are two or more orders of magnitude stronger than those obtained in [16] and at least three orders of magnitude below the experimental limits given in [15].
- vi) The neutrino mass implications for the couplings $g_{LR,RL}^{S,T}$ are more subtle. Of the twelve independent four-fermion operators that contribute to these couplings, only eight are directly constrained by the scale of neutrino mass and naturalness considerations. Based on one-loop matching, we expect that their contributions to the $g_{LR,RL}^{S,T}$ are generally $\sim 10^4$ times smaller than the present experimental bounds, and $\sim 10^3$ times smaller than obtained in the analysis of [16]. We show, however, that the flavor structure of the remaining four operators allows them to evade constraints implied by either one-loop matching or two-loop mixing. While from a theoretical perspective one might not expect their contributions to be substantially larger than those from the constrained operators, experimental efforts to determine the $g_{LR,RL}^{S,T}$ remain a worthwhile endeavor.

A summary of our results is given in Table 3.1. In the remainder of the chapter we give

⁴Since the computation of [16] did not employ gauge invariant operators, we consider the results to give at best reasonable estimates of constraints implied by two-loop mixing.

Table 3.1: Constraints on μ -decay couplings $g_{e\mu}^\gamma$. The first eight rows give naturalness expectations in units of $(v/\Lambda)^2 \times (m_\nu/1\text{ eV})$ on contributions from $n = 6$ muon decay operators (defined in Section 3.2 below) based on one-loop matching with the $n = 4$ neutrino mass operators. For $\Lambda \sim v$, the bounds on $g_{LR,RL}^V$ obtained from one-loop mixing are similar to those listed. The ninth row gives upper bounds derived from a recent global analysis of [15], while the last row gives estimated bounds from [16] derived from two-loop mixing of $n = 6$ muon decay and mass operators. A “-” indicates that the operator does not contribute to the given $g_{e\mu}^\gamma$, while “None” indicates that the operator gives a contribution unconstrained by neutrino mass. The subscript D runs over the two generations of RH Dirac neutrinos.

Source	$ g_{LR}^S $	$ g_{LR}^T $	$ g_{RL}^S $	$ g_{RL}^T $	$ g_{LR}^V $	$ g_{RL}^V $
$\mathcal{O}_{F,122D}^{(6)}$	4×10^{-7}	2×10^{-7}	-	-	-	-
$\mathcal{O}_{F,212D}^{(6)}$	4×10^{-7}	-	-	-	-	-
$\mathcal{O}_{F,112D}^{(6)}$	None	None	-	-	-	-
$\mathcal{O}_{F,211D}^{(6)}$	-	-	8×10^{-5}	4×10^{-5}	-	-
$\mathcal{O}_{F,121D}^{(6)}$	-	-	8×10^{-5}	-	-	-
$\mathcal{O}_{F,221D}^{(6)}$	-	-	None	None	-	-
$\mathcal{O}_{\tilde{V},2D}^{(6)}$	-	-	-	-	8×10^{-7}	-
$\mathcal{O}_{\tilde{V},1D}^{(6)}$	-	-	-	-	-	2×10^{-4}
Global [15]	0.088	0.025	0.417	0.104	0.036	0.104
Two-loop [16]	10^{-4}	10^{-4}	10^{-2}	10^{-2}	10^{-4}	10^{-2}

the details of our analysis. In Section 3.2, we write down the complete set of independent operators through $n = 6$ that contribute to m_ν^{AB} and/or μ -decay. Section 3.3 gives our analysis of operator mixing and matching considerations, while in Section 3.4 we discuss the resulting constraints on the $g_{LR,RL}^\gamma$ that follow from this analysis and the present upper bounds on the neutrino mass scale. We summarize in Section 3.5⁵.

The material presented in this chapter was published in [37].

3.2 Operator Basis

To set notation, we follow [17] and consider the effective Lagrangian

$$\mathcal{L}_{\text{eff}} = \sum_{n,j} \frac{C_j^n(\mu)}{\Lambda^{n-4}} \mathcal{O}_j^{(n)}(\mu) + \text{h.c.} \quad (3.2)$$

⁵This work was done in collaboration with Jennifer Kile, Michael Ramsey-Musolf, and Peng Wang.

where μ is the renormalization scale, $n \geq 4$ is the operator dimension, and j is an index running over all independent operators of a given dimension. The lowest dimension neutrino mass operator is

$$\mathcal{O}_{M,AD}^{(4)} = \bar{L}^A \tilde{\phi} \nu_R^D \quad (3.3)$$

where L^A is the left-handed (LH) lepton doublet for generation A , ν_R^D is a RH neutrino for generation D , and $\tilde{\phi} = i\tau_2 \phi^*$ with ϕ being the Higgs doublet field. After spontaneous symmetry breaking, one has

$$\phi \rightarrow \begin{pmatrix} 0 \\ v/\sqrt{2} \end{pmatrix} \quad (3.4)$$

so that

$$\begin{aligned} C_{M,AD}^4 \mathcal{O}_{M,AD}^{(4)} &\rightarrow -m_\nu^{AD} \bar{\nu}_L^A \nu_R^D \\ m_\nu^{AD} &= -C_{M,AD}^4 v/\sqrt{2}. \end{aligned} \quad (3.5)$$

The other $n = 4$ operators are those of the SM and we do not write them down explicitly here.

For the case of Dirac neutrinos that we consider here, there exist no gauge-invariant $n = 5$ operators. In considering those with dimension six, it is useful to group them according to the number of fermion, Higgs, and gauge boson fields that enter:

Four-fermion:

$$\begin{aligned} &\bar{L}\gamma^\mu L \bar{L}\gamma_\mu L \\ &\bar{\ell}_R\gamma^\mu \ell_R \bar{\ell}_R\gamma_\mu \ell_R \\ &\bar{\ell}_R\gamma^\mu \ell_R \bar{\nu}_R\gamma_\mu \nu_R \\ &\bar{\nu}_R\gamma^\mu \nu_R \bar{\nu}_R\gamma_\mu \nu_R \\ &\bar{L}\ell_R \bar{\ell}_R L \\ &\bar{L}\nu_R \bar{\nu}_R L \\ &\epsilon^{ij} \bar{L}_i \ell_R \bar{L}_j \nu_R \end{aligned}$$

Here ℓ_R is the right-handed charged lepton field. Several of the operators appearing in this list can contribute to μ -decay, but only the last one can also contribute to m_ν^{AD} through

radiative corrections. Including flavor indices, we refer to this operator as

$$\mathcal{O}_{F,ABCD}^{(6)} = \epsilon^{ij} \bar{L}_i^A \ell_R^C \bar{L}_j^B \nu_R^D \quad (3.6)$$

where the indices i, j refer to the weak isospin components of the LH doublet fields and $\epsilon^{12} = -\epsilon^{21} = 1$.

Fermion-Higgs:

$$\begin{aligned} & i(\bar{L}^A \gamma^\mu L^B)(\phi^+ D_\mu \phi) \\ & i(\bar{L}^A \gamma^\mu \tau^a L^B)(\phi^+ \tau^a D_\mu \phi) \\ & i(\bar{\ell}_R^A \gamma^\mu \ell_R^B)(\phi^+ D_\mu \phi) \\ & i(\bar{\nu}_R^A \gamma^\mu \nu_R^B)(\phi^+ D_\mu \phi) \\ & i(\bar{\ell}_R^A \gamma^\mu \nu_R^B)(\phi^+ D_\mu \tilde{\phi}) \end{aligned} \quad (3.7)$$

Neither of the first two operators in the list (3.7) can contribute significantly to m_ν^{AD} since they contain no RH neutrino fields. Any loop graph through which they radiatively induce m_ν^{AD} would have to contain operators that contain both LH and RH fields, such as $\mathcal{O}_{M,AB}^{(4)}$ or other $n = 6$ operators. In either case, the resulting constraints on the operator coefficients will be weak. For similar reasons, the third and fourth operators cannot contribute substantially because they contain an even number of neutrino fields having the same chirality and since the neutrino mass operator contains one LH and one RH neutrino field. Only the last operator

$$\mathcal{O}_{\tilde{V},AD}^{(6)} \equiv i(\bar{\ell}_R^A \gamma^\mu \nu_R^D)(\phi^+ D_\mu \tilde{\phi}) \quad (3.8)$$

can contribute significantly to m_ν since it contains a single RH neutrino. It also contributes to the μ -decay amplitude after SSB via the graph of Fig. 3.1a since the covariant derivative D_μ contains charged W -boson fields. We also write down the $n = 6$ neutrino mass operators

$$\mathcal{O}_{M,AD}^{(6)} = (\bar{L}^A \tilde{\phi} \nu_R^D)(\phi^+ \phi) \quad (3.9)$$

as well as the charged lepton mass operator $(\bar{L} \phi \ell_R)(\phi^+ \phi)$ that we do not use in the present analysis.

Fermion-Higgs-Gauge:

$$\begin{aligned}
& \bar{L}\tau^a\gamma^\mu D^\nu LW_{\mu\nu}^a \\
& \bar{L}\gamma^\mu D^\nu LB_{\mu\nu} \\
& \bar{\ell}_R\gamma^\mu D^\nu \ell_R B_{\mu\nu} \\
& \bar{\nu}_R\gamma^\mu D^\nu \nu_R B_{\mu\nu} \\
& g_2(\bar{L}\sigma^{\mu\nu}\tau^a\phi)\ell_R W_{\mu\nu}^a \\
& g_1(\bar{L}\sigma^{\mu\nu}\phi)\ell_R B_{\mu\nu} \\
& g_2(\bar{L}\sigma^{\mu\nu}\tau^a\tilde{\phi})\nu_R W_{\mu\nu}^a \\
& g_1(\bar{L}\sigma^{\mu\nu}\tilde{\phi})\nu_R B_{\mu\nu}
\end{aligned} \tag{3.10}$$

As for the fermion-Higgs operators, the operators in (3.10) that contain an even number of ν_R fields will not contribute significantly to m_ν^{AB} , so only the last two in the list are relevant:

$$\mathcal{O}_{B,AD}^{(6)} = g_1(\bar{L}^A\sigma^{\mu\nu}\tilde{\phi})\nu_R^D B_{\mu\nu} \tag{3.11}$$

$$\mathcal{O}_{W,AD}^{(6)} = g_2(\bar{L}^A\sigma^{\mu\nu}\tau^a\tilde{\phi})\nu_R^D W_{\mu\nu}^a \tag{3.12}$$

In addition to these operators, there exist additional $n = 6$ operators that contain two derivatives. However, as discussed in [17], they can either be related to $\mathcal{O}_{B,AD}^{(6)}$ and $\mathcal{O}_{W,AD}^{(6)}$ through the equations of motion or contain derivatives acting on the ν_R fields so that they do not contribute to the neutrino mass operator. Consequently, we need not consider them here. We also observe that the operator $\mathcal{O}_{W,AD}^{(6)}$ will also contribute to the μ -decay amplitude via graphs as in Fig. 3.1b. We have computed its contributions to the Michel parameters and find that they are suppressed by $\sim (m_\mu/\Lambda)^2 \lesssim 1.7 \times 10^{-7}$ relative to the effects of the other $n = 6$ operators. This suppression arises from the presence of the derivative acting on the gauge field and the absence of an interference between the corresponding amplitude and that of the SM. Finally, we note that the operators whose chiral structure suppresses their contributions to the neutrino mass operator (as discussed above) may, in general, contribute to muon decay via the terms in Eq. (3.1) having $\epsilon = \mu$. We do not consider these terms in this study.

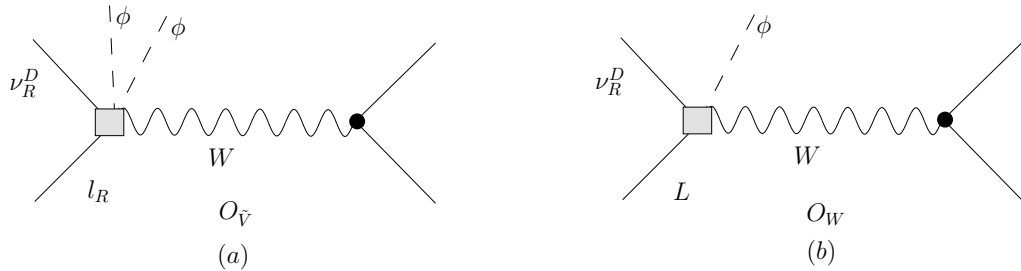


Figure 3.1: Contributions from the operators (a) $\mathcal{O}_{\bar{V},AD}^{(6)}$ and (b) $\mathcal{O}_{W,AD}^{(6)}$ (denoted by the shaded box) to the amplitude for μ -decay. Solid, dashed, and wavy lines denote fermions, Higgs scalars, and gauge bosons, respectively. After SSB, the neutral Higgs field is replaced by its vev, yielding a four-fermion μ -decay amplitude.

3.3 Operator Renormalization: Mixing and Matching Considerations

In analyzing the renormalization of operators that contribute to both μ -decay and m_ν^{AD} it is useful to consider separately two cases: (i) one-loop matching conditions at the scale Λ involving the $n = 6$ operators that enter μ -decay and the $n = 4$ mass operator, $\mathcal{O}_{M,AD}^{(4)}$, and (ii) mixing among the relevant $n = 6$ operators. In general, contributions to m_ν^{AD} involving the second case will be smaller than those implied by matching with $\mathcal{O}_{M,AD}^{(4)}$ by $\sim (v/\Lambda)^2$, since $\mathcal{O}_{M,AD}^{(4)}$ contains an additional factor of $(\phi^\dagger\phi)/\Lambda^2$. We first consider this case and employ dimensional analysis to derive neutrino mass naturalness expectations for the $n = 6$ operator coefficients. For v not too different from Λ , the impact of the $n = 6$ mixing can also be important, and in this case we can employ a full renormalization group (RG) analysis to derive robust naturalness bounds.

3.3.1 Matching with $\mathcal{O}_{M,AD}^{(4)}$

The analysis of [16] employed dimensional regularization (DR) to regularize the one- and two-loop graphs through which four-fermion operators containing a single ν_R field contribute to the $n = 6$ mass operator. Mixing with lower-dimension operators does not arise in DR since the relevant graphs are quadratically divergent and must be proportional to the square of a mass scale. For $\mu > v$, all fields are massless, and μ itself appears only logarithmically. Since the mass operator exists for zero external momentum, all quadratically-divergent

graphs vanish in this case.

The $n = 4$ mass operator will nevertheless receive contributions at the scale Λ associated with loop graphs containing the $n = 6$ operators. Simple power counting shows that these contributions go as $\sim \Lambda^2/(4\pi)^2$ times a product $n = 6$ operator coefficient C^6/Λ^2 and the gauge couplings $\sim g^2$ appearing in the loop. Thus, matching of the effective theory with the full theory (unspecified) at the scale Λ implies the presence of a contribution to C_M^4 of order $\sim \alpha C^6/4\pi$. As emphasized in [25], the precise numerical coefficient that enters this matching contribution cannot be computed without knowing the theory above the scale Λ . One may, however, estimate the size of these contributions either using a gauge-invariant regulator, such as the generalized Pauli-Villars regulator of [26], or using naive dimensional analysis. Since we are interested in order-of-magnitude expectations, use of the latter is sufficient. We emphasize that these expectations can only be relaxed in specific models that suppress the matching conditions.

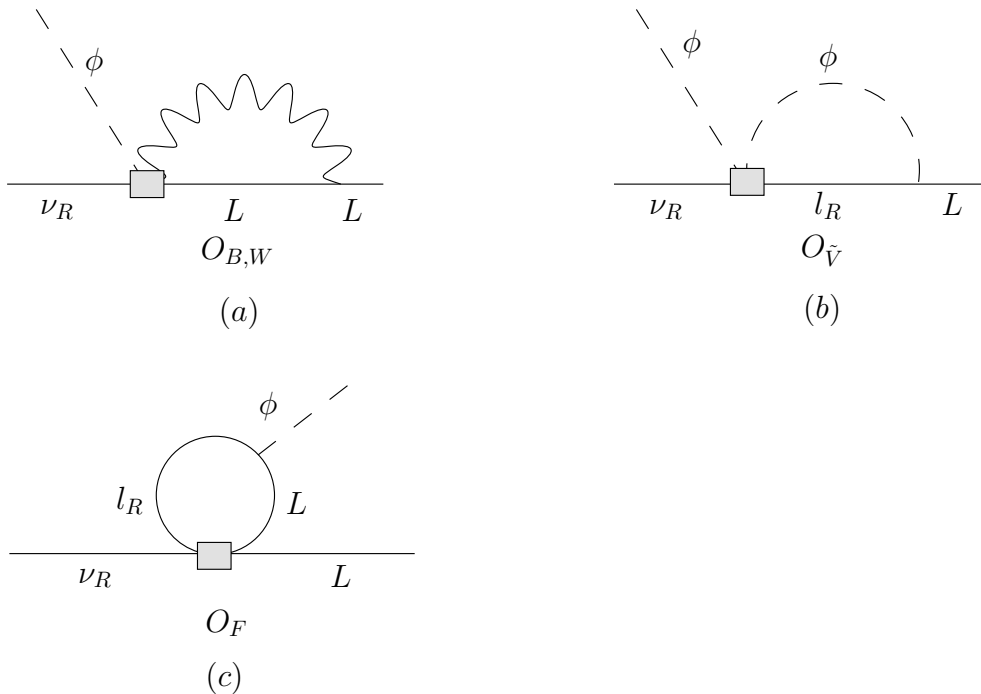


Figure 3.2: One-loop graphs for the matching contributions of the $n = 6$ operators (denoted by the shaded box) to the $n = 4$ mass operator $\mathcal{O}_{M, AD}^{(4)}$. Solid, dashed, and wavy lines denote fermions, Higgs scalars, and gauge bosons, respectively. Panels (a, b, c) illustrate contributions from $\mathcal{O}_{B,W}^{(6)}$, $\mathcal{O}_{\tilde{V}}^{(6)}$, and $\mathcal{O}_F^{(6)}$, respectively, to $\mathcal{O}_{M, AD}^{(4)}$.

The relevant one-loop graphs are shown in Fig. 3.2. For the matching of the four-fermion operators $\mathcal{O}_{F,ABCD}^{(6)}$ onto $\mathcal{O}_{M,AD}^{(4)}$, two topologies are possible, associated with either the fields (\bar{L}^A, ν_R^D) or (\bar{L}^B, ν_R^D) living on the external lines. For the matching of $\mathcal{O}_{F,ABCD}^{(6)}$ as well as of $\mathcal{O}_{V,AB}^{(6)}$ into $\mathcal{O}_{M,AD}^{(4)}$, one insertion of the Yukawa interaction $f_{AC}^* \bar{l}_R^C L^A$ is needed to convert the internal, RH lepton into a LH one. In contrast, no Yukawa insertion is required for the matching of $\mathcal{O}_{B,AD}^{(6)}$ and $\mathcal{O}_{W,AD}^{(6)}$ onto $\mathcal{O}_{M,AD}^{(4)}$.

To simplify the analysis of matching involving the $\mathcal{O}_{F,ABCD}^{(6)}$ we note that one may always redefine the fields L^A and ℓ_R^D so that the charged lepton Yukawa matrix f_{AD} is diagonal. Specifically, we take

$$\begin{aligned} L^A &\rightarrow L^{A'} = S_{AB} L^B \\ \ell_R^C &\rightarrow \ell^{C'} = T_{CD} \ell^D \end{aligned} \quad (3.13)$$

with S_{AB} and T_{CD} chosen so that

$$\bar{L} \tilde{f} \ell = \bar{L}' \tilde{f}_{\text{diag}} \ell' \quad (3.14)$$

where L, L' denote vectors in flavor space, \tilde{f} denotes the Yukawa matrix in the original basis, and $\tilde{f}_{\text{diag}} = \tilde{S}^\dagger \tilde{f} \tilde{T}$. We note that the field redefinition (3.13) differs from the conventional flavor rotation used for quarks, since we have performed identical rotations on both isospin components of the left-handed doublet. Consequently, gauge interactions in the new basis entail no transitions between generations. We also note that Eq. (3.13) also implies a redefinition of the operator coefficients $C_{M,AD}^4, C_{F,ABCD}^6$, etc. For example, one has

$$\begin{aligned} C_{M,A'D}^{4,6} &= C_{M,AD}^{4,6} S_{M,A'A} \\ C_{F,A'B'C'D}^{6'} &= C_{F,ABCD}^6 S_{A'A} S_{B'B} T_{C'C}^* \end{aligned} \quad (3.15)$$

where a sum over repeated indices is implied. Diagonalization of the neutrino mass matrix requires additional, independent rotations of the $\nu_{L,R}^D$ fields after inclusion of radiative contributions to the coefficients $C_{M,AD}^{4,6}$ generated by physics above the weak scale. Since we are concerned only with contributions generated above the scale of SSB, we will not perform the latter diagonalization and carry out computations using the L', ℓ'_R basis⁶.

⁶For notational simplicity, we henceforth omit the prime superscripts.

In this case, the only four fermion operators $\mathcal{O}_{F,ABCD}^{(6)}$ that can contribute substantially to m_ν^{AD} are those having either $A = C$ or $B = C$. Thus, we obtain the following estimates of the contributions from the $n = 6$ operators to the coefficient of the $n = 4$ mass operator:

$$\begin{aligned}
\mathcal{O}_{B,AD}^{(6)} &\rightarrow C_{M,AD}^4(\Lambda) \sim \frac{\alpha}{4\pi \cos^2 \theta_W} C_{B,AD}^6(\Lambda) \\
\mathcal{O}_{W,AD}^{(6)} &\rightarrow C_{M,AD}^4(\Lambda) \sim \frac{3\alpha}{4\pi \sin^2 \theta_W} C_{W,AD}^6(\Lambda) \\
\mathcal{O}_{\tilde{V},AD}^{(6)} &\rightarrow C_{M,AD}^4(\Lambda) \sim \frac{f_{AA}}{16\pi^2} C_{\tilde{V},AD}^6(\Lambda) \\
\mathcal{O}_{F,ABAD}^{(6)} &\rightarrow C_{M,BD}^4(\Lambda) \sim \frac{f_{AA}}{8\pi^2} C_{F,ABAD}^6(\Lambda) \\
\mathcal{O}_{F,ABBD}^{(6)} &\rightarrow C_{M,AD}^4(\Lambda) \sim \frac{f_{BB}}{16\pi^2} C_{F,ABBD}^6(\Lambda)
\end{aligned} \tag{3.16}$$

where θ_W is the weak mixing angle and where we have made the dependence on the matching scale Λ explicit⁷.

The relative factor of $3 \cot^2 \theta_W$ for the mixing of $\mathcal{O}_{W,AD}^{(6)}$ compared to the mixing of $\mathcal{O}_{B,AD}^{(6)}$ arises from the ratio of gauge couplings $(g/g')^2$ and the presence of a $\vec{\tau} \cdot \vec{\tau}$ appearing in Fig. 3.2a. The factor of two that enters the mixing of $\mathcal{O}_{F,ABAD}^{(6)}$ compared to that of $\mathcal{O}_{F,ABBD}^{(6)}$ arises from the trace associated with the closed chiral fermion loop that does not arise for $\mathcal{O}_{F,ABBD}^{(6)}$.

We observe that there exist two four-fermion operators that contribute to μ -decay that do not contribute to $C_{M,AD}^4$ in the basis giving a diagonal f_{AB} : $\mathcal{O}_{F,AABD}^{(6)}$ with either $A = 1, B = 2$ or $A = 2, B = 1$. It is similarly straightforward to see that these operators do not mix with $C_{M,AD}^6$, since in the basis of charged lepton mass eigenstates, there exist no Yukawa interactions that couple lepton doublet and charged lepton singlet fields of different generations. As we discuss in Section 3.4, the operators $\mathcal{O}_{F,AABD}^{(6)}$ with either $A = 1, B = 2$ or $A = 2, B = 1$ contribute to $g_{LR}^{S,T}$ and $g_{RL}^{S,T}$, respectively. Consequently, the magnitudes of these couplings are not directly bounded by m_ν and naturalness considerations, as indicated in Table 3.1.

These conclusions differ from those in [16], which did not take into account operators that contribute to μ -decay but do not mix with the neutrino mass operators. The corresponding bounds on $g_{LR}^{S,T}$ and $g_{RL}^{S,T}$ obtained in that work are, thus, not general and would apply

⁷In relating the coefficients $C(\Lambda)$ to those at the weak scale as needed for the analysis of both μ -decay and m_ν , we will neglect corrections to the relations in Eq. (3.16) generated by running, as they are higher order in the gauge couplings and numerically insignificant for our purposes.

only in scenarios for which $C_{F,112D}^6$ and $C_{F,221D}^6$ vanish. From a theoretical standpoint, one might expect the magnitudes of $C_{F,112D}^6$ and $C_{F,221D}^6$ to be comparable to those of the other four-fermion operator coefficients in models that are consistent with the scale of neutrino mass. Nevertheless, we cannot *a priori* rule out order of magnitude or more differences between operator coefficients.

3.3.2 Mixing among $n = 6$ operators

Because $\mathcal{O}_{M,AD}^{(6)}$ contains one power of $(\phi^\dagger\phi)/\Lambda^2$ compared to $\mathcal{O}_{M,AD}^{(4)}$, the constraints obtained from mixing with the former will generally be weaker than the one-loop $n = 4$ matching contributions by $\sim (v/\Lambda)^2$. However, for Λ not too different from the weak scale, the $n = 6$ mixing can be of comparable importance to the $n = 4$ matching. Here, we study the mixing among $n = 6$ operators by computing all one-loop graphs that contribute using DR and performing a renormalization group (RG) analysis. Doing so provides the exact result for contributions to the one-loop mixing from scales between Λ and v , summed to all orders in $f_{AA} \ln(v/\Lambda)$ and $\alpha \ln(v/\Lambda)$.

In carrying out this analysis, it is necessary to identify a basis of operators that close under renormalization. We find that the minimal set consists of seven operators that contribute to μ -decay and m_ν^{AD} :

$$\mathcal{O}_{B,AD}^{(6)}, \mathcal{O}_{W,AD}^{(6)}, \mathcal{O}_{M,AD}^{(6)}, \mathcal{O}_{\tilde{V},AD}^{(6)}, \mathcal{O}_{F,AABD}^{(6)}, \mathcal{O}_{F,ABBD}^{(6)}, \mathcal{O}_{F,BABD}^{(6)}. \quad (3.17)$$

For simplicity, we have included a single RH neutrino field ν_R^D in all seven operators. While one could, in principle, allow for different ν_R generation indices, the essential physics can be extracted from an analysis of this minimal basis.

The classes of graphs relevant to mixing among these operators are illustrated in Fig. 3.3, where we show representative contributions to operator self-renormalization and mixing among the various operators. The latter include mixing of all operators into $\mathcal{O}_{M,AD}^{(6)}$ (a–c); mixing of $\mathcal{O}_{M,AD}^{(6)}$, $\mathcal{O}_{B,AD}^{(6)}$, and $\mathcal{O}_{W,AD}^{(6)}$ into $\mathcal{O}_{\tilde{V},AD}^{(6)}$ (d, e); and mixing between the four-fermion operators and the magnetic moment operators (f, g). Representative self-renormalization graphs are given in Fig. 3.3(h–j). As noted in [16], the mixing of the the four-fermion operators into $\mathcal{O}_{M,AD}^{(6)}$ contains three powers of the lepton Yukawa couplings and is highly suppressed. In contrast, all other mixing contains at most one Yukawa inser-

tion.

Working to first order in the f_{AA} we find a total of 59 graphs that must be computed, not including wavefunction renormalization graphs that are not shown. Twenty-two of these graphs were computed by the authors of [17] in their analysis of the mixing between $\mathcal{O}_{M,AD}^{(6)}$ and the magnetic moment operators. Here, we compute the remaining 37. As in [17], we work with the background field gauge [27] in $d = 4 - 2\epsilon$ spacetime dimensions. We renormalize the operators using minimal subtraction, wherein counterterms simply remove the divergent $1/\epsilon$ terms from the one-loop amplitudes. The resulting renormalized operators $\mathcal{O}_{jR}^{(6)}$ are expressed in terms of the unrenormalized operators $\mathcal{O}_j^{(6)}$ as

$$\mathcal{O}_{jR}^{(6)} = \sum_k Z_{jk}^{-1} Z_L^{n_L/2} Z_\phi^{n_\phi/2} \mathcal{O}_k^{(6)} = \sum_k Z_{jk}^{-1} \mathcal{O}_{k0}^{(6)}, \quad (3.18)$$

where

$$\mathcal{O}_{j0}^{(6)} = Z_L^{n_L/2} Z_\phi^{n_\phi/2} \mathcal{O}_j^{(6)} \quad (3.19)$$

are the μ -independent bare operators. $Z_L^{1/2}$ and $Z_\phi^{1/2}$ are the wavefunction renormalization constants for the fields L^A and ϕ , respectively; n_L and n_ϕ are the number of LH lepton and Higgs fields appearing in a given operator; and $Z_{jk}^{-1} Z_L^{n_L/2} Z_\phi^{n_\phi/2}$ are the counterterms that remove the $1/\epsilon$ divergences.

Since the bare operators $\mathcal{O}_{j0}^{(6)}$ do not depend on the renormalization scale, whereas the Z_{jk}^{-1} and the $\mathcal{O}_j^{(6)}$ do, the operator coefficients C_j^6 must carry a compensating μ -dependence to ensure that \mathcal{L}_{eff} is independent of scale. This requirement leads to the RG equation for the operator coefficients:

$$\mu \frac{d}{d\mu} C_j^6 + \sum_k C_k^6 \gamma_{kj} = 0 \quad (3.20)$$

where

$$\gamma_{kj} = \sum_\ell \left(\mu \frac{d}{d\mu} Z_{k\ell}^{-1} \right) Z_{\ell j}. \quad (3.21)$$

is the anomalous dimension matrix. We obtain⁸

$$\gamma_{jk} = \begin{pmatrix} -\frac{3(\alpha_1-3\alpha_2)}{16\pi} & \frac{3\alpha_1}{8\pi} & -6\alpha_1(\alpha_1+\alpha_2) & -\frac{9\alpha_1 f_{AA}^*}{8\pi} & -\frac{9\alpha_1 f_{AA}}{4\pi} & -\frac{9\alpha_1 f_{BB}}{2\pi} & \frac{9\alpha_1 f_{BB}}{4\pi} \\ \frac{9\alpha_2}{8\pi} & \frac{3(\alpha_1-3\alpha_2)}{16\pi} & 6\alpha_2(\alpha_1+3\alpha_2) & \frac{27\alpha_2 f_{AA}^*}{8\pi} & -\frac{9\alpha_2 f_{AA}}{4\pi} & -\frac{9\alpha_2 f_{BB}}{2\pi} & \frac{9\alpha_2 f_{BB}}{4\pi} \\ 0 & 0 & \frac{9(\alpha_1+3\alpha_2)}{16\pi} - \frac{3\lambda}{2\pi^2} & 0 & 0 & 0 & 0 \\ 0 & 0 & \frac{9\alpha_2 f_{AA}}{8\pi} - \frac{3f_{AA}\lambda}{8\pi^2} & \frac{3\alpha_1}{4\pi} & 0 & 0 & 0 \\ -\frac{3f_{AA}^*}{128\pi^2} & -\frac{f_{AA}^*}{128\pi^2} & 0 & 0 & \frac{3(3\alpha_1-\alpha_2)}{8\pi} & 0 & 0 \\ -\frac{3f_{BB}^*}{128\pi^2} & -\frac{f_{BB}^*}{128\pi^2} & 0 & 0 & 0 & \frac{3(\alpha_1+\alpha_2)}{8\pi} & \frac{3(\alpha_1-\alpha_2)}{4\pi} \\ 0 & 0 & 0 & 0 & 0 & \frac{3(\alpha_1-\alpha_2)}{4\pi} & \frac{3(\alpha_1+\alpha_2)}{8\pi} \end{pmatrix} \quad (3.22)$$

where the $\alpha_i = g_i^2/(4\pi)$ and λ is the Higgs self coupling defined by the potential $V(\phi) = \lambda[(\phi^\dagger\phi) - v^2/2]^2$.

Using this result for γ_{ij} and the one-loop β functions for α_1 , α_2 , and the lepton Yukawa couplings, we solve the RG equations to determine the operator coefficients $C_k^6(\mu)$ as a function of their values at the scale Λ . As in [17] we find that the the running of the gauge and Yukawa couplings has a negligible impact on the evolution of the $C_k^6(\mu)$. It is instructive to consider the results obtained by retaining only the leading logarithms $\ln(\mu/\Lambda)$ and terms

⁸The term in γ_{33} proportional to λ differs from that of [17], which contains an error. However, this change does not affect the bounds on the neutrino magnetic moments obtained in that work.

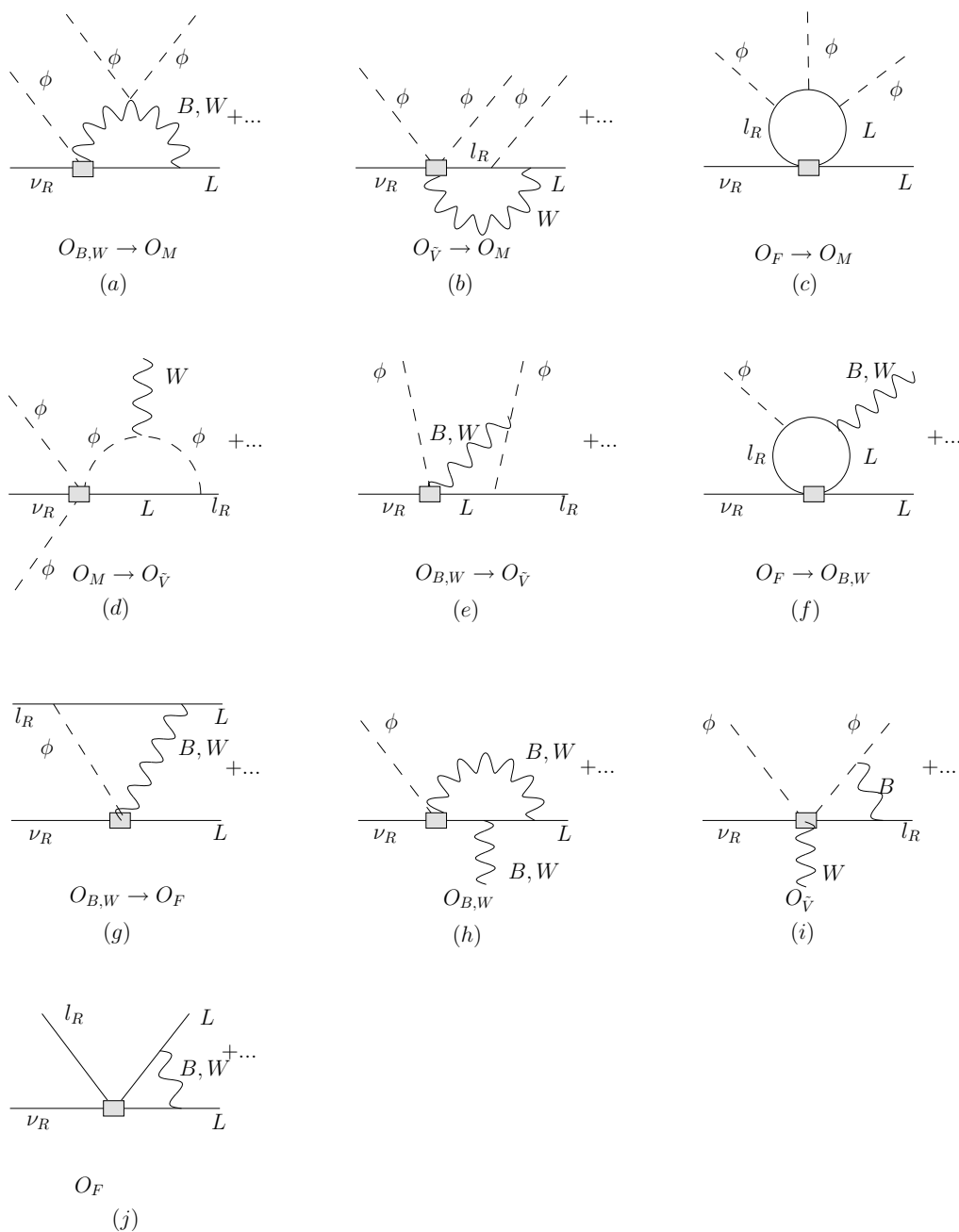


Figure 3.3: One-loop graphs for the mixing among $n = 6$ operators. Notation is as in previous figures. Various types of mixing (a–g) and self-renormalization (h–j) are as discussed in the text.

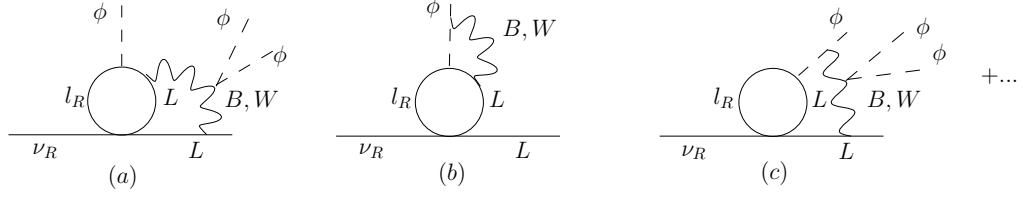


Figure 3.4: Two-loop graphs for the mixing of the $n = 6$ operators. Only representative graphs for the mixing of the four-fermion operators $\mathcal{O}_{F,ABCD}^{(6)}$ into $\mathcal{O}_{M,AD}^{(6)}$ are shown.

at most first order in the Yukawa couplings. We find

$$\begin{aligned}
C_{M,AD}^6(\mu) &= C_{M,AD}^6(\Lambda) \left[1 - \gamma_{33} \ln \frac{\mu}{\Lambda} \right] \\
&\quad - \left[\gamma_- C_-^6(\Lambda) + \gamma_+ C_+^6(\Lambda) + \gamma_{43} C_{V,AD}^6(\Lambda) \right] \ln \frac{\mu}{\Lambda} \\
C_+^6(\mu) &= C_+^6(\Lambda) \left[1 - \tilde{\gamma} \ln \frac{\mu}{\Lambda} \right] \\
&\quad + \left[(f_{AA}^*/32\pi^2) C_{F,AAAD}^6(\Lambda) + (f_{BB}^*/32\pi^2) C_{F,ABBD}^6(\Lambda) \right] \ln \frac{\mu}{\Lambda} \\
\tilde{C}^6(\mu) &= \tilde{C}^6(\Lambda) \left[1 + \tilde{\gamma} \ln \frac{\mu}{\Lambda} \right] \\
&\quad + \left[(3f_{AA}/128\pi^2) (\alpha_1 - \alpha_2) C_{F,AAAD}^6(\Lambda) \right. \\
&\quad \left. + (3f_{BB}/128\pi^2) (\alpha_1 - \alpha_2) C_{F,ABBD}^6(\Lambda) \right] \ln \frac{\mu}{\Lambda} \\
C_{V,AD}^6(\mu) &= C_{V,AD}^6(\Lambda) \left[1 - \gamma_{44} \ln \frac{\mu}{\Lambda} \right] + (9f_{AA}/8\pi) \tilde{C}^6(\Lambda) \ln \frac{\mu}{\Lambda} \\
C_{F,AAAD}^6(\mu) &= C_{F,AAAD}^6(\Lambda) \left[1 + \frac{3(\alpha_2 - 3\alpha_1)}{8\pi} \ln \frac{\mu}{\Lambda} \right] \\
&\quad + (9f_{AA}/4\pi) \left[C_{B,AD}^6(\Lambda) \alpha_1 + C_{W,AD}^6(\Lambda) \alpha_2 \right] \ln \frac{\mu}{\Lambda} \\
C_{F,ABBD}^6(\mu) &= C_{F,ABBD}^6(\Lambda) \left[1 - \frac{3(\alpha_1 + \alpha_2)}{8\pi} \ln \frac{\mu}{\Lambda} \right] \\
&\quad - \frac{3(\alpha_1 - \alpha_2)}{4\pi} C_{F,BABD}^6(\Lambda) \ln \frac{\mu}{\Lambda} \\
&\quad + (9f_{BB}/2\pi) \left[C_{B,AD}^6(\Lambda) \alpha_1 + C_{W,AD}^6(\Lambda) \alpha_2 \right] \ln \frac{\mu}{\Lambda} \\
C_{F,BABD}^6(\mu) &= C_{F,BABD}^6(\Lambda) \left[1 - \frac{3(\alpha_1 + \alpha_2)}{8\pi} \ln \frac{\mu}{\Lambda} \right] \\
&\quad - \frac{3(\alpha_1 - \alpha_2)}{4\pi} C_{F,ABBD}^6(\Lambda) \ln \frac{\mu}{\Lambda} \\
&\quad - (9f_{BB}/4\pi) \left[C_{B,AD}^6(\Lambda) \alpha_1 + C_{W,AD}^6(\Lambda) \alpha_2 \right] \ln \frac{\mu}{\Lambda}
\end{aligned} \tag{3.23}$$

where

$$\begin{aligned}
C_{\pm}^6(\mu) &\equiv C_{B,AD}^6(\mu) \pm C_{W,AD}^6(\mu) \\
\tilde{C}^6(\mu) &\equiv \alpha_1 C_{B,AD}^6(\mu) - 3\alpha_2 C_{W,AD}^6(\mu) \\
\gamma_{\pm} &\equiv (\gamma_{13} \pm \gamma_{23})/2 \\
\tilde{\gamma} &\equiv 3(\alpha_1 + 3\alpha_2)/16\pi
\end{aligned} \tag{3.24}$$

We note that the combination of coefficients $C_+^6(v)$ enters the neutrino magnetic moment. Its RG evolution was obtained in [17] to zeroth order in the Yukawa couplings; here we obtain the corrections that are linear in f_{AA} and f_{BB} . The corresponding contributions to the neutrino mass matrix δm_{ν}^{AD} and magnetic moment matrix μ_{ν}^{AD} are then given by

$$\delta m_{\nu}^{AD} = - \left(\frac{v^3}{2\sqrt{2}\Lambda^2} \right) C_{M,AD}^6(v) \tag{3.25}$$

$$\frac{\mu_{\nu}^{AD}}{\mu_B} = -4\sqrt{2} \left(\frac{m_e v}{\Lambda^2} \right) \text{Re} \{ C_+^6(v) \} . \tag{3.26}$$

From Eqs. (3.23), (3.25), and (3.26) we observe that to linear order in the lepton Yukawa couplings, $C_{M,AD}^6(\mu)$ receives contributions from the two magnetic moment operators and $\mathcal{O}_{\tilde{V}}^{(6)}$ but not from the four fermion operators. This result is consistent with the result obtained by the authors of [16], who computed one-loop graphs containing the four-fermion operators of Eq. (3.1) using massive charged leptons and found that contributions to $m_{\nu} \propto m_{\ell}^3$. In the effective theory used here, the latter result corresponds to a one-loop computation with three insertions of the Yukawa interaction. However, mixing with $\mathcal{O}_{\tilde{V}}^{(6)}$ was not considered in [16], and our result that this operator mixes with $\mathcal{O}_{M,AD}^{(6)}$ to linear order in the Yukawa couplings represents an important difference with the former analysis.

We agree with the observation of [16] that the four fermion operators can mix with $\mathcal{O}_{M,AD}^{(6)}$ to linear order in the f_{AA} via two-loop graphs, such as those indicated in Fig. 3.4. These graphs were estimated in [16] by considering loops with massive W^{\pm} and Z^0 bosons that correspond in our framework to the diagrams of Fig. 3.4a. We observe, however, that the two-loop constraints will be weaker than those obtained by one-loop matching with $\mathcal{O}_{M,AD}^{(4)}$ by $\sim (\alpha/4\pi)(v/\Lambda)^2$ (modulo logarithmic and model-dependent corrections), so we do not consider this two-loop mixing in detail here. Moreover, because we work at a scale $\mu > v$ for which the use of massless fields is appropriate, and because we adopt a basis in

which the Yukawa matrix and gauge interactions are flavor diagonal (but m_ν^{AD} is not), the operators $\mathcal{O}_{F,112D}^{(6)}$ and $\mathcal{O}_{F,221D}^{(6)}$ will not mix with $\mathcal{O}_{M,AD}^{(6)}$ even at two-loop order.

3.4 Neutrino Mass Constraints

To arrive at neutrino mass naturalness expectations for the $g_{\epsilon\mu}^\gamma$ coefficients, it is useful to tabulate their relationships with the dimension six operator coefficients. In some cases, one must perform a Fierz transformation in order to obtain the operator structures in Eq. (3.1).

Letting

$$g_{\epsilon\mu}^\gamma = \kappa \left(\frac{v}{\Lambda}\right)^2 C_k^6(v) \quad (3.27)$$

we give in Table 3.2 the κ s corresponding to the various dimension six operators.

Using the entries in Table 3.2 and the estimates in Eq. (3.16), we illustrate how the bounds in Table 3.1 were obtained. For the operator $\mathcal{O}_{F,122D}^{(6)}$, for example, we have from Eqs. (3.5) and (3.16)⁹

$$|C_{F,122D}^6| \lesssim 16\pi^2 \left(\frac{\delta m_\nu^{1D}}{m_\mu}\right) \quad (3.28)$$

leading to

$$|g_{LR}^S| \lesssim 4\pi^2 \left(\frac{\delta m_\nu^{1D}}{m_\mu}\right) \left(\frac{v}{\Lambda}\right)^2 \quad |g_{LR}^T| \lesssim 2\pi^2 \left(\frac{\delta m_\nu^{1D}}{m_\mu}\right) \left(\frac{v}{\Lambda}\right)^2 \quad (3.29)$$

where δm_ν^{AD} denotes the radiative contribution to m_ν^{AD} . Choosing $\Lambda = v$ and $\delta m_\nu^{1D} = 1\text{eV}$ (corresponding to the scale of upper bounds derived from ^3H β -decay studies [28, 29]) leads to the bounds in the first row of Table 3.1. Similar arguments yield the other entries in the table. Note that the bounds become smaller as Λ is increased from v .

The constraints on the $g_{LR,RL}^V$ that arise from mixing among the $n = 6$ operators follow straightforwardly from Eqs. (3.23) and (3.25) and Table 3.2. We obtain

$$g_{LR}^V = \left(\frac{\delta m_\nu^{2D}}{m_\mu}\right) \left(\frac{8\pi \sin^2 \theta_W}{9}\right) \left(\alpha - \frac{\lambda \sin^2 \theta_W}{3\pi}\right)^{-1} \left(\ln \frac{\Lambda}{v}\right)^{-1}. \quad (3.30)$$

A similar expression holds for g_{RL}^V but with $m_\mu \rightarrow m_e$ and $\delta m_\nu^{2D} \rightarrow \delta m_\nu^{1D}$. Note that in arriving at Eq. (3.30) we have ignored the running of the $C_{V,AD}^6(\mu)$ between Λ and v , since the impact on the $g_{LR,RL}^V$ is higher order in the gauge and Yukawa couplings. To derive numerical bounds on the $g_{LR,RL}^V$ from Eq. (3.30) we use the running couplings in the $\overline{\text{MS}}$

⁹In what follows, we suppress the scale dependence of the $C(\mu)$ and, as indicated earlier, neglect the effects of running in translating the one-loop matching bounds into constraints at the weak scale.

scheme $\alpha = \hat{\alpha}(M_Z) \approx 1/127.9$, $\sin^2 \hat{\theta}_W(M_Z) \approx 0.2312$ and the tree-level relation between the Higgs quartic coupling λ , the Higgs mass m_H , and v : $2\lambda = (m_H/v)^2$. We quote two results, corresponding to the direct search lower bound on $m_H \gtrsim 114$ GeV and the one-sided 95 % C.L. upper bound from analysis of precision electroweak measurements, $m_H \lesssim 186$ GeV [30]. We obtain

$$\begin{aligned} |g_{LR}^V| &= \left(\frac{\delta m_\nu^{2D}}{1 \text{ eV}} \right) \left(\ln \frac{\Lambda}{v} \right)^{-1} \begin{cases} 1.2 \times 10^{-6}, & m_H = 114 \text{ GeV} \\ 7.5 \times 10^{-6}, & m_H = 186 \text{ GeV} \end{cases} \\ |g_{RL}^V| &= \left(\frac{\delta m_\nu^{1D}}{1 \text{ eV}} \right) \left(\ln \frac{\Lambda}{v} \right)^{-1} \begin{cases} 2.5 \times 10^{-4}, & m_H = 114 \text{ GeV} \\ 1.5 \times 10^{-3}, & m_H = 186 \text{ GeV}. \end{cases} \end{aligned} \quad (3.31)$$

For $\Lambda \sim 1$ TeV, the logarithms are $\mathcal{O}(1)$ so that for $\delta m_\nu \sim 1$ eV, the bounds on the $g_{LR,RL}^V$ derived from $n = 6$ mixing are comparable in magnitude to those estimated from one-loop matching with the $n = 4$ mass operators.

Although the four fermion operators do not mix with $\mathcal{O}_{M,AD}^{(6)}$ at linear order in the Yukawa couplings, they do contribute to the magnetic moment operators $\mathcal{O}_{B,AD}^{(6)}$ and $\mathcal{O}_{W,AD}^{(6)}$ at this order. From Eqs. (3.23) and (3.26) we have

$$\frac{\delta \mu_\nu^{AD}}{\mu_B} = \frac{\sqrt{2}}{8\pi^2} \left(\frac{m_e}{v} \right) \left(\frac{v}{\Lambda} \right)^2 \text{Re} [f_{AA}^* C_{F,AAAD}^6 + f_{BB}^* C_{F,ABBD}^6] \ln \frac{\Lambda}{v}, \quad (3.32)$$

where $\delta \mu_\nu^{AD}$ denotes the contribution to the magnetic moment matrix and μ_B is a Bohr magneton. While $\mathcal{O}_{F,AAAD}^{(6)}$ does not contribute to μ -decay, the operator $\mathcal{O}_{F,ABBD}^{(6)}$ does, and its presence in Eq. (3.32) implies constraints on its coefficient from current bounds on neutrino magnetic moments. The most stringent constraints arise for $A = 1$, $B = 2$ for which we find

$$|C_{F,122D}^6| \left(\frac{v}{\Lambda} \right)^2 \lesssim 5 \times 10^{10} \left(\ln \frac{\Lambda}{v} \right)^{-1} \left(\frac{\mu_\nu^{1D}}{\mu_B} \right). \quad (3.33)$$

Current experimental bounds on $|\mu_\nu^{\text{exp}}/\mu_B|$ range from $\sim 10^{-10}$ from observations of solar and reactor neutrinos [31, 32, 33, 34] to $\sim 3 \times 10^{-12}$ from the non-observation of plasmon decay into $\bar{\nu}\nu$ in astrophysical objects [35]. Assuming that the logarithm in Eq. (3.33) is of order unity, these limits translate into bounds on g_{LR}^S and g_{LR}^T ranging from $\sim 1 \rightarrow 0.03$ and $\sim 0.3 \rightarrow 0.01$, respectively. The solar and reactor neutrino limits on $|\mu_\nu^{\text{exp}}/\mu_B|$

Table 3.2: Coefficients κ that relate $g_{\epsilon\mu}^\gamma$ to the dimension six operator coefficients C_k^6 via Eq. (3.27).

Coefficient	g_{LR}^S	g_{LR}^T	g_{RL}^S	g_{RL}^T	g_{LR}^V	g_{RL}^V
$C_{F,122D}^6$	1/4	1/8	-	-	-	-
$C_{F,212D}^6$	1/2	-	-	-	-	-
$C_{F,112D}^6$	3/4	1/8	-	-	-	-
$C_{F,211D}^6$	-	-	1/4	1/8	-	-
$C_{F,121D}^6$	-	-	1/2	-	-	-
$C_{F,221D}^6$	-	-	3/4	1/8	-	-
$C_{\tilde{V},2D}^6$	-	-	-	-	-1/2	-
$C_{\tilde{V},1D}^6$	-	-	-	-	-	-1/2

imply bounds on the $g_{LR}^{S,T}$ that are weaker than those obtained from the global analysis of μ -decay measurements, while those associated with the astrophysical magnetic moment limits are comparable to the global values. Nevertheless, the bounds derived from neutrino magnetic moments are several orders of magnitude weaker than those derived from the scale of neutrino mass.

The naturalness expectations for the C_k^6 associated with the scale of m_ν have implications for the interpretation of μ -decay experiments. Because the coefficients $C_{F,112D}^6$ and $C_{F,221D}^6$ that contribute to $g_{LR,RL}^{S,T}$ are not directly constrained by m_ν , none of the eleven Michel parameters is directly constrained by neutrino mass alone. Instead, it is more relevant to compare the results of global analyses from which limits on the $g_{\epsilon\mu}^\gamma$ are obtained with the m_ν naturalness bounds, since the latter imply tiny values for the couplings $g_{LR,RL}^V$. Should future experiments yield a value for either of these couplings that is considerably larger than our expectations in Table 3.1, the new physics above Λ would have to exhibit either fine-tuning or a symmetry in order to evade unacceptably large contributions to m_ν . In addition, should future global analyses find evidence for non-zero $g_{LR,RL}^{S,T}$ with magnitudes considerably larger than given by the m_ν naturalness expectations listed in Table 3.1, then one would have evidence for a non-trivial flavor structure in the new physics that allows considerably larger effects from the operators $\mathcal{O}_{F,112D}^{(6)}$ and $\mathcal{O}_{F,221D}^{(6)}$ than from the other four fermion operators.

Finally, we note that one may use a combination of neutrino mass and direct studies of

the Michel spectrum to derive bounds on a subset of the Michel parameters that are more stringent than one obtains from μ -decay experiments alone. To illustrate, we consider the parameters δ and α , for which one has

$$\frac{3}{4} - \rho = \frac{3}{4} |g_{LR}^V|^2 + \frac{3}{2} |g_{LR}^T|^2 + \frac{3}{4} \text{Re} (g_{LR}^S g_{LR}^{T*}) + (L \leftrightarrow R) \quad (3.34)$$

$$\alpha = 8 \text{Re} \{ g_{RL}^V (g_{LR}^{S*} + 6g_{LR}^{T*}) + (L \leftrightarrow R) \} . \quad (3.35)$$

From Table 3.1, we observe that the magnitudes of the $g_{LR,RL}^V$ contributions to ρ and α are expected to be several orders of magnitude below the current experimental sensitivities, based on neutrino mass naturalness considerations. In contrast, the contributions to $g_{LR,RL}^{S,T}$ that arise from $\mathcal{O}_{F,112D}^{(6)}$ and $\mathcal{O}_{F,221D}^{(6)}$ are only directly constrained by μ -decay experiments and not neutrino mass. Thus, we may use the current experimental results for ρ to bound the operator coefficients $C_{F,112D}^6$ and $C_{F,221D}^6$ and subsequently employ the results — together with the m_ν bounds on the $g_{LR,RL}^V$ — to derive expectations for the magnitude of α . For simplicity, we consider only the contributions from $C_{F,112D}^6$ to ρ , and using the current experimental uncertainty in this parameter, we find

$$|C_{F,112D}^6| \left(\frac{v}{\Lambda} \right)^2 \lesssim 0.1 . \quad (3.36)$$

In the parameter α , this coefficient interferes with $C_{\tilde{V},1D}^6$:

$$\alpha = -6 \left(\frac{v}{\Lambda} \right)^4 \text{Re} \left(C_{\tilde{V},1D}^6 C_{F,112D}^{6*} + \dots \right) , \quad (3.37)$$

where the “ $+\dots$ ” indicates contributions from the other coefficients that we will assume to be zero for purposes of this discussion. From Eq. (3.36) and the m_ν limits on $C_{\tilde{V},1D}^6$ we obtain

$$|\alpha| \lesssim 2 \times 10^{-4} \left(\frac{v}{\Lambda} \right)^2 \left(\frac{m_\nu^{1D}}{1 \text{ eV}} \right) . \quad (3.38)$$

For $\Lambda = v$, this expectation for $|\alpha|$ is more than two orders of magnitude below the present experimental sensitivity and will fall rapidly as Λ increases from v . A similar line of reasoning can be used to obtain expectations for the parameter α' in terms of m_ν and the CP-violating phases that may enter the effective operator coefficients.

3.5 Conclusions

The existence of the small, non-zero masses of neutrinos have provided our first direct evidence for physics beyond the minimal Standard Model, and the incorporation of m_ν into SM extensions is a key element of beyond the SM model building. At the same time, the existence of non-vanishing neutrino mass — together with its scale — have important consequences for the properties of neutrinos and their interactions that can be delineated in a model-independent manner [17, 18, 16, 36]. In this chapter, we have analyzed those implications for the decay of muons, using the effective field theory approach of [17] and concentrating on the case of Dirac neutrinos. We have derived model-independent naturalness expectations for the contributions to the Michel parameters from various $n = 6$ operators that also contribute to the neutrino mass matrix via radiative corrections.

Our work has been motivated by the ideas in [16], but our conclusions differ in important respects. In particular, we find — after properly taking into account $SU(2)_L \times U(1)_Y$ gauge invariance and mixing between $n = 6$ μ -decay and neutrino mass operators — that the dominant constraints on the contributions from $g_{RL,LR}^V$ to the Michel parameters occur at one-loop order, rather than through two-loop effects as in [16]. Consequently, the naturalness bounds we derive on these contributions are two orders of magnitude stronger than those of [16]. Based on one-loop matching considerations that cannot be analyzed in the context of dimensional regularization, we also obtain expectations for contributions from various four-fermion operators to effective scalar and tensor interactions that are substantially smaller than the two-loop mixing constraints appearing in that earlier work. We emphasize that these expectations can only be relaxed in the presence of fine-tuning or model-dependent suppression of the matching conditions at the scale Λ .

In addition, we carefully study the flavor structure of the operators that can contribute to μ -decay and find that there exist four-fermion μ -decay operators that do not contribute to the neutrino mass matrix through radiative corrections. Since these operators contribute to the effective scalar and tensor couplings $g_{LR,RL}^{S,T}$ of Eq. (3.1), no model-independent neutrino mass naturalness bounds exist for these couplings, contrary to the conclusions of [16]. In contrast, all operators that generate the $g_{LR,RL}^V$ terms contribute to m_ν^{AD} , so these effective couplings do have neutrino-mass naturalness bounds. From a model-building perspective it might seem reasonable to expect the coefficients of the unconstrained four-fermion operator

coefficients to have the same magnitude as those that are constrained by m_ν , but it is important for precise muon decay experiments to test this expectation.

While we have focused on the implications of Dirac mass terms, a similar analysis for the Majorana neutrinos is clearly called for. Indeed, in the case of neutrino magnetic moments, the requirement of flavor non-diagonality for Majorana magnetic moments can lead to substantially weaker naturalness bounds than for Dirac moments [17, 18, 19]. While we do not anticipate similar differences between the Majorana and Dirac case for operators that contribute to μ -decay, a detailed comparison will appear in the next chapter.

Chapter 4

Majorana Neutrinos and μ -decay

4.1 Introduction

The existence of small nonzero neutrino masses has provided our first direct evidence of physics beyond the Standard Model. Since direct experimental study of the neutrino mass and of neutrino-matter interactions is difficult, and the number of candidates for physics beyond the SM is large, model-independent studies of neutrino-matter interactions combined with the study of neutrino mass are valuable tools in the search for new physics.

The study of Majorana neutrinos and muon decay has the potential to set bounds on beyond the SM parameters that may soon be accessible by experiment. These bounds are on some of the Michel parameters [10, 11] that contain information about contributions to muon decay from unknown physics. In the SM, there are well-known predictions for what these parameters should be. A previous study [37] looked at the limits that a Dirac neutrino mass could put on the muon decay Michel parameters. Here we do the same for Majorana neutrinos, and we closely follow the approach of that paper. However, in order to analyze the effect of Majorana neutrino masses on the Michel parameters, we will need to cover some background material.

We will first examine the motivations behind the development of Majorana neutrinos, both how they emerge from higher-dimensional operators and why they are, from a theoretical perspective, appealing. In Section 4.2, we write down the complete set of independent operators through $n = 7$ that contribute to m_ν^{AE} and μ -decay. Section 4.3 gives our analysis of operator mixing and matching considerations, while in Section 4.4 we discuss the resulting constraints on the $g_{LR,RL}^\gamma$ that follow from this analysis and the present upper bounds on the neutrino mass scale. We summarize in Section 4.5.

4.1.1 Majorana neutrinos

Contributions to muon decay are typically parameterized as

$$\mathcal{L}^{\mu\text{-decay}} = -\frac{4G_\mu}{\sqrt{2}} \sum_{\gamma, \alpha, \beta} g_{\alpha\beta}^\gamma \bar{e}_\alpha \Gamma^\gamma \nu^e \bar{\nu}^\mu \Gamma_{\gamma\mu\beta}, \quad (4.1)$$

where we sum over Dirac matrices $\Gamma^\gamma = 1$ (S), γ^α (V), and $\sigma^{\alpha\beta}/\sqrt{2}$ (T) and the subscripts α and β indicate the chirality (R, L) of the muon and final state lepton, respectively¹. In the SM, $g_{LL}^V = 1$ and all other $g_{\alpha\beta}^\gamma = 0$. A recent, global analysis by Gagliardi, Tribble, and Williams [15] give the present experimental bounds on the $g_{\alpha\beta}^\gamma$ that include the results of the latest TRIUMF and PSI measurements. When referring to Eq. (4.1) with Majorana neutrinos, note that $\nu_R \rightarrow \overline{\nu}_L^c$.

We use the effective Lagrangian

$$\mathcal{L}_{\text{eff}} = \sum_{n,j} \frac{C_j^n(\mu)}{\Lambda^{n-4}} \mathcal{O}_j^{(n)}(\mu) + \text{h.c.}, \quad (4.2)$$

where μ is the renormalization scale, $n \geq 4$ is the operator dimension, and j is an index running over all independent operators of a given dimension. There are several ways of modifying the SM to allow nonzero neutrino masses. One of the “easiest” ways is to give up on renormalizability of the Lagrangian [41]: by regarding the standard model as a low-energy effective field theory, we find that there is only one gauge-invariant dimension five operator allowed by SM gauge invariance and particle content:

$$\mathcal{L}_5 = \frac{C^{(5)}}{\Lambda} (\overline{L^c} \epsilon H) (H^T \epsilon L) + \text{h.c.}, \quad (4.3)$$

where $\overline{L^c} = L^T C$ (C is the charge conjugation operator). This operator clearly violates lepton number, by two units. When the Higgs field acquires a vacuum expectation value,

$$\langle \phi \rangle = \begin{pmatrix} 0 \\ v/\sqrt{2} \end{pmatrix} \quad (4.4)$$

we acquire a Majorana mass for the neutrino,

$$\mathcal{L}_M = -\frac{C^{(5)}}{\Lambda} \frac{v^2}{2} \overline{\nu}_L^c \nu_L + \text{h.c.} \quad (4.5)$$

¹The normalization of the tensor terms corresponds to the convention adopted in [14]

As an aside, the neutrino has obtained a Majorana mass only because \mathcal{L}_5 violated lepton number, which here is a low-energy accidental symmetry and is in general violated by higher-dimensional operators. Since, in this formulation, neutrino masses are naturally of order v^2/Λ , if $\Lambda \gg v$, this is an attractive explanation of why neutrinos are much lighter than the other fermions [40].

The Majorana mass, written in terms of Dirac spinors, is given by (see Sec. 1.1):

$$\mathcal{L} = -\frac{1}{2}m(\overline{L^c}L + \text{h.c.}) . \quad (4.6)$$

By comparing this with the $n = 5$ mass operator, Eq. (4.3),

$$\frac{C_M^{5, AE}}{\Lambda}(\overline{L^c}^A \epsilon H)(H^T \epsilon L^E) \leftrightarrow -\frac{1}{2}m_\nu^{AE}(\overline{\nu_L^c}^A \nu_L^E) , \quad (4.7)$$

we see that after spontaneous symmetry breaking,

$$\frac{C_M^{5, AE}}{\Lambda}\mathcal{O}_{M, AE}^{(5)} = \frac{C_M^{5, AE}}{\Lambda}(-H_0^2 \overline{\nu_L^c}^A \nu_L^E) ,$$

an upper bound on the neutrino mass contribution is obtained:

$$m_\nu^{AE} \lesssim \frac{v^2}{\Lambda}C_M^{5, AE} . \quad (4.8)$$

It is important to realize that the $n = 5$ neutrino mass operator, Eq. (4.3), is symmetric with respect to the lepton flavors. This means that, if we label the flavors as A and E , the $SU(2)$ indices beginning with i, j, \dots and the Dirac indices beginning with a, b, \dots :

$$\mathcal{O}_{M, AE}^{(5)} = L_{i,a}^A \epsilon_{ij} C_{ab} H_j H_k \epsilon_{kl} L_{l,b}^E ,$$

then by moving L^E past L^A (putting in a -1 for interchanging the fermion fields), we get

$$\mathcal{O}_{M, EA}^{(5)} = -L_{l,b}^E \epsilon_{lk} C_{ab} H_k H_j \epsilon_{ji} L_{i,a}^A ,$$

which is just

$$\mathcal{O}_{M, EA}^{(5)} = -(L^{TE} C^T \epsilon H)(H^T \epsilon L^A) .$$

Since $\overline{L^c} = -L^T C^T$, we get the original 5D mass operator back,

$$\mathcal{O}_{M,EA}^{(5)} = (\overline{L^c}^E \epsilon H)(H^T \epsilon L^E) = \mathcal{O}_{M,AE}^{(5)} .$$

We will use $\mathcal{O}_{M,AE}^{(5)}$ and $\mathcal{O}_{M,EA}^{(5)}$ interchangeably to refer to the same operator.

4.2 Operator Basis

In order to begin the analysis we will first examine our operator basis by writing down some of the operators up to dimension seven that contain Majorana neutrinos and contribute to the $n = 5$ and $n = 7$ Majorana neutrino mass operators. Here we will make use of the list of operators outlined in [38]. We will then take a careful look at the flavor structure of our operators, and in the process discover that some of the operators that superficially appear relevant to our analysis actually give contributions to μ -decay that are unconstrained by neutrino mass.

4.2.1 $n = 7$ operators contributing to neutrino mass

As before, the lowest dimension Majorana neutrino mass operator, which is a 5D operator, is

$$\mathcal{O}_{M,AE}^{(5)} = (\overline{L^c}^A \epsilon H)(H^T \epsilon L^E) . \quad (4.9)$$

For Majorana neutrinos there are no gauge-invariant $n = 6$ operators. Here, we group the operators with dimension seven according to the number of fermion, Higgs, and gauge boson fields they contain. The 7D mass operator is:

$$\mathcal{O}_{M,AE}^{(7)} = (\overline{L^c}^A \epsilon H)(H^T \epsilon L^E)(H^\dagger H) , \quad (4.10)$$

There are three independent operators with two derivatives. Only the last one can contribute to muon decay after SSB:

$$\begin{aligned} \mathcal{O}_{D(a),AE}^{(7)} &= (\overline{L^c}^A \epsilon L^E)(H^T \overleftarrow{D}_\mu \epsilon D^\mu H) , \\ \mathcal{O}_{D(b),AE}^{(7)} &= (\overline{L^c} \epsilon D^\mu H)(H^T \overleftarrow{D}_\mu \epsilon L) , \\ \mathcal{O}_{D(c),AE}^{(7)} &= (\overline{L^c} \epsilon H)(H^T \overleftarrow{D}_\mu \epsilon D^\mu L) . \end{aligned} \quad (4.11)$$

Due to the presence of the derivative acting on the external fermion field, this contribution is suppressed and will not be considered here.

There is one independent operator with one derivative; it contributes to g_{RL}^V and g_{LR}^V :

$$\mathcal{O}_{\check{V}, AE}^{(7)} = i \overline{\ell}_R^{cA} \gamma^\mu (H^T \epsilon L^E) (H^T \epsilon \overrightarrow{D}_\mu H) . \quad (4.12)$$

There are two independent four-fermion scalar operators. Each one corresponds to a different Lorentz contraction. These operators contribute to g_{RL}^S , g_{LR}^S , g_{RL}^T , and g_{LR}^T :

$$\begin{aligned} \mathcal{O}_{F(a), ABDE}^{(7)} &= \epsilon_{ij} \epsilon_{kl} (\overline{L}_i^{cA} L_k^B) (\overline{L}_j^D \ell_R^{cE}) H_l , \\ \mathcal{O}_{F(b), ABDE}^{(7)} &= \epsilon_{ij} \epsilon_{kl} (\overline{L}_i^{cA} L_j^B) (\overline{L}_k^D \ell_R^{cE}) H_l , \end{aligned} \quad (4.13)$$

where $\ell_R^c = C \overline{\ell}_R^{cT}$. These are the only independent $SU(2)$ contractions. For example, the contraction:

$$\mathcal{O}_F = \epsilon_{ij} \epsilon_{kl} (\overline{L}_i^c \ell_R^c) (\overline{L}_j L_k) H_l ,$$

can, by renaming $i \leftrightarrow j$, be shown to be simply $-\mathcal{O}_{F(a)}$.

We also note that any four-fermion tensor operators, for example:

$$\mathcal{O}_{\check{F}(a), ABDE}^{(7)} = \epsilon_{ij} \epsilon_{kl} (\overline{L}_i^{cA} \sigma^{\alpha\beta} L_k^B) (\overline{L}_j^D \sigma_{\alpha\beta} \ell_R^{cE}) H_l ,$$

are merely linear combinations of the scalar operators and are not independent². This can be seen by starting with the operator

$$\epsilon_{ij} \epsilon_{kl} (\overline{L}_i^{cA} \ell_R^{cE}) (\overline{L}_j^D L_k^B) H_l ,$$

and Fierz-transforming to obtain the ordering of the original operator, $\mathcal{O}_{\check{F}(a), ABDE}^{(7)}$:

$$\epsilon_{ij} \epsilon_{kl} \left[\frac{1}{2} (\overline{L}_i^{cA} L_k^B) (\overline{L}_j^D \ell_R^{cE}) + \frac{1}{8} (\overline{L}_i^{cA} \sigma^{\alpha\beta} L_k^B) (\overline{L}_j^D \sigma_{\alpha\beta} \ell_R^{cE}) \right] H_l ,$$

²The tensor operators referred to in [38], $\epsilon_{ij} \epsilon_{kl} (L_i^{TA} \sigma^{\alpha\beta} L_k^B) (L_j^{TD} \sigma_{\alpha\beta} \ell_R^{cE}) H_l$ and $\epsilon_{ij} \epsilon_{kl} (L_i^{TA} \sigma^{\alpha\beta} L_j^B) (L_k^{TD} \sigma_{\alpha\beta} \ell_R^{cE}) H_l$, are not Lorentz invariant.

which means that the tensor operator can be re-expressed as:

$$\begin{aligned} \frac{1}{8}\epsilon_{ij}\epsilon_{kl}(\overline{L}_i^{cA}\sigma^{\alpha\beta}L_k^B)(\overline{L}_j^{cD}\sigma_{\alpha\beta}\ell_R^{cE}) &= \epsilon_{ij}\epsilon_{kl}[(\overline{L}_i^{cA}\ell_R^{cE})(\overline{L}_j^{cD}L_k^B) \\ &- \frac{1}{2}(\overline{L}_i^{cA}L_k^B)(\overline{L}_j^{cD}\ell_R^{cE})]H_l, \end{aligned}$$

or

$$\frac{1}{8}\mathcal{O}_{\tilde{F}(a), ABDE}^{(7)} = -\mathcal{O}_{F(a), DBAE}^{(7)} - \frac{1}{2}\mathcal{O}_{F(a), ABDE}^{(7)}.$$

Finally, there is one independent W charged gauge boson operator that can contribute to muon decay, and a B operator that does not:

$$\begin{aligned} \mathcal{O}_{W, AE}^{(7)} &= (\overline{L}^{cA}\epsilon H)\sigma^{\mu\nu}(H^T\epsilon\tau^a L^E)W_{\mu\nu}^a, \\ \mathcal{O}_{B, AE}^{(7)} &= (\overline{L}^{cA}\epsilon H)\sigma^{\mu\nu}(H^T\epsilon L^E)B_{\mu\nu}. \end{aligned}$$

The operator $\mathcal{O}_{B, AE}^{(7)}$ is lepton flavor antisymmetric. The operator $\mathcal{O}_{W, AE}^{(7)}$, which is the most general $n = 7$ operator involving $W_{\mu\nu}^a$, is neither flavor symmetric nor antisymmetric. We will choose to express it in terms of operators with definite flavor symmetry, $\mathcal{O}_{W, AE}^{(7)\pm}$:

$$\mathcal{O}_{W, AE}^{(7)\pm} = \frac{1}{2}\left(\mathcal{O}_{W, AE}^{(7)} \pm \mathcal{O}_{W, EA}^{(7)}\right). \quad (4.14)$$

However, like the two-derivative operators, the contribution of the W operator is suppressed (by a factor of m_μ^4/Λ^4) by the derivative acting on the gauge field and, again, will not be considered in this analysis.

4.2.2 Flavor structure

In order to examine the neutrino mass constraints on the $g_{\alpha\beta}^\gamma$ coefficients, we must determine how the operators under consideration are related to these coefficients. For most, a Fierz transformation [39] must be done to move the fields into the order in Eq. (4.1). By defining

$$g_{\alpha\beta}^\gamma = -\kappa\left(\frac{v}{\Lambda}\right)^3 C_k^\gamma, \quad (4.15)$$

we can find the κ s of the various dimension seven operators. These results are summarized in Table 4.1; we explain how to obtain these numbers in the following.

For the six possible flavor combinations for the two scalar operators $\mathcal{O}_{F(a), ABDE}^{(7)}$ and $\mathcal{O}_{F(b), ABDE}^{(7)}$, two are not constrained by neutrino mass. By writing out the $SU(2)$ indices we can examine the flavor structure more closely:

$$\begin{aligned}\mathcal{O}_{F(a), ABDE}^{(7)} &= \epsilon_{ij}\epsilon_{kl}(\overline{L}_i^{cA} L_k^B)(\overline{L}_j^{cD} \ell_R^{cE}) H_l \\ &= H^0(\overline{\nu}_L^c{}^A \nu_L^B \overline{\ell}_L^{cD} \ell_R^{cE} - \overline{\ell}_L^{cA} \nu_L^B \overline{\nu}_L^{cD} \ell_R^{cE}) \\ &\quad + H^+(\overline{\ell}_L^{cA} \ell_L^B \overline{\nu}_L^{cD} \ell_R^{cE} - \overline{\nu}_L^c{}^A \ell_L^B \overline{\ell}_L^{cD} \ell_R^{cE}),\end{aligned}\quad (4.16)$$

$$\begin{aligned}\mathcal{O}_{F(b), ABDE}^{(7)} &= \epsilon_{ij}\epsilon_{kl}(\overline{L}_i^{cA} L_j^B)(\overline{L}_k^{cD} \ell_R^{cE}) H_l \\ &= H^0(\overline{\nu}_L^c{}^A \ell_L^B \overline{\nu}_L^{cD} \ell_R^{cE} - \overline{\ell}_L^{cA} \nu_L^B \overline{\nu}_L^{cD} \ell_R^{cE}) \\ &\quad + H^+(\overline{\ell}_L^{cA} \nu_L^B \overline{\ell}_L^{cD} \ell_R^{cE} - \overline{\nu}_L^c{}^A \ell_L^B \overline{\ell}_L^{cD} \ell_R^{cE}).\end{aligned}\quad (4.17)$$

For example, we can obtain the $g_{\alpha\beta}^\gamma$ coefficients for the flavor combination $\mathcal{O}_{F(a)}^{e\mu\mu e}$ by first Fierz transforming and then exchanging fields. The different parts of the expanded operator (using only the neutral Higgs part) contain information about muon decay or neutrino mass:

$$\mathcal{O}_{F(a)}^{e\mu\mu e} \Rightarrow H^0 \underbrace{(\overline{\nu}_L^c{}^e \nu_L^\mu \overline{\ell}_L^{c\mu} \ell_R^{c^e})}_{\mu \text{ decay}} - \underbrace{(\overline{\ell}_L^{c^e} \nu_L^\mu \overline{\nu}_L^{c\mu} \ell_R^{c^e})}_{\nu \text{ mass}}. \quad (4.18)$$

After Fierz transforming the muon decay part, we have:

$$\mathcal{O}_{F(a)}^{e\mu\mu e} \Rightarrow \frac{H^0}{4} (2 \overline{\nu}_L^c{}^e \ell_R^{c^e} \overline{\ell}_L^{c\mu} \nu_L^\mu + \frac{1}{2} \overline{\nu}_L^c{}^e \sigma^{\alpha\beta} \ell_R^{c^e} \overline{\ell}_L^{c\mu} \sigma_{\alpha\beta} \nu_L^\mu). \quad (4.19)$$

Next, we exchange the fields in the first position with the fields in the second position, and similarly with the fields in the third and fourth positions, taking care to keep track of minus signs from fermion anticommutation and the transposition of the charge conjugation operator. Using the relations

$$\overline{w}_L^{c(1)} w_R^{c(2)} = \overline{w}_R^{(2)} w_L^{(1)}, \quad (4.20)$$

$$\overline{w}_L^{c(1)} w_L^{(2)} = \overline{w}_L^{c(2)} w_L^{(1)}, \quad (4.21)$$

$$\overline{w}_L^{c(1)} \sigma^{\alpha\beta} w_R^{c(2)} = -\overline{w}_R^{(2)} \sigma^{\alpha\beta} w_L^{(1)}, \quad (4.22)$$

$$\overline{w}_L^{c(1)} \sigma^{\alpha\beta} w_L^{(2)} = -\overline{w}_L^{c(2)} \sigma^{\alpha\beta} w_L^{(1)}, \quad (4.23)$$

Table 4.1: Coefficients κ that relate $g_{\alpha\beta}^\gamma$ to the dimension seven four-fermion scalar and vector operator coefficients C_k^7 via Eq. (4.15). A “-” indicates that the associated operator does not contribute to that g in muon decay.

κ	g_{LR}^S	g_{LR}^T	g_{RL}^S	g_{RL}^T	g_{LR}^V	g_{RL}^V
$C_{F(a)}^{7e\mu\mu e}$	-	-	$\frac{-1}{4\sqrt{2}}$	$\frac{-1}{8\sqrt{2}}$	-	-
$C_{F(a)}^{7\mu e e \mu}$	$\frac{-1}{4\sqrt{2}}$	$\frac{-1}{8\sqrt{2}}$	-	-	-	-
$C_{F(a)}^{7e\mu e \mu}$	-	$\frac{-1}{8\sqrt{2}}$	-	-	-	-
$C_{F(a)}^{7\mu e \mu e}$	-	-	-	$\frac{-1}{8\sqrt{2}}$	-	-
$C_{F(a)}^{7\mu\mu ee}$	-	-	$\frac{1}{2\sqrt{2}}$	-	-	-
$C_{F(a)}^{7ee\mu\mu}$	$\frac{1}{2\sqrt{2}}$	-	-	-	-	-
$C_{F(b)}^{7e\mu\mu e}$	-	-	$\frac{-1}{4\sqrt{2}}$	$\frac{1}{8\sqrt{2}}$	-	-
$C_{F(b)}^{7\mu e e \mu}$	$\frac{-1}{4\sqrt{2}}$	$\frac{1}{8\sqrt{2}}$	-	-	-	-
$C_{F(b)}^{7e\mu e \mu}$	$\frac{1}{4\sqrt{2}}$	$\frac{-1}{8\sqrt{2}}$	-	-	-	-
$C_{F(b)}^{7\mu e \mu e}$	-	-	$\frac{1}{4\sqrt{2}}$	$\frac{-1}{8\sqrt{2}}$	-	-
$C_{F(b)}^{7\mu\mu ee}$	-	-	-	0	-	-
$C_{F(b)}^{7ee\mu\mu}$	-	0	-	-	-	-
$C_{\hat{V}}^{7ee}$	-	-	-	-	-	$\frac{-1}{2\sqrt{2}}$
$C_{\hat{V}}^{7\mu\mu}$	-	-	-	-	$\frac{-1}{2\sqrt{2}}$	-

the operator becomes:

$$\mathcal{O}_{F(a)}^{e\mu\mu e} \Rightarrow \frac{H^0}{4} \left(2 \underbrace{\overline{\ell}_R^e \nu_L^e \overline{\nu}_L^{c\mu} \ell_L^\mu}_{g_{RL}^S} + \frac{1}{2} \underbrace{\overline{\ell}_R^e \sigma^{\alpha\beta} \nu_L^e \overline{\nu}_L^{c\mu} \sigma_{\alpha\beta} \ell_L^\mu}_{g_{RL}^T} \right). \quad (4.24)$$

Comparing these coefficients with the coefficient of Eq. (4.1), we find that $g_{RL}^S = \frac{-1}{4\sqrt{2}} \left(\frac{v}{\Lambda}\right)^3 C_\kappa^7$ and $g_{RL}^T = \frac{-1}{8\sqrt{2}} \left(\frac{v}{\Lambda}\right)^3 C_\kappa^7$. A summary of these results can be found in Table 4.1.

Finally, the values for g_V^{RL} and g_V^{LR} are found by calculating the diagram in Fig. 4.1 with the Standard Model vertex $\overline{L}^\mu i/DL_\mu$ and the new physics vertex with the operator $\mathcal{O}_{\hat{V},AE}^{(7)} = i \overline{\ell}_R^{cA} \gamma^\mu (H^T \epsilon L^E) (H^T \epsilon \overrightarrow{D}_\mu H)$, where $A, E = e, e$ (g_{RL}^V) or $A, E = \mu, \mu$ (g_{LR}^V). We find that the coefficients for both cases are given by $-\frac{1}{2\sqrt{2}}$ (Table 4.1). The difference from

the Dirac case, where the coefficient is $1/2$, arises from the additional Higgs field in $\mathcal{O}_{V,AE}^{(7)}$.

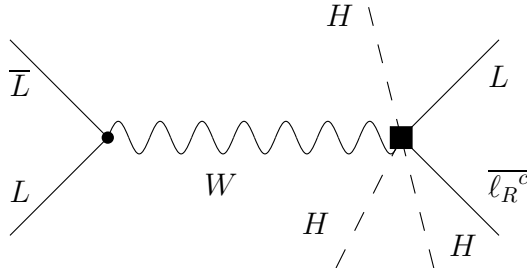


Figure 4.1: Contributions of the operators $\mathcal{O}_{V,AE}^{(7)}$ and $\mathcal{O}_{V,EA}^{(7)}$ (denoted by the solid box) to muon decay. Solid, dashed, and wavy lines denote fermions, Higgs scalars, and gauge bosons, respectively. After SSB, the neutral Higgs field is replaced by its vev, yielding a four-fermion μ -decay amplitude.

4.3 Operator Renormalization: Matching and Mixing

In order to determine the effect of neutrino mass on muon decay, we must consider both the contributions from matching the $n = 7$ operators discussed in Section 4.2 to the $n = 5$ mass operator, and also from mixing among the relevant $n = 7$ operators. We expect the results from the latter case to be approximately $(v/\Lambda)^2$ larger than those from $7D \rightarrow 5D$ matching, since the $7D$ mass operator has an additional factor of $(H^\dagger H)/\Lambda^2$. The matching case is considered first.

4.3.1 $7D \rightarrow 5D$ matching

Here we analyze the matching of the $n = 7$ operators to the $n = 5$ mass operator with naive dimensional analysis. Dimensional regularization (DR) is inapplicable here because in that scheme operators of a given dimension do not mix with operators of lower dimension.

To simplify the analysis of matching involving the $\mathcal{O}_{F,ABDE}^{(7)}$ we note that one may always redefine the fields L^A and ℓ_R^E so that the charged lepton Yukawa matrix f_{AE} is diagonal. Specifically, we take

$$\begin{aligned}
L^A &\rightarrow L^{A'} = S_{AB}L^B \\
\ell_R^E &\rightarrow \ell^{E'} = T_{ED}\ell^D
\end{aligned}
\tag{4.25}$$

with S_{AB} and T_{ED} chosen so that

$$\bar{L} \tilde{f} \ell = \bar{L}' \tilde{f}_{\text{diag}} \ell' \tag{4.26}$$

where L, L' denote vectors in flavor space, \tilde{f} denotes the Yukawa matrix in the original basis, and $\tilde{f}_{\text{diag}} = \tilde{S}^\dagger \tilde{f} \tilde{T}$. We note that the field redefinition (4.25) differs from the conventional flavor rotation used for quarks, since we have performed identical rotations on both isospin components of the left-handed doublet. Consequently, gauge interactions in the new basis entail no transitions between generations. We carry out computations using the L', ℓ'_R basis³.

To calculate the contribution of the scalar four-fermion operators in Eq. (4.13) to the five-dimensional mass operator, we have one diagram to consider, Fig. 4.2(a). From Section 4.2.2, we know that there are two charged fermions in the part of the operators associated with the neutral Higgs field, so there are two ways to contract the charged leptons belonging to the four-fermion operators and the Yukawa vertex. In general, each contraction gives a different result for the matching contribution. These results are summarized in the next section.

For the one-derivative operator in Eq. (4.12), there is one diagram to consider (Fig. 4.2(b)). The evaluation of this graph using dimensional analysis is straightforward.

As noted previously, the only scalar $n = 7$ four-fermion operators that can contribute to the $n = 5$ neutrino mass operator are those with either $A = E$ or $A = B$. For the scalar four-fermion operators, the contribution from the $7D$ operators to the $5D$ mass operator

³For notational simplicity, we henceforth omit the prime superscripts.

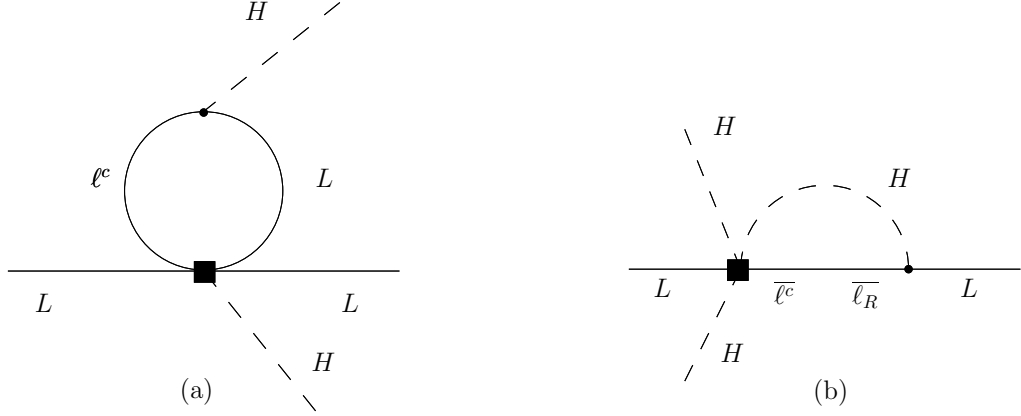


Figure 4.2: One-loop graphs for the matching of the $n = 7$ operators (denoted by the box) into the $n = 5$ mass operator $\mathcal{O}_{M,AE}^{(5)}$. Solid, dashed, and wavy lines denote fermions, Higgs scalars, and gauge bosons, respectively. Panels (a, b) illustrate mixing of $\mathcal{O}_F^{(7)}$ and $\mathcal{O}_4^{(7)}$, respectively, into $\mathcal{O}_{M,AE}^{(5)}$.

from dimensional analysis are:

$$\begin{aligned}
\mathcal{O}_{F(a)}^{7,ABBA} &\rightarrow C_M^{5,BB} \sim \frac{f_{AA}}{16\pi^2} C_{F(a)}^{7,ABBA}, \\
\mathcal{O}_{F(a)}^{7,AABB} &\rightarrow C_M^{5,AA} \sim \frac{f_{BB}}{4\pi^2} C_{F(a)}^{7,AABB}, \\
\mathcal{O}_{F(b)}^{7,ABBA} &\rightarrow C_M^{5,BB} \sim \frac{f_{AA}}{16\pi^2} C_{F(b)}^{7,ABBA}, \\
\mathcal{O}_{F(b)}^{7,ABAB} &\rightarrow C_M^{5,AA} \sim \frac{f_{BB}}{16\pi^2} C_{F(b)}^{7,ABAB}.
\end{aligned} \tag{4.27}$$

Certain flavor combinations ($\mathcal{O}_{F(a)}^{7,ABAB}$ and $\mathcal{O}_{F(b)}^{7,AABB}$) are missing because, although they contribute to μ -decay, they are unconstrained by neutrino mass and do not contribute to C_M^5 .

When we calculate the contribution of the $7D$ one-derivative operator, $\mathcal{O}_{V,AE}^{(7)}$ or $\mathcal{O}_{V,EA}^{(7)}$, to the $5D$ mass operator, we find:

$$\begin{aligned}
\mathcal{O}_4^{7,AE} &\rightarrow C_M^{5,EA} \sim \frac{f_{AA}^*}{16\pi^2} C_4^{7,AE}, \\
\mathcal{O}_4^{7,EA} &\rightarrow C_M^{5,AE} \sim \frac{f_{EE}^*}{16\pi^2} C_4^{7,EA}.
\end{aligned} \tag{4.28}$$

In performing these calculations, the well-known relation $C^{-1}\gamma_\mu = -\gamma_\mu^T C^{-1}$ was useful.

4.3.2 Mixing among the 7D operators

In order to study the mixing of the $n = 7$ operators, we use a partial renormalization group (RG) analysis to derive the neutrino mass naturalness bounds.

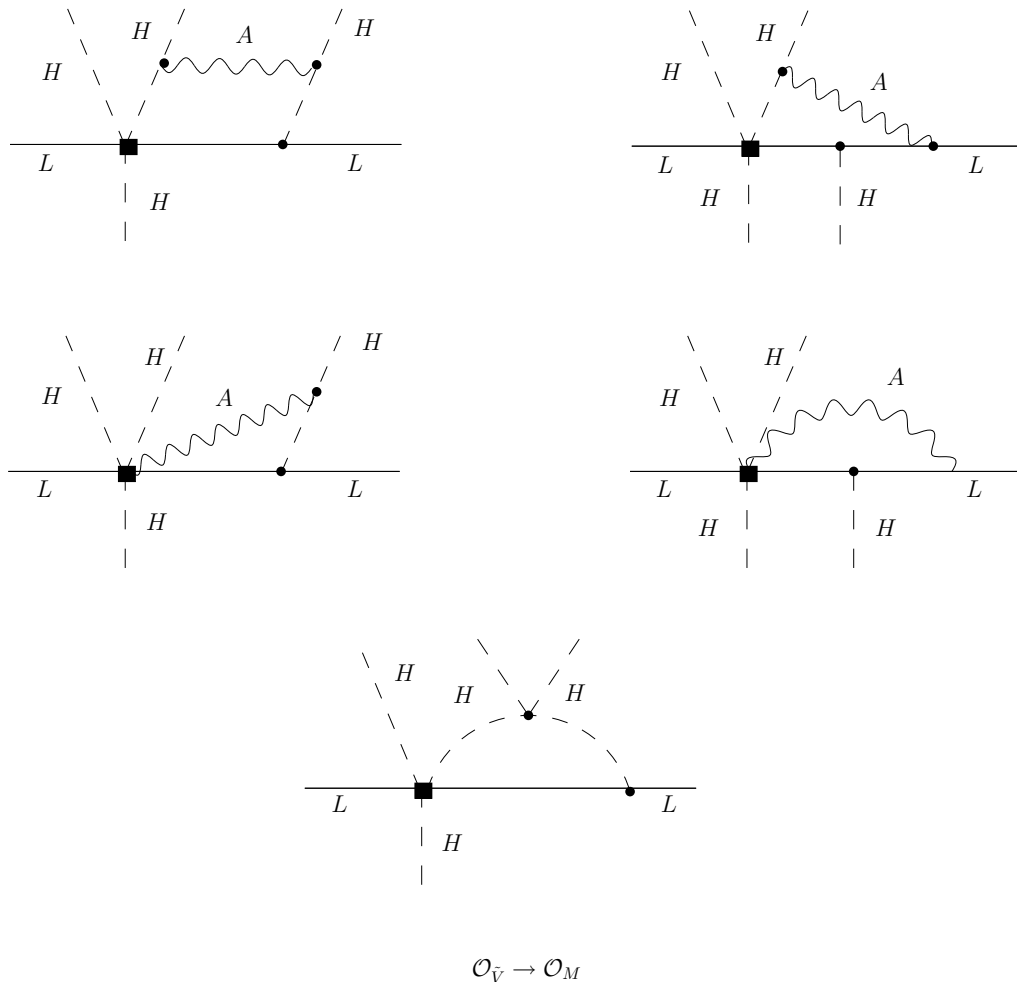


Figure 4.3: One-loop graphs for the mixing of the $n = 7$ operator $\mathcal{O}_{\tilde{V}}^{(7)}$ (denoted by the box) into the $n = 7$ mass operator $\mathcal{O}_{M,AE}^{(7)}$. Solid, dashed, and wavy lines denote fermions, Higgs scalars, and gauge bosons, respectively.

Because $\mathcal{O}_{M,AE}^{(7)}$ contains one power of $(H^\dagger H)/\Lambda^2$ compared to $\mathcal{O}_{M,AE}^{(5)}$, the constraints obtained from mixing with the former will generally be weaker by $\sim (v/\Lambda)^2$. However, we will see that for $\Lambda \sim 1$ TeV, the $n = 7$ mixing can be of comparable importance to the $n = 5$ case.

We will be calculating the contributions from the $n = 7$ operator $\mathcal{O}_{\tilde{V},AE}^{(7)}$ to the 7D mass

operator using DR and performing a renormalization group (RG) analysis. The contributions of the other $n = 7$ operators will be ignored because their contributions to neutrino mass are suppressed (in the case of the four-fermion operators, by three powers of the Yukawa coupling) or because their contributions to muon decay are suppressed (in the case of the two-derivative operators and the magnetic moment operators).

To first order in Yukawa couplings, there are five graphs to be calculated (see Fig. 4.3). The background field gauge is used with $d = 4 - 2\epsilon$; the operators are renormalized with minimal subtraction, and the renormalized operators are then expressed in terms of the unrenormalized operators:

$$\mathcal{O}_{jR}^{(7)} = \sum_k Z_{jk}^{-1} Z_L^{n_L/2} Z_H^{n_H/2} Z_{\ell_R}^{n_{\ell_R}/2} \mathcal{O}_k^{(7)} = \sum_k Z_{jk}^{-1} \mathcal{O}_{k0}^{(7)} \quad , \quad (4.29)$$

where

$$\mathcal{O}_{j0}^{(7)} = Z_L^{n_L/2} Z_H^{n_H/2} Z_{\ell_R}^{n_{\ell_R}/2} \mathcal{O}_j^{(7)} \quad (4.30)$$

are the μ -independent bare operators. $Z_L^{1/2}$ and $Z_H^{1/2}$ are the wavefunction renormalization constants for the fields L^A and H , respectively, n_L and n_H are the number of LH lepton and Higgs fields appearing in a given operator, and $Z_{jk}^{-1} Z_L^{n_L/2} Z_H^{n_H/2} Z_{\ell_R}^{n_{\ell_R}/2}$ are the counterterms that remove the $1/\epsilon$ divergences.

Since the bare operators $\mathcal{O}_{j0}^{(7)}$ do not depend on the renormalization scale, whereas the Z_{jk}^{-1} and the $\mathcal{O}_j^{(7)}$ do, the operator coefficients C_j^7 must carry a compensating μ -dependence to ensure that \mathcal{L}_{eff} is independent of scale. This requirement leads to the RG equation for the operator coefficients:

$$\mu \frac{d}{d\mu} C_j^7 + \sum_k C_k^7 \gamma_{kj} = 0 \quad (4.31)$$

where

$$\gamma_{kj} = \sum_{\ell} \left(\mu \frac{d}{d\mu} Z_{k\ell}^{-1} \right) Z_{\ell j} \quad . \quad (4.32)$$

is the anomalous dimension matrix. However, since we are only calculating *one element* of the matrix — corresponding to the mixing of $\mathcal{O}_{\tilde{V}, AE}^{(7)}$ into $\mathcal{O}_{M, AE}^{(7)}$ — we easily find

$$\gamma_{43} = \frac{9\alpha_2 f_A^*}{8\pi} - \frac{3f_A^* \lambda}{8\pi^2} \quad , \quad (4.33)$$

where the “4” labels $\mathcal{O}_{V,AE}^{(7)}$ and “3” labels $\mathcal{O}_{M,AE}^{(7)}$, in the notation of [37], and where the $\alpha_i = g_i^2/(4\pi)$ and λ is the Higgs self-coupling defined by the potential $V(\phi) = \lambda[(\phi^\dagger\phi) - v^2/2]^2$.

Using this result for γ_{43} and the one-loop β functions for α_2 and the lepton Yukawa couplings, we solve the RG equation to determine the operator coefficient $C_M^7(\mu)$ as a function of its values at the scale Λ . As in [17] and [37] we find that the the running of the gauge and Yukawa couplings has a negligible impact on the evolution of $C_M^7(\mu)$. We obtain

$$C_{M,AE}^7(\mu) = -\gamma_{43} C_{V,AE}^7(\Lambda) \ln \frac{\mu}{\Lambda} + \frac{3\alpha_2}{4\pi} \frac{m_A^2 - m_E^2}{v^2} C_{W,AE}^{(7)-}(\Lambda) + \dots, \quad (4.34)$$

where we have included the antisymmetric magnetic moment operator contribution. There is also a contribution from the mass operator self-renormalization; while this has not, to our knowledge, been previously calculated, we do not need its value in this analysis because we are assuming that $C_{M,AE}^7(\Lambda) = 0$, so that δm_ν is generated entirely by radiative corrections involving insertions of $C_{V,AE}^7$. Combining Eq. (4.34) with the contribution to the neutrino mass matrix δm_ν^{AE} given by

$$\delta m_\nu^{AE} \lesssim - \left(\frac{v^4}{2\Lambda^3} \right) C_{M,AE}^7(v), \quad (4.35)$$

we will find the neutrino mass constraints in the next section.

4.4 Neutrino Mass Constraints

Using Eq. (4.8) and Eqs. (4.27) and (4.28), we can calculate the bounds shown in Table 4.2. We will demonstrate this with an example. For the operator $\mathcal{O}_{F(a)}^{e\mu\mu e}$, we have from Eq. (4.8) and Eq. (4.27):

$$m_{\nu L} \lesssim \frac{v^2}{\Lambda} \frac{f}{16\pi^2} C_{F(a)}^{7e\mu\mu e},$$

giving a bound on the C coefficient of the four-fermion operator:

$$|C_{F(a)}^{7e\mu\mu e}| \lesssim \frac{16\pi^2}{\sqrt{2}} \left(\frac{\delta m_\nu}{m} \right) \left(\frac{\Lambda}{v} \right). \quad (4.36)$$

By referring to the entries in Table 4.1 we see that

$$|g_{RL}^S| \lesssim 2\pi^2 \left(\frac{\delta m_\nu}{m_e} \right) \left(\frac{v^2}{\Lambda^2} \right) \quad |g_{RL}^T| \lesssim \pi^2 \left(\frac{\delta m_\nu}{m_e} \right) \left(\frac{v^2}{\Lambda^2} \right) \quad (4.37)$$

where δm_ν are the radiative corrections to m_ν . If we choose $\Lambda/v \approx 1$ and $\delta m_\nu \approx 1\text{eV}$, which we take from tritium β -decay measurements [28], [29], we find the bounds in the first row of Table 4.2. The other bounds are found in a similar manner. It is interesting to note that, due to the factor of v^2/Λ^2 , as the size of Λ increases, the bounds become smaller.

The constraints on the $g_{LR,RL}^V$ that follow from the mixing of the $n = 7$ operator $\mathcal{O}_{M,AE}^{(7)}$ into the mass operator $\mathcal{O}_{M,AE}^{(7)}$ follow straightforwardly from Eqs. (4.34) and (4.35), and Table 4.1. We find

$$g_{LR}^V \lesssim \frac{1}{2} \left(\frac{\delta m_\nu^{\mu\mu}}{m_\mu} \right) \left(\frac{8\pi \sin^2 \theta_W}{9} \right) \left(\alpha - \frac{\lambda \sin^2 \theta_W}{3\pi} \right)^{-1} \left(\ln \frac{v}{\Lambda} \right)^{-1}. \quad (4.38)$$

A similar expression holds for g_{RL}^V but with $m_\mu \rightarrow m_e$ and $\delta m_\nu^{\mu\mu} \rightarrow \delta m_\nu^{ee}$. Compared to the Dirac case, Eq. 4.38 has an additional factor of 1/2; this comes from a combination of the additional Higgs field in the $n = 7$ mass operator, the factor of 1/2 in the Lagrangian for the Majorana neutrino mass, and the value of $\kappa = \frac{1}{2\sqrt{2}}$ in Table 4.1 (instead of $\kappa = 1/2$ in the Dirac case). To derive numerical bounds on the $g_{LR,RL}^V$ from Eq. (3.30) we use the running couplings in the $\overline{\text{MS}}$ scheme $\alpha = \hat{\alpha}(M_Z) \approx 1/127.9$, $\sin^2 \hat{\theta}_W(M_Z) \approx 0.2312$ and the tree-level relation between the Higgs quartic coupling λ , the Higgs mass m_H , and v : $2\lambda = (m_H/v)^2$. We quote two results, corresponding to the direct search lower bound on $m_H \gtrsim 114$ GeV and the one-sided 95 % C.L. upper bound from analysis of precision electroweak measurements, $m_H \lesssim 186$ GeV [30]. We obtain

$$|g_{LR}^V| \lesssim \left(\frac{\delta m_\nu^{\mu\mu}}{1\text{eV}} \right) \left(\ln \frac{\Lambda}{v} \right)^{-1} \begin{cases} 5.9 \times 10^{-7}, & m_H = 114 \text{ GeV} \\ 3.8 \times 10^{-6}, & m_H = 186 \text{ GeV} \end{cases} \quad (4.39)$$

$$|g_{RL}^V| \lesssim \left(\frac{\delta m_\nu^{ee}}{1\text{eV}} \right) \left(\ln \frac{\Lambda}{v} \right)^{-1} \begin{cases} 1.2 \times 10^{-4}, & m_H = 114 \text{ GeV} \\ 8.0 \times 10^{-4}, & m_H = 186 \text{ GeV}. \end{cases}$$

For $\Lambda \sim 1$ TeV, the logarithms are $\mathcal{O}(1)$ so that for $\delta m_\nu \sim 1$ eV, the bounds on the $g_{LR,RL}^V$ derived from $n = 7$ mixing are comparable in magnitude to those estimated from mixing

Table 4.2: Constraints on μ -decay couplings $g_{\alpha\beta}^\gamma$ from the scalar four-fermion operator and the vector operator. The first fourteen rows give naturalness bounds in units of $(v/\Lambda)^2 \times (m_\nu/1 \text{ eV})$ on contributions from $n = 7$ muon decay operators (defined in Section 4.2) based on one-loop matching with the $n = 5$ neutrino mass operators. The third to last row gives upper bounds derived from a recent global analysis of [15], the second to last row gives upper bounds from a recent analysis using Dirac neutrinos [37], and the last row gives estimated bounds from [16] derived from two-loop mixing of $n = 6$ muon decay and neutrino mass operators. A “-” indicates that the operator does not contribute to the given $g_{\alpha\beta}^\gamma$, while “None” indicates that the operator gives a contribution unconstrained by neutrino mass.

Source	$ g_{LR}^S $	$ g_{LR}^T $	$ g_{RL}^S $	$ g_{RL}^T $	$ g_{LR}^V $	$ g_{RL}^V $
$\mathcal{O}_{F(a)}^{7\epsilon\mu\mu e}$	-	-	4×10^{-5}	2×10^{-5}	-	-
$\mathcal{O}_{F(a)}^{7\mu e e \mu}$	2×10^{-7}	8×10^{-8}	-	-	-	-
$\mathcal{O}_{F(a)}^{7\epsilon\mu e \mu}$	-	None	-	-	-	-
$\mathcal{O}_{F(a)}^{7\mu e \mu e}$	-	-	-	None	-	-
$\mathcal{O}_{F(a)}^{7\mu\mu e e}$	-	-	2×10^{-5}	-	-	-
$\mathcal{O}_{F(a)}^{7\epsilon e \mu \mu}$	1×10^{-7}	-	-	-	-	-
$\mathcal{O}_{F(b)}^{7\epsilon\mu\mu e}$	-	-	4×10^{-5}	2×10^{-5}	-	-
$\mathcal{O}_{F(b)}^{7\mu e e \mu}$	2×10^{-7}	8×10^{-8}	-	-	-	-
$\mathcal{O}_{F(b)}^{7\epsilon\mu e \mu}$	2×10^{-7}	8×10^{-8}	-	-	-	-
$\mathcal{O}_{F(b)}^{7\mu e \mu e}$	-	-	4×10^{-5}	2×10^{-5}	-	-
$\mathcal{O}_{F(b)}^{7\mu\mu e e}$	-	-	-	None	-	-
$\mathcal{O}_{F(b)}^{7\epsilon e \mu \mu}$	-	None	-	-	-	-
$\mathcal{O}_{\tilde{V}}^{7\mu\mu}$	-	-	-	-	4×10^{-7}	-
$\mathcal{O}_{\tilde{V}}^{7ee}$	-	-	-	-	-	8×10^{-5}
Global [15]	0.088	0.025	0.417	0.104	0.036	0.104
Dirac [37]	4×10^{-7}	2×10^{-7}	8×10^{-5}	4×10^{-5}	8×10^{-7}	2×10^{-4}
Two-loop [16]	10^{-4}	10^{-4}	10^{-2}	10^{-2}	10^{-4}	10^{-2}

with the $n = 5$ mass operators (see Table 4.2). Due to the difference in numerical factors between Eq. (4.38) and its equivalent in [37], the bounds from operator mixing obtained here are slightly smaller than the bounds from the Dirac case.

4.5 Conclusions

We have used experimental limits on the Majorana neutrino mass to put constraints on the muon decay Michel parameters. Specifically, we have derived model-independent naturalness contributions to the Michel parameters from various dimension seven operators that also contribute to neutrino mass through radiative corrections. The resulting constraints are much smaller than current experimental limits and are approximately the same as the constraints obtained from Dirac neutrinos. They are also a few orders of magnitude better than those obtained in a previous two-loop study [16] using Dirac neutrinos. It is interesting to note that as neutrino mass bounds become tighter with future experiments, our limits on the g coupling constants in muon decay become tighter as well. At the same time, as the TWIST experiment improves its sensitivity to the Michel parameters it will be looking for deviations from our predictions.

After taking the flavor structure of operators contributing to muon decay and neutrino mass into account, we have found that, similar to the Dirac case, there are some four-fermion operators that do not contribute to neutrino mass through radiative corrections. While all of the operators that contribute to the vector coupling constants g^V have neutrino mass naturalness bounds, those contributing to the scalar and tensor coupling constants $g^{S,T}$ do not. It is reasonable to expect the coefficients of the unconstrained operators to be of the same order of magnitude as the constrained coefficients, but without more precise measurements from muon decay experiments we cannot say for certain.

Appendix A

Perturbative Renormalization for Domain-Wall Fermions

A.1 Introduction

Understanding the non-perturbative dynamics that govern the internal structure and interactions of hadrons is a central goal of nuclear physics. Experimentally, substantial efforts are underway using electron scattering and relativistic heavy ion collisions to probe the interactions of quarks and gluons at distance scales and temperatures where non-perturbative dynamics are expected to dominate. Theoretically, a variety of approaches are being pursued to derive insight into these dynamics. Hadronic models have been remarkably successful in accounting for a variety of non-perturbative phenomena while providing important guidance as to the essential elements that drive them. Similarly, effective field theories such as chiral perturbation theory or heavy quark effective theory that incorporate approximate symmetries of Quantum Chromodynamics (QCD) have proven to be powerful tools in systematically correlating a limited number of existing measurements in order to make predictions for as yet unmeasured observables. Each of these approaches, however, requires parameterizing one's ignorance of various aspects of non-perturbative QCD in terms of a set of input parameters that must be taken from experiment. Ideally, one would like to derive these parameters from first principles in QCD. To date, the only viable method for doing so is to put QCD on the lattice.

The implementation of lattice QCD itself entails numerically approximating the full theory in a way that reproduces it in the continuum limit. However, at finite lattice spacing a , various symmetries of continuum QCD — such as Lorentz invariance — are broken. In

order to obtain results that realistically describe the continuum limit, one must understand the effect of these symmetry breakdowns in a systematic way. One of the most important of these is the approximate $SU(3)_L \times SU(3)_R$ chiral symmetry of the QCD Lagrangian associated with the three lightest quarks. It is well known that the widely used Wilson and Kogut-Suskind (KS) lattice actions do not fully reflect this chiral symmetry. The Wilson action breaks the degeneracy of physical quarks and the unphysical doublers by including a chiral symmetry-breaking mass parameter. Consequently, a certain degree of fine-tuning of lattice parameters is needed to compensate for this effect when computing quantities, such as the pion decay constant or nucleon polarizabilities, that are chirally sensitive. The KS action introduces no such mass parameter, but the corresponding spectrum does not contain the full set of Goldstone bosons implied by spontaneously broken $SU(3)_L \times SU(3)_R$ symmetry.

In the past decade or so, the development of lattice actions for quarks satisfying the Ginsparg-Wilson relation has allowed one to implement chiral symmetry on the lattice while removing the problematic doublers and maintaining locality and gauge invariance. For computations aimed at understanding the properties of light quark systems, the state of the art clearly lies in the use of Ginsparg-Wilson quarks. Here, we focus on one variety, namely, domain-wall (DW) quarks introduced by Kaplan [44] and subsequently formulated by Shamir [45]. The DW action places physical quarks and their gauge interactions on the four-dimensional boundaries of a five-dimensional space, where the size of the fifth dimension is N . In the $N \rightarrow \infty$ limit, the chiral symmetry is exact, while for finite N , the effects of chiral symmetry-breaking are exponentially suppressed roughly as $\exp\{-N\}$.

A number of quantities have been computed using DW quarks, and it has been demonstrated that the chiral behavior of various observables is reproduced in the continuum limit (see, e.g. [46]). More generally, the observables one would like to study with DW quarks and compare with experiment involve matrix elements of renormalized operators. The simplest example are matrix elements of twist-two operators that give the lowest moments of structure functions obtained in deep inelastic scattering. These matrix elements depend on the renormalization scale μ in such a way as to compensate for the μ -dependence of the corresponding Wilson coefficients, with the precise definition of each dependent on the choice of renormalization scheme. In most instances, dimensional regularization (DR) with modified minimal subtraction ($\overline{\text{MS}}$) scheme is used in continuum QCD. Since the lattice

regulator differs by construction from DR, the corresponding renormalization scheme is not the same as $(\overline{\text{MS}})$. Consequently, a direct comparison between lattice results and experimental values for matrix elements of renormalized operators is not meaningful. In general, one has

$$\langle h' | \hat{O}_j | h \rangle_{\overline{\text{MS}}} = \sum_k \bar{Z}_{jk}(\mu a) \langle h' | \hat{O}_k | h \rangle_{\text{lat}} \quad (\text{A.1})$$

where, at one-loop order, the matching coefficients $\bar{Z}_{jk}(\mu a)$ contain a logarithmic dependence on μa plus a (μ, a) -independent term that reflects the difference between $(\overline{\text{MS}})$ and lattice renormalization, *viz*

$$\bar{Z}_{jk}(\mu a) = \delta_{jk} + \frac{g^2}{16\pi^2} C_F [(\gamma_{jk} + \gamma_2 \delta_{jk}) \ln(\mu a) + R_{jk}] \quad (\text{A.2})$$

where γ_{jk} is the anomalous dimension matrix, γ_2 arises from wavefunction renormalization, and the R_{jk} contain the scheme-dependent differences¹. The goal of the present study is to compute the \bar{Z}_{jk} for DW fermions for a variety of twist-two operators.

Ideally, one would compute the \bar{Z}_{jk} using non-perturbative methods, but doing so is neither feasible nor desirable in all cases. It is well known, for example, that the breaking of Lorentz invariance by the lattice regulator implies additional operator mixing not present in the continuum. Accounting for this mixing when approaching the continuum limit can be prohibitively expensive when done non-perturbatively (for a more extensive discussion, see, e.g. [51]). Similarly, weak interaction operators, such as those governing the non-leptonic decays of K - and B -mesons, undergo mixing even in the continuum limit. Thus, in both cases, having in hand analytic, perturbative computations for the \bar{Z}_{jk} can be advantageous. For this reason, we present here $\mathcal{O}(\alpha_s)$ perturbative computations of the Z_{jk} for DW fermions.

As a practical matter, perturbative lattice renormalization can also provide for more precise determinations of the \bar{Z}_{jk} than can be obtained at present with non-perturbative methods. The extent to which perturbative, one-loop computations provide a reliable method for obtaining precise values for the \bar{Z}_{jk} depends on knowing that the truncation error associated with higher-order contributions is sufficiently small. So long as the R_{jk} are $\mathcal{O}(1)$, the size of this truncation error is governed by the coupling $g_s(a)$. It has been known for

¹In summing over k in Eq. (A.1) we have allowed for operator mixing that arises both in the continuum limit as well as mixing generated by the breaking of Lorentz invariance on the lattice.

some time, however, that one-loop computations using standard link variables can yield $|R_{jk}| \gg 1$, thereby undermining the convergence properties that undergird the use of perturbation theory. This situation is remedied to some degree by employing “smeared” or “fat” links. The primary motivation for the use of smeared links has been to reduce the impact of short distance fluctuations and exceptional configurations in the computation of various matrix elements. As a by-product, however, carrying out perturbative renormalization with smeared links is equivalent to introducing momentum-space form factors into one-loop computations that suppress large contributions to the R_{jk} . Smeared links have been used in a variety of Wilson and KS perturbative computations, leading to R_{jk} of $\mathcal{O}(1)$. To our knowledge, no computations for DW have been carried out using smeared links. While the paper from which this appendix is excerpted employs smeared links, all of the results presented here will be in terms of unsmeared links.

The primary results of our work are numerical values for the \bar{Z}_{jk} for matrix elements of operators listed in Table A.1. To provide as many cross checks as possible, we also compare our results in various limits with those obtained by Aoki et al. for the quark self energy and bilinears using DW quarks and standard (unsmeared) link variables and [51] for Wilson fermions without smearing. In all cases, we find agreement with existing results. In the case of DW quarks, in the original paper we find that smearing generally reduces the magnitude of the R_{jk} by factors of three or four and, in some cases, substantially more, but that will not be discussed here.

As in the work of [47] and [48], we also find that the magnitude of the wavefunction renormalization constant, Z_q , for physical quarks that live only on the boundaries of the fifth dimension is quite sizeable. As we discuss below, the origin of the large contributions to Z_q is a renormalization of the physical quark field that is distinct from the wavefunction renormalization of the individual DW quark fields living anywhere in the fifth dimension. We isolate this effect by writing $Z_q = Z_2 Z_w$, where Z_2 is the wavefunction renormalization constant for the individual DW quarks and Z_w is the additional renormalization of the physical quark fields. We argue that Z_w is essentially a non-perturbative quantity, and we identify a method for obtaining it from ratios of non-perturbative matrix elements. In contrast, Z_2 and the individual operator renormalization constants Z_{jk} appear to be perturbative. Since the matching coefficients \bar{Z}_{jk} depend on products of the Z_{jk}^{-1} and Z_q , since the latter contain the non-perturbative Z_w contribution, and since the R_{jk} are

observable	H(4)	mixing	\vec{P}	lattice operator
$\langle x \rangle_q^{(a)}$	$\mathbf{6}_3^+$	no	1	$\bar{q}\gamma_{\{1}\vec{D}_4}q$
$\langle x \rangle_q^{(b)}$	$\mathbf{3}_1^+$	no	0	$\bar{q}\gamma_4\vec{D}_4q - \frac{1}{3}(\bar{q}\gamma_1\vec{D}_1q + \bar{q}\gamma_2\vec{D}_2q + \bar{q}\gamma_3\vec{D}_3q)$
$\langle x^2 \rangle_q$	$\mathbf{8}_1^-$	yes	1	$\bar{q}\gamma_{\{1}\vec{D}_1\vec{D}_4}q - \frac{1}{2}\bar{q}(\gamma_{\{2}\vec{D}_2\vec{D}_4} + \gamma_{\{3}\vec{D}_3\vec{D}_4})q$
$\langle x^3 \rangle_q$	$\mathbf{2}_1^+$	no*	1	$\bar{q}\gamma_{\{1}\vec{D}_1\vec{D}_4\vec{D}_4}q + \bar{q}\gamma_{\{2}\vec{D}_2\vec{D}_3\vec{D}_3}q - (3 \leftrightarrow 4)$
$\langle 1 \rangle_{\Delta q}$	$\mathbf{4}_4^+$	no	0	$\bar{q}\gamma^5\gamma_3q$
$\langle x \rangle_{\Delta q}^{(a)}$	$\mathbf{6}_3^-$	no	1	$\bar{q}\gamma^5\gamma_{\{1}\vec{D}_3}q$
$\langle x \rangle_{\Delta q}^{(b)}$	$\mathbf{6}_3^-$	no	0	$\bar{q}\gamma^5\gamma_{\{3}\vec{D}_4}q$
$\langle x^2 \rangle_{\Delta q}$	$\mathbf{4}_2^+$	no	1	$\bar{q}\gamma^5\gamma_{\{1}\vec{D}_3\vec{D}_4}q$
$\langle 1 \rangle_{\delta q}$	$\mathbf{6}_1^+$	no	0	$\bar{q}\gamma^5\sigma_{34}q$
$\langle x \rangle_{\delta q}$	$\mathbf{8}_1^-$	no	1	$\bar{q}\gamma^5\sigma_{3\{4}\vec{D}_1}q$
d_1	$\mathbf{6}_1^+$	no**	0	$\bar{q}\gamma^5\gamma_{[3}\vec{D}_4]q$
d_2	$\mathbf{8}_1^-$	no**	1	$\bar{q}\gamma^5\gamma_{[1}\vec{D}_{\{3}\vec{D}_4}q$

Table A.1: Operators used to measure moments of quark distributions. Different lattice operators corresponding to the same continuum operator are denoted by superscripts *a* and *b*. Subscripts of irreducible representations of $H(4)$ distinguish different representations of the same dimensionality and superscripts denote charge conjugation C . In the operator mixing column, *no** indicates a case in which mixing generically could exist but vanishes perturbatively for Wilson or overlap fermions, and *no*** indicates perturbative mixing with lower dimension operators for Wilson fermions but no mixing for overlap fermions. The entry in column \vec{P} denotes the number of spatial components of the nucleon momentum, \vec{P} , that must be chosen non-zero. Operators requiring one non-zero component have been written for \vec{P} in the 1-direction and \vec{S} in the 3-direction.

meaningful only in the context of one-loop perturbation theory, we quote results for the \bar{Z}_{jk} rather than for the R_{jk} .

A secondary aim of this chapter is to provide a brief, pedagogical introduction to perturbative renormalization with DW quarks for readers who may be unfamiliar with the subject. An extensive review of perturbative renormalization that focuses largely on Wilson fermions and unsmearred links can be found in [51], and the present work should be read in tandem with that paper. Here, we discuss in some detail elements of perturbative renormalization that are unique to DW quarks, and include a few detailed examples for illustration. We also provide rather general expressions that may be used by others in constructing codes to carry out perturbative renormalization.

Our presentation of these points is organized as follows: In Section A.2, we review the DW action and discuss the structure of the various tree-level quark propagators needed for

the one-loop computations. In Section A.3, we give an extensive discussion of perturbative renormalization, including the issues involving Z_q mentioned above, the treatment of infrared singularities, and detailed computations of quark self-energies and bilinear operators $\bar{q}\Gamma q$. This section contains most of the formalism needed to understand the subsequent discussion of twist-two operators. Because the notation and definitions employed in the lattice community differ in some cases from the standard field theory notation, we also provide a translation guide for converting from one to the other. Section A.4 contains the computation of the \bar{Z}_{jk} for the twist-two operators listed in Table A.1, and in Section A.5 we give a summary. Additional formal, pedagogical, and computational details are contained in a following appendix².

A.2 Domain-Wall Action and Propagators

Domain-wall fermions live in five spacetime dimensions and possess gauge interactions in the four-dimensional subspace that corresponds to ordinary spacetime. The fifth dimension is taken to be of finite size, with physical quark fields corresponding to linear combinations of the fields that live on the boundaries of the fifth dimension. For pedagogical purposes, however, it is useful to first consider the fifth dimension to be of infinite size. One may decompose the 5D Lagrangian into the usual 4D Wilson Lagrangian, \mathcal{L}_4 , plus a component that couples fields in the fifth dimension, \mathcal{L}_5 [45]. One has, then³,

$$\begin{aligned} \mathcal{L}_4 = & -\frac{1}{2a} \sum_{x,s,\mu} \left[\bar{\psi}_s(x)(r - \gamma_\mu)U_\mu(x)\psi_s(x + a\hat{\mu}) + \bar{\psi}_s(x + a\hat{\mu})(r + \gamma_\mu)U_\mu^\dagger(x)\psi_s(x) \right] \\ & + \sum_{x,s} \bar{\psi}_s(x) \left(M + \frac{rd}{a} \right) \psi_s(x), \end{aligned} \quad (\text{A.3})$$

where x and s denote the usual spacetime co-ordinates and those for the fifth dimension, respectively, and μ indicates any one of the directions in the ordinary $d = 4$ spacetime dimensions, and the gauge link is defined

$$U_\mu(x) = e^{iag_0 A_\mu(x+a\hat{\mu}/2)}. \quad (\text{A.4})$$

²The work in Appendices A and B was done in collaboration with Bojan Bistrotić.

³When comparing formulas, one has to take into account that different authors use different sign-conventions for the r term

The other notation in Eq. (A.3) corresponds to that of the standard Wilson Lagrangian: M is the 5D mass parameter, and the terms containing r break the degeneracy of doublers in the $M \rightarrow 0$ limit. Although one may allow r to take on any value in the range $-1 \leq r < 0$, we will take $r = -1$ in order to avoid the presence of additional time doublers that disappear in the continuum limit. Note that the link fields $U_\mu(x)$ are independent of s .

The Lagrangian \mathcal{L}_5 couples fermions at different values of s without involving the gauge degrees of freedom:

$$\mathcal{L}_5 = \frac{-1}{2a_5} \sum_{x,s} [\bar{\psi}_s(x)(r_5 - \gamma_5)\psi_{s+1}(x) + \bar{\psi}_s(x)(r_5 + \gamma_5)\psi_{s-1}(x)] + \sum_{x,s} \bar{\psi}_s(x) \frac{r_5}{a_5} \psi_s(x), \quad (\text{A.5})$$

where we have allowed for the spacing a_5 , and the discretized second derivative (proportional to r_5/a_5) in the fifth dimension to differ from the corresponding quantities in the other four dimensions. Note that since \mathcal{L}_5 involves no gauge couplings, one may think of the coordinates s as labeling an internal degree of freedom, or “flavor,” for the fermion fields. The total Lagrangian $\mathcal{L} = \mathcal{L}_4 + \mathcal{L}_5$ then corresponds to an infinite tower of ordinary 4D Wilson Lagrangians for fermions labeled by s with “nearest flavor” couplings given by \mathcal{L}_5 .

For the purpose of carrying out renormalization, it is most convenient to work in momentum space. The DW action is

$$S_{DW} = a^d \sum_x \mathcal{L}_{DW} = \int_{-\pi/a}^{\pi/a} \frac{d^d p}{(2\pi)^d} \sum_{s,s'} \bar{\psi}_s(p) D_{s,s'}^0(p) \psi_{s'}(p), \quad (\text{A.6})$$

with

$$D_{s,s'}^0(p) = \left[i\bar{p} \cdot \gamma - \frac{a}{2} \hat{p}^2 + \left(\frac{r_5}{a_5} + M \right) \right] \delta_{s,s'} - \frac{r_5 - \gamma_5}{2a_5} \delta_{s+1,s'} - \frac{r_5 + \gamma_5}{2a_5} \delta_{s-1,s'}. \quad (\text{A.7})$$

Throughout the chapter we will use the notation

$$\hat{p}_\mu \equiv \frac{2}{a} \sin \frac{ap_\mu}{2}, \quad \bar{p}_\mu \equiv \frac{1}{a} \sin ap_\mu, \quad \tilde{p}_\mu \equiv \cos \frac{ap_\mu}{2}, \quad (\text{A.8})$$

so that

$$\hat{p}^2 \equiv \sum_\mu \left(\frac{\sin ap_\mu/2}{a/2} \right)^2, \quad \bar{p}^2 \equiv \sum_\mu \left(\frac{\sin ap_\mu}{a} \right)^2, \quad \tilde{p}^2 \equiv \sum_\mu \left(\cos \frac{ap_\mu}{2} \right)^2. \quad (\text{A.9})$$

Since we will not take a continuum limit in the fifth dimension, we are not concerned with the implications of the choice of r_5 for the approach to the continuum theory. In this case, it is convenient to choose $r_5 = -1$ in order to obtain chirality projection operators in $D_{s,s'}^0(p)$:

$$D_{s,s'}^0(p) = [i\bar{p} \cdot \gamma - W(p)] \delta_{s,s'} + \frac{1}{a_5} (P_+ \delta_{s+1,s'} + P_- \delta_{s-1,s'}) \quad (\text{A.10})$$

$$W(p) = \left(\frac{1}{a_5} - M \right) + \frac{a}{2} \hat{p}^2. \quad (\text{A.11})$$

The propagator for the semi-infinite and finite dimensions will be determined by restricting the range of s, s' in $D_{s,s'}^0(p)$.

The DW propagator is obtained by inverting the Dirac operator $D_{s,s'}^0(p)$. A detailed discussion of the procedure for doing so is given in Appendix B. In practice, we work with a fifth dimension of finite extent ($s = 1, \dots, N$) and quarks having non-zero mass, m . As discussed below, physical quarks are defined as linear combinations of the quarks living at $s = 1$ and $s = N$, we add a mass term only on the boundaries of the Dirac operator. The resulting form is

$$\hat{D}_{s,s'}(m) = \theta(s-1)\theta(s'-1)\theta(N-s)\theta(N-s')D_{s,s'}^0 + mP_- \delta_{s,1}\delta_{s',N} + mP_+ \delta_{s,N}\delta_{s',1}. \quad (\text{A.12})$$

The propagator for the 5D quarks is just the inverse of \hat{D} and is given by (see Appendix B)

$$\hat{S}_{ss'}(p) = -i\bar{p} \cdot \gamma \left(\hat{G}_{ss'}^+ P_+ + \hat{G}_{ss'}^- P_- \right) + S_{ss'}^+ P_+ + S_{ss'}^- P_-, \quad (\text{A.13})$$

where

$$S_{ss'}^+ = \sum_t \left(-W\delta_{s,t} + \frac{1}{a_5}\delta_{s,t+1} + m\delta_{s,1}\delta_{t,N} \right) \hat{G}_{ts'}^+ \quad (\text{A.14})$$

$$S_{ss'}^- = \sum_t \left(-W\delta_{s,t} + \frac{1}{a_5}\delta_{s,t-1} + m\delta_{s,N}\delta_{t,1} \right) \hat{G}_{ts'}^-. \quad (\text{A.15})$$

with

$$\hat{G}_{s,s'}^\pm = A^0 e^{-\alpha|s-s'|} + \hat{A}_\pm e^{-\alpha(s+s'-2)} + \hat{A}_\mp e^{-\alpha(2N-s-s')} + \hat{A}_m \left(e^{-\alpha(N-s+s')} + e^{-\alpha(N+s-s')} \right), \quad (\text{A.16})$$

where formulas for coefficients A_0 , \hat{A}_\pm , and \hat{A}_m are given in Appendix B.

A.2.1 Physical quarks

The computation of hadronic matrix elements on the lattice requires the construction of sources that contain quark interpolating fields. From the standpoint of chiral symmetry, one uses interpolating fields whose $m_q \rightarrow 0$ properties are chosen to reflect most closely those of the physical quarks of QCD. One advantage of DW quarks is that in the $N \rightarrow \infty$ limit, mass renormalization is multiplicative. Indeed, as shown in [47], the existence of a massless mode χ_0

$$\chi = \sqrt{1 - w_0^2} \left(P_+ w_0^{s-1} \psi_s(x) + P_- w_0^{N-s} \psi_s(x) \right) \quad (\text{A.17})$$

is stable under one-loop renormalization. In principle, one would like to construct hadronic sources and operators from the χ_0 fields, but due to the non-local structure of that field it is more practical to build interpolating fields from linear combinations of the fields on the boundaries, ψ_1 and ψ_N . Denoting the interpolating, or ‘‘physical,’’ quark field as $q(x)$ one has

$$q(x) = P_+ \psi_1(x) + P_- \psi_N(x), \quad \bar{q}(x) = \bar{\psi}_1(x) P_- + \bar{\psi}_N(x) P_+. \quad (\text{A.18})$$

As discussed below, it is necessary to know the DW propagators involving the physical quark fields as well as those arising from one physical and one of the $\psi_s(x)$ fields. To that end, we define the following propagators:

$$S_{qs}(x, y) = \langle q(x) \bar{\psi}_s(y) \rangle \quad (\text{A.19})$$

$$S_{sq}(x, y) = \langle \psi_s(x) \bar{q}(y) \rangle \quad (\text{A.20})$$

$$S_{qq}(x, y) = \langle q(x) \bar{q}(y) \rangle. \quad (\text{A.21})$$

Using our previous expressions for $\hat{S}_{st}(k)$ we obtain the following explicit expressions for these propagators:

$$\hat{S}_{qs}(k) = -i\bar{k} \cdot \gamma [g_+(s, k) P_+ + g_-(s, k) P_-] + \sigma_+(s, k) P_+ + \sigma_-(s, k) P_- \quad (\text{A.22})$$

$$\hat{S}_{sq}(k) = [g_+(s, k) P_+ + g_-(s, k) P_-] (-i\bar{k} \cdot \gamma) + \sigma_+(s, k) P_+ + \sigma_-(s, k) P_- \quad (\text{A.23})$$

$$\hat{S}_{qq}(k) = \frac{i\bar{k} \cdot \gamma - m(1 - |b| a_5 e^{-\alpha})}{f_N(m)} \quad (\text{A.24})$$

where

$$g_+(s, k) = - \left[\frac{e^{-\alpha(N-s)} + ma_5 e^{-\alpha} e^{-\alpha(s-1)}}{f_N(m)} \right] \quad (\text{A.25})$$

$$g_-(s, k) = - \left[\frac{e^{-\alpha(s-1)} + ma_5 e^{-\alpha} e^{-\alpha(N-s)}}{f_N(m)} \right] \quad (\text{A.26})$$

$$\sigma_+ = m (1 - Wa_5 e^{-\alpha}) g_+ - a_5 e^{-\alpha} e^{-\alpha(s-1)} \quad (\text{A.27})$$

$$\sigma_+ = m (1 - Wa_5 e^{-\alpha}) g_- - a_5 e^{-\alpha} e^{-\alpha(N-s)} \quad (\text{A.28})$$

$$f_N(m) = \frac{1}{a_5^2} (1 - |b| a_5 e^\alpha) - m^2 (1 - |b| a_5 e^{-\alpha}) . \quad (\text{A.29})$$

A.3 Renormalization

Deriving the matching coefficients $\tilde{Z}_{jk}(\mu, a)$ requires that one carefully delineate the contributions from both quark field renormalization and proper vertices involving operator insertions. In doing so, it is useful begin with the standard reduction formulae for operator matrix elements. Since we work at momentum scales $p \sim 1/a$ that are well above the confinement scale, we may consider matrix elements between initial and final states containing free quarks of well-defined momenta. To illustrate, consider matrix elements of the quark bilinear, given at tree-level by

$$\hat{O}_j(x) = \bar{q}(x) \Gamma_j q(x) . \quad (\text{A.30})$$

After renormalization, one replaces the fields $q(x)$ by the bare fields $q_0(x)$:

$$q_0(x) = \sqrt{\tilde{Z}_q} q(x) \quad (\text{A.31})$$

where \tilde{Z}_q is the regulator-dependent wavefunction renormalization constant defined in a particular renormalization scheme. Any additional ultraviolet divergences in the operator matrix elements that are not removed by the wavefunction renormalization (A.31) are eliminated by operator renormalization:

$$\hat{O}_{Rj}(x) = \sum_k \tilde{Z}_{jk}^{-1} \hat{O}_{0k}(x) = \sum_k \tilde{Z}_{jk}^{-1} \tilde{Z}_q^{N_q/2} \hat{O}_j(x) , \quad (\text{A.32})$$

where $\hat{O}_{Rj}(x)$ is the renormalized bilinear, $\hat{O}_{0k}(x) = \bar{q}_0(x) \Gamma_j q_0(x)$ is the bare operator, and $N_q = 2$ is the number of quark fields appearing in $O_j(x)$.

The finite matrix elements of $\hat{O}_{Rj}(x)$ are then given by the reduction formula in terms of amputated, one-particle irreducible matrix elements:

$$\begin{aligned} \langle k | \hat{O}_j^R(x) | p \rangle &= \text{disc} + \left(\frac{-i}{\sqrt{Z_q}} \right)^2 \int d^4 y \int d^4 z e^{i(k \cdot z - p \cdot y)} \bar{u}(k) \vec{D}_z \\ &\times \langle 0 | T \left[q(z) \hat{O}_j^R(x) \bar{q}(y) e^{iS_{\text{int}}} \right] | 0 \rangle \overleftarrow{D}_y^\dagger u(k) \end{aligned} \quad (\text{A.33})$$

where the ‘‘disc’’ denotes contributions from disconnected diagrams, and where we have gone to the interaction representation, with $S_{\text{int}} = \int d^4 x \mathcal{L}_{\text{int}}$. The operators \vec{D}_z are just the Dirac operators (either continuum or lattice) and Z_q is the finite wavefunction renormalization constant for the quark field $q(x)$. In the $\overline{\text{MS}}$ scheme, the Z_q gives the residue of the pole of the renormalized quark propagator. In the case of lattice regularization, Z_q may differ from unity even at tree-level. From Eq. (A.17) we observe that for the physical quark fields defined in Eq. (A.18), one has

$$(Z_q)_{\text{lat, tree}} = 1 - w_0^2. \quad (\text{A.34})$$

It is useful to express Eq. (A.30) in terms of the propagators \hat{S}_{ts} , \hat{S}_{qs} , etc., and the proper vertices Λ_{ts}^j that contain insertions of the unrenormalized operators $\hat{O}_j(x)$. Transforming to momentum space leads to

$$\begin{aligned} \int d^4 x e^{iq \cdot x} \langle k | \hat{O}_{Rj}(x) | p \rangle &= (2\pi)^4 \delta(p - q - k) \left(\frac{1}{\sqrt{Z_q}} \right)^2 \sum_k Z_{jk}^{-1} \\ &\times \left[\hat{S}_{qq}(k)^{-1} \right]^{\text{tree}} \hat{S}_{qs}(k) \Lambda_{st}^j(k, p) \hat{S}_{tq}(p) \left[\hat{S}_{qq}(p)^{-1} \right]^{\text{tree, } \dagger}, \end{aligned} \quad (\text{A.35})$$

where we have replaced \vec{D}_z and $\overleftarrow{D}_y^\dagger$ in momentum space by $[\hat{S}_{qq}(k)^{-1}]^{\text{tree}}$ and $[\hat{S}_{qq}(p)^{-1}]^{\text{tree, } \dagger}$, respectively. At tree-level, $\Lambda_{st}^j(k, p) \rightarrow \Lambda_{qq}^j(k, p)$ since $\hat{O}_j(x)$ contains only physical quark fields, and $Z_{jk}^{-1} \rightarrow \delta_{jk}$. Similarly, $Z_q = 1$ ($\overline{\text{MS}}$) or $1 - w_0^2$ (DW quarks) and the inverse propagators simply amputate the renormalized, external propagators $\hat{S}_{qq}(k)$ and $\hat{S}_{qq}(x, y)$ that arise from contractions of the $\bar{q}(z)$ and $q(y)$ with the fields appearing in $\hat{O}_j(x)$.

At one-loop order, several effects must be taken into account. First, one must account for renormalization of the propagators \hat{S}_{qs} and \hat{S}_{tq} arising from external leg corrections. Since $\hat{O}_j(x)$ contains only the physical quark fields $q(x)$, one need consider only the external

leg corrections to \hat{S}_{qq} to this order. Second, one must include operator renormalization generated by vertex corrections. The latter give rise to non-vanishing Λ_{st}^k , Λ_{sq}^k , and Λ_{qs}^k since the internal lines can contain any one of the propagators \hat{S}_{qt} , \hat{S}_{sq} , or \hat{S}_{qq} . In this case, one may use the tree-level external propagators \hat{S}_{qs} appearing in Eq. (A.35). Finally, the one-loop expression for the residue Z_q in Eq. (A.35) must be used.

Once this renormalization has been carried out, Eq. (A.32) can be used to convert matrix elements computed on the lattice to the matrix elements of renormalized operators in the continuum in the $\overline{\text{MS}}$ scheme. To do so, we observe that the matrix element of \hat{O}_{Rj} between quark states, $\langle q | \hat{O}_{Rj} | q \rangle$ in any scheme is given by

$$\langle q | \hat{O}_{Rj} | q \rangle = \sum_k Z_{jk}^{-1} Z_q^{N_q/2} \langle q | \hat{O}_k | q \rangle_{\text{tree}} , \quad (\text{A.36})$$

where the Z_{jk} and Z_q without the tilde denote the finite parts of the one-loop matrix elements after the divergences have been removed by renormalization. Moreover, the tree-level matrix elements (in the continuum limit) are identical for all schemes. Thus, we have in the continuum limit

$$\begin{aligned} \langle q | \hat{O}_{Rj} | q \rangle_{\overline{\text{MS}}} &= \sum_{\ell} \left(Z_{j\ell}^{-1} \right)_{\overline{\text{MS}}} \left(Z_q^{N_q/2} \right)_{\overline{\text{MS}}} \langle q | \hat{O}_{\ell} | q \rangle_{\text{tree}} \\ &= \sum_{\ell} \left(Z_{j\ell}^{-1} \right)_{\overline{\text{MS}}} \left(Z_q^{N_q/2} \right)_{\overline{\text{MS}}} \sum_{\ell} (Z_{\ell k})_{\text{lat}} \left(Z_q^{-N_q/2} \right)_{\text{lat}} \langle q | \hat{O}_{Rk} | q \rangle_{\text{lat}} , \end{aligned} \quad (\text{A.37})$$

so that the matching coefficients \bar{Z}_{jk} of Eq. (A.1) are given by

$$\bar{Z}_{jk} = \sum_{\ell} \left(Z_{j\ell}^{-1} \right)_{\overline{\text{MS}}} (Z_{\ell k})_{\text{lat}} \left(Z_q^{N_q/2} \right)_{\overline{\text{MS}}} \left(Z_q^{-N_q/2} \right)_{\text{lat}} . \quad (\text{A.38})$$

The interpretation of Eq. (A.38) is clear. To obtain the renormalized matrix elements in $\overline{\text{MS}}$ from those computed on the lattice, one must divide out the finite artifacts of lattice regularization that contribute to wavefunction renormalization [the $(Z_q^{-N_q/2})_{\text{lat}}$ factor] and operator renormalization [the $(Z_{\ell k})_{\text{lat}}$ factor]. For operators and operator mixing involving different numbers of quark and/or gluon fields, Eq. (A.38) can be generalized in a straightforward way. Note that for the physical quarks of Eq. (A.18), the tree-level matching coefficients $Z_{jk} = \delta_{jk} (1 - w_0^2)^{-N_q/2}$.

The notation used in the foregoing discussion is the standard employed in most textbook

treatments of renormalization. Indeed, the anomalous dimension matrix γ_{jk} is given in terms of the logarithmic derivatives of the Z_{jk}^{-1} :

$$\gamma_{jk} = \sum_{\ell} \left(\mu \frac{d}{d\mu} Z_{j\ell}^{-1} \right) Z_{\ell k}. \quad (\text{A.39})$$

The operator renormalization constants used in the lattice literature, however, are defined with a slightly different notation. In [47] and [48], for example, the matching constant \bar{Z}_{Γ} for quark bilinears $\bar{q}\Gamma q$ is given by

$$\bar{Z}_{\Gamma} = (1 - w_0^2)^{-1} Z_w^{-1} Z_{\Gamma}(\mu a), \quad (\text{A.40})$$

where the $(1 - w_0^2)^{-1} Z_w^{-1}$ arises from the $(Z_q^{-N_q/2})_{\text{lat}}$ factor in Eq. (A.38) with $N_q = 2$, and where $Z_{\Gamma}(\mu a)$ contains the Z_2^{-1} from 5D DW quark wavefunction renormalization and the $(Z_{\Gamma}^{-1})_{\overline{\text{MS}}}(Z_{\Gamma})_{\text{lat}}(Z_q)_{\overline{\text{MS}}}$ factors⁴.

The extraction of the one-loop $(Z_q)_{\text{lat}}$ factors in lattice perturbation theory involves special considerations that we discuss before treating specific examples. First, we note from Eq. (A.35) that we require the products

$$\left[\hat{S}_{qq}(k)^{-1} \right]^{\text{tree}} \hat{S}_{qs}(k)^{\text{tree}} \quad \text{and} \quad \hat{S}_{tq}(p)^{\text{tree}} \left[\hat{S}_{qq}(p)^{-1} \right]^{\text{tree}, \dagger} \quad (\text{A.41})$$

that occur in tandem with the one-loop vertex corrections and

$$\left[\hat{S}_{qq}(k)^{-1} \right]^{\text{tree}} \hat{S}_{qq}(k) \quad \text{and} \quad \hat{S}_{qq}(p) \left[\hat{S}_{qq}(p)^{-1} \right]^{\text{tree}, \dagger} \quad (\text{A.42})$$

associated with the external leg corrections to the physical quark propagators. For future reference, it is useful to work out explicit expressions for the former:

$$\begin{aligned} \bar{S}_s^{OUT}(p) &= \left[\hat{S}_{qq}(p)^{-1} \right]^{\text{tree}} \hat{S}_{qs}(p)^{\text{tree}} \\ &= -i\bar{p} \cdot \gamma (\bar{g}_+ P_+ + \bar{g}_- P_-) + \bar{\sigma}_+ P_+ + \bar{\sigma}_- P_- \end{aligned} \quad (\text{A.43})$$

$$\begin{aligned} \bar{S}_s^{IN}(p) &= \hat{S}_{qq}(p) \left[\hat{S}_{qq}(p)^{-1} \right]^{\text{tree}, \dagger} \\ &= (\bar{g}_- P_+ + \bar{g}_+ P_-) (-i\bar{p} \cdot \gamma) + \bar{\sigma}_- P_+ + \bar{\sigma}_+ P_- \end{aligned} \quad (\text{A.44})$$

⁴The quark bilinears introduce no operator mixing, so the sum over operator labels does not appear.

with

$$\bar{g}_+(p) = \frac{a_5 e^{-\alpha} f_N(m)}{\bar{p}^2 + m^2 (1 - |b(p)| a_5 e^{-\alpha(p)})^2} e^{-\alpha(s-1)} \quad (\text{A.45})$$

$$\bar{g}_-(p) = \frac{a_5 e^{-\alpha} f_N(m)}{\bar{p}^2 + m^2 (1 - |b(p)| a_5 e^{-\alpha(p)})^2} e^{-\alpha(N-s)} \quad (\text{A.46})$$

$$\bar{\sigma}_+(p) = m(1 - W a_5 e^{-\alpha}) \bar{g}_+ + m a_5 e^{-\alpha} e^{-\alpha(s-1)} + e^{-\alpha(N-s)} \quad (\text{A.47})$$

$$\bar{\sigma}_-(p) = m(1 - W a_5 e^{-\alpha}) \bar{g}_- + m a_5 e^{-\alpha} e^{-\alpha(N-s)} + e^{-\alpha(s-1)}. \quad (\text{A.48})$$

In practice we will need $p \rightarrow 0$ expansions of formulas for \bar{g}_\pm and $\bar{\sigma}_\pm$

$$\bar{g}_+(0) = \mathcal{A} w_0^{s-1}, \quad \bar{g}_-(0) = \mathcal{A} w_0^{N-s}, \quad \bar{\sigma}_+(0) = w_0^{N-s}, \quad \bar{\sigma}_-(0) = w_0^{s-1}, \quad (\text{A.49})$$

with $\mathcal{A} = \frac{a_5 w_0}{1 - w_0^2}$.

The products $[\hat{S}_{qq}(k)^{-1}]^{\text{tree}} \hat{S}_{qq}(k)$ and $\hat{S}_{qq}(p) [\hat{S}_{qq}(p)^{-1}]^{\text{tree}, \dagger}$ are each equal to the residue⁵ Z_q . As we discuss in detail below, Z_q receives two contributions that may be seen by considering the one-loop renormalized \hat{S}_{qq} :

$$\hat{S}_{qq}(p) = \hat{S}_{qq}(p)^{\text{tree}} + \sum_{s,t} \hat{S}_{qs}(p)^{\text{tree}} \Sigma_{st}(p) \hat{S}_{tq}(p)^{\text{tree}}, \quad (\text{A.50})$$

where $\Sigma_{st}(p)$ defines the one-loop self energy matrix:

$$\Sigma_{st}(p) = i A_{st} p \cdot \gamma + B_{st}. \quad (\text{A.51})$$

In the continuum limit, we have

$$\hat{S}_{qq}(p) \rightarrow \frac{1 - w_0^2}{ip \cdot \gamma (1 + A) + m(1 - w_0^2)(1 + B)}, \quad (\text{A.52})$$

where A and B indicate the finite, one-loop contributions, m is the quark mass parameter appearing in the lattice action, and $Z_q = (1 - w_0^2)(1 + A)^{-1}$. The second term in Eq. (A.50) contributes to A in two ways: (a) via the A_{st} component of $\Sigma_{st}(p)$ that corresponds to wavefunction renormalization of the 5D quarks and (b) through the B_{st} component in combination with the $ip \cdot \gamma$ appearing in $\hat{S}_{qs}^{\text{tree}}$ and $\hat{S}_{tq}^{\text{tree}}$ in the second term of Eq. (A.50).

⁵In the following discussion, we drop the “lat” subscript for simplicity, except where it is needed to distinguish the lattice and $\overline{\text{MS}}$ cases.

Denoting the contribution of type (a) as Z_2 and that of type (b) as Z_w we have

$$Z_q = Z_2 Z_w (1 - w_0^2) . \quad (\text{A.53})$$

Physically, the effect of Z_w corresponds to a change in the normalization of the physical quark fields defined in Eq. (A.18) that is distinct from the renormalization of the ψ_1 and ψ_N components. As we discuss below, the magnitude of the one-loop contribution to $Z_2 - 1$ is roughly $\mathcal{O}(\alpha_s/4\pi)$, as one would expect, whereas the magnitude of $Z_w - 1$ is considerably larger. The presence of anomalously large one-loop contributions is obviously troubling from the standpoint of the perturbative expansion. In order to remedy this difficulty, we identify below a method to obtain Z_w non-perturbatively by taking appropriate ratios of axial current matrix elements. We also discuss an *ansatz* for resumming the large one-loop contributions to Z_w that produces good agreement with the non-perturbative value.

Before proceeding with the detailed discussion of one-loop computations, we modify our earlier definition of the physical quark fields $q(x)$ to absorb the $1 - w_0^2$ factor appearing in Z_q . In what follows, we take

$$q(x) = \frac{1}{\sqrt{1 - w_0^2}} [P_+ \psi_1(x) + P_- \psi_N(x)] , \quad \bar{q}(x) = \frac{1}{\sqrt{1 - w_0^2}} [\bar{\psi}_1(x) P_- + \bar{\psi}_N(x) P_+] . \quad (\text{A.54})$$

The corresponding mass parameter in the action becomes

$$\tilde{m} = (1 - w_0^2)m . \quad (\text{A.55})$$

Note that with the definition in Eq. (A.54) one has $Z_q = 1$ at tree level.

A.3.1 Wavefunction renormalization

It is instructive to discuss in detail the computation of the wavefunction renormalization constant Z_q in order to highlight several features of the DW renormalization program: (a) the general procedure for computing one-loop amplitudes; (b) the treatment of *bona fide* infrared singularities as well as numerical divergences that arise in computing IR-finite graphs in the vicinity of zero loop momentum; and (c) the non-perturbative extraction of Z_w . In doing so, it is also instructive to identify three classes of contributions: those that contribute to Z_2 , those giving Z_w , and those that renormalize the mass parameter \tilde{m} .

Letting

$$\Sigma_q(p) = \left[\hat{S}_{qq}(p)^{-1} \right]^{\text{tree}} \hat{S}_{qq}(p) \left[\hat{S}_{qq}(p)^{-1} \right]^{\text{tree}, \dagger} - (ip \cdot \gamma + \tilde{m}), \quad (\text{A.56})$$

we may write $\Sigma_q(p)$ as

$$\Sigma_q(p) = \frac{g_0^2 C_F}{16\pi^2} \left[ip \cdot \gamma \left(\tilde{\Sigma}_2 - \mathcal{A} \tilde{\Sigma}_w \right) + \tilde{m} \tilde{\Sigma}_m \right], \quad (\text{A.57})$$

where C_F is the quadratic Casimir for $\text{SU}(3)$; $\tilde{\Sigma}_2$, $\tilde{\Sigma}_w$, and $\tilde{\Sigma}_m$ give the one-loop contributions to Z_2 , Z_w , and \tilde{m} renormalization, respectively; and

$$\mathcal{A} = \frac{a_5 w_0}{1 - w_0^2}. \quad (\text{A.58})$$

Because of the chiral symmetry of the DW action, the mass parameter \tilde{m} is multiplicatively renormalized. Thus, it is convenient to introduce the mass renormalization constant Z_m defined by

$$\tilde{m} + \delta\tilde{m} \equiv Z_w Z_m^{-1} \tilde{m}, \quad (\text{A.59})$$

where $\delta\tilde{m}$ indicates the momentum-independent part of $\Sigma_q(p)$.

The diagrams that contribute to $\Sigma_q(p)$ are shown in Figs. A.1 and A.2. We discuss the computation of each in turn.

A.3.1.1 Sunset diagram

The amplitude $\Sigma_{s,t}$ (see Eq. (A.50)) for the sunset diagram is given by

$$\Sigma_{st}(a, p) = \int_{-\pi/a}^{\pi/a} \frac{d^d k}{(2\pi)^d} \sum_{\lambda, \rho} G_{\lambda\rho}(p - k) V_\rho(k, p) [S_F(k)]_{st} V_\lambda(p, k). \quad (\text{A.60})$$

After rescaling the loop momentum $k_\mu \rightarrow k_\mu/a$, we have

$$\begin{aligned}
\Sigma_{st}(a, p) &= \int_{-\pi}^{\pi} \frac{d^d k}{(2\pi)^d} \sum_{\lambda, \rho} G_{\lambda\rho}(ap - k) V_\rho(k, ap) S_F(k) V_\lambda(ap, k) \\
&= g_0^2 C_F \int_{-\pi}^{\pi} \frac{d^d k}{(2\pi)^d} \frac{1}{a^4} \sum_{\mu} \left[\frac{a^2 g_{\rho\sigma}}{(\widehat{ap - k})^2} \right] \left[\frac{r}{2} (\widehat{ap + k})_\rho + i\gamma_\rho (\widetilde{ap + k})_\rho \right] \\
&\quad \times a [(-i\gamma \cdot \bar{k}(G_+ P_+ + G_- P_-) + S_+ P_+ + S_- P_-)] \\
&\quad \times \left[\frac{r}{2} (\widehat{ap + k})_\sigma + i\gamma_\sigma (\widetilde{ap + k})_\sigma \right] \\
&\equiv g_0^2 C_F \int_{-\pi}^{\pi} \frac{d^d k}{(2\pi)^d} I_{st}(ap, k)
\end{aligned} \tag{A.61}$$

where we have suppressed 5D indices on G_\pm and S_\pm for simplicity. After performing the γ -matrix algebra we separate the integrand into terms having odd or even numbers of γ matrices

$$\Sigma_{st}(ap) = g_0^2 C_F \int_{-\pi/a}^{\pi/a} \frac{d^d k}{(2\pi)^d} ([I_{odd}^+]_{st} P_+ + [I_{odd}^-]_{st} P_- + [I_{even}^+]_{st} P_+ + [I_{even}^-]_{st} P_-) \tag{A.62}$$

where I^\pm are given by

$$\begin{aligned}
[I_{odd}^\pm]_{st} &= \frac{1}{a} \frac{g_{\rho\sigma}}{(\widehat{ap - k})^2 + \lambda^2} \left\{ -i\bar{k} \cdot \gamma \left(\frac{r^2}{4} (\widehat{ap + k})_\rho (\widehat{ap + k})_\sigma [G_\pm]_{st} + g_{\rho\sigma} (\widetilde{ap + k})_\rho^2 [G_\mp]_{st} \right) \right. \\
&\quad + 2i (\widetilde{ap + k})_\rho (\widetilde{ap + k})_\sigma \gamma_\rho \bar{k}_\sigma [G_\mp]_{st} \\
&\quad \left. + \frac{r}{2} (\widehat{ap + k})_\rho (\widetilde{ap + k})_\sigma i\gamma_\sigma [(S_\pm + S_\mp)]_{st} \right\}
\end{aligned} \tag{A.63}$$

$$\begin{aligned}
[I_{even}^\pm]_{st} &= \frac{1}{a} \frac{g_{\rho\sigma}}{(\widehat{ap - k})^2 + \lambda^2} \left\{ \frac{r^2}{4} (\widehat{ap + k})_\rho (\widehat{ap + k})_\sigma [S_\pm]_{st} - g_{\rho\sigma} (\widetilde{ap + k})_\rho^2 [S_\mp]_{st} \right. \\
&\quad \left. + \frac{r}{2} (\widehat{ap + k})_\rho (\widetilde{ap + k})_\sigma (\bar{k} \cdot \gamma \gamma_\sigma [G_\mp]_{st} + \gamma_\sigma \bar{k} \cdot \gamma [G_\pm]_{st}) \right\}.
\end{aligned} \tag{A.64}$$

The contribution to $\Sigma_q(a, p)$ generated by $\Sigma_{st}(a, p)$ is obtained by multiplying by \bar{S}_s^{OUT} and \bar{S}_t^{IN} on the left and right, respectively (see Eqs. (A.50) and (A.56)). The corresponding

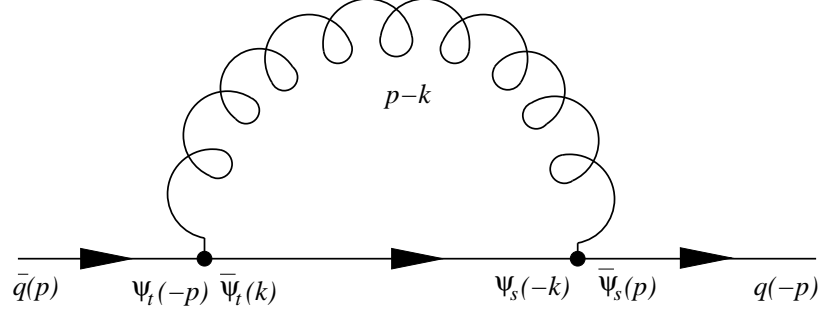


Figure A.1: *Sunset diagram for physical quarks. Solid and curly lines represent fermions and gluons, respectively.*

integrand $I_q(a, p)$ appearing in $\Sigma_q(a, p)$ is, thus,

$$\begin{aligned}
I_q &= \bar{S}_s^{OUT} I_{st} \bar{S}_t^{IN} \\
&= (1 - w_0^2) \left[-ip \cdot \gamma \mathcal{A} \left(w_0^{N-s} P_- + w_0^{s-1} P_+ \right) + \left(w_0^{s-1} P_- + w_0^{N-s} P_+ \right) \right]_s I_{st} \\
&\quad \times \left[\left(w_0^{N-t} P_+ + w_0^{t-1} P_- \right) (-ip \cdot \gamma \mathcal{A}) + \left(w_0^{t-1} P_+ + w_0^{N-t} P_- \right) \right]_t. \quad (\text{A.65})
\end{aligned}$$

Now we use

$$I_{odd} P_{\pm} = P_{\mp} I_{odd}, \quad I_{even} P_{\pm} = P_{\pm} I_{even} \quad (\text{A.66})$$

to get

$$\begin{aligned}
I_q^{odd}(ap, k) &= (-ip \cdot \gamma \mathcal{A}) \bar{I}_{odd}^-(ap, k) (-ip \cdot \gamma \mathcal{A}) + \bar{I}_{odd}^+(ap, k) \\
&\quad + (-ip \cdot \gamma \mathcal{A}) \tilde{I}_{odd}^-(ap, k) + \tilde{I}_{odd}^+(ap, k) (-ip \cdot \gamma \mathcal{A}) \quad (\text{A.67})
\end{aligned}$$

$$\begin{aligned}
I_q^{even}(ap, k) &= (-ip \cdot \gamma \mathcal{A}) \tilde{I}_{even}^+(ap, k) (-ip \cdot \gamma \mathcal{A}) + \tilde{I}_{even}^-(ap, k) \\
&\quad + (-ip \cdot \gamma \mathcal{A}) \bar{I}_{even}^+(ap, k) + \bar{I}_{even}^-(ap, k) (-ip \cdot \gamma \mathcal{A}), \quad (\text{A.68})
\end{aligned}$$

where

$$\bar{I}^{\pm} \equiv (1 - w_0^2) \sum w_0^{s-1} I^{\pm} w_0^{t-1} \equiv (1 - w_0^2) \sum w_0^{N-s} I^{\mp} w_0^{N-t}, \quad (\text{A.69})$$

$$\tilde{I}^{\pm} \equiv (1 - w_0^2) \sum w_0^{s-1} I^{\pm} w_0^{N-t} \equiv (1 - w_0^2) \sum w_0^{N-s} I^{\mp} w_0^{t-1}. \quad (\text{A.70})$$

To evaluate the renormalization of the self energy, we only need to keep terms to $\mathcal{O}(p)$:

$$\begin{aligned}
I_q(ap, k) &= \bar{I}_{odd}^+(0, k) + p_\mu \left. \frac{\partial \bar{I}_{odd}^+(ap, k)}{\partial p_\mu} \right|_{p_\mu=0} - i\mathcal{A} \left[p \cdot \gamma \tilde{I}_{odd}^-(0, k) + \tilde{I}_{odd}^+(0, k) p \cdot \gamma \right] \\
&\quad + \tilde{I}_{even}^-(0, k) + p_\mu \left. \frac{\partial \tilde{I}_{even}^-(0, k)}{\partial p_\mu} \right|_{p_\mu=0} \\
&\quad - i\mathcal{A} \left[p \cdot \gamma \bar{I}_{even}^+(0, k) + \bar{I}_{even}^-(0, k) p \cdot \gamma \right] \\
&\quad + \mathcal{O}(p^2).
\end{aligned} \tag{A.71}$$

The terms $p \cdot \gamma \tilde{I}_{odd}^-(0, k) + \tilde{I}_{odd}^+(0, k) p \cdot \gamma$, $\bar{I}_{odd}^+(0, k)$ and $p_\mu \frac{\partial \tilde{I}_{even}^-(0, k)}{\partial p_\mu}$ vanish after integration since they are also odd in k_μ , so we are left with

$$I_q(ap, k) = \tilde{I}_{even}^-(0, k) - i\mathcal{A} \left[p \cdot \gamma \bar{I}_{even}^+(0, k) + \bar{I}_{even}^-(0, k) p \cdot \gamma \right] + p_\mu \left. \frac{\partial \bar{I}_{odd}^+(ap, k)}{\partial p_\mu} \right|_{p \rightarrow 0}. \tag{A.72}$$

A.3.1.2 Numerical evaluation of the sunset diagram

Obtaining an analytic expression for the expansion of I_q in powers of the external momentum p is a formidable task. Moreover, when we consider below the twist-two operators with n derivatives, we will require all terms through $\mathcal{O}(p^n)$ in the one-loop amplitudes. Arriving at analytic expressions in the latter case — though possible in principle — is practically inefficient for obtaining numerical results. An alternate approach, which we follow here, involves evaluating the momentum integral numerically using the full expression for I_q and projecting out the required spacetime structures using the properties of γ matrices. To this end, we let

$$\Sigma_q(a, p) = g_0^2 C_F \int_{-\pi/a}^{\pi/a} \frac{d^d k}{(2\pi)^d} I_q(a, p, k) \tag{A.73}$$

and note that $J(q)$ is a 4×4 matrix that can be decomposed in terms of Dirac matrices:

$$\Sigma_q(a, p) = \frac{g_0^2 C_F}{16\pi^2} J_q(a, p) = \frac{g_0^2 C_F}{16\pi^2} \left[J_S(p) + J_P(p) \gamma_5 + J_V^\mu(p) \gamma_\mu + J_A^\mu(p) \gamma_\mu \gamma_5 + J_T^{\mu\nu}(p) \sigma_{\mu\nu} \right] \tag{A.74}$$

where

$$\begin{aligned}
J_S(p) &= \frac{1}{4} \text{Tr}_D [J_q(p)] & J_P(p) &= \frac{1}{4} \text{Tr}_D [J_q(p) \gamma_5] \\
J_V^\mu(p) &= \frac{1}{4} \text{Tr}_D [J_q(p) \gamma_\mu] & J_A^\mu(p) &= \frac{1}{4} \text{Tr}_D [J_q(p) \gamma_5 \gamma_\mu] \\
J_T^{\mu\nu}(p) &= \frac{1}{8} \text{Tr}_D [J_q(p) \sigma_{\mu\nu}]
\end{aligned} \tag{A.75}$$

and we have suppressed the a -dependence for simplicity. Parity symmetry implies that $J_P = 0 = J_A^\mu$, while $J_T^{\mu\nu}$ vanishes for $p \rightarrow 0$. The J_V^μ term must be proportional to p_μ :

$$J_V^\mu(p) = ip_\mu [J_2(p) + \mathcal{A}J_W(p)] \quad (\text{A.76})$$

where $J_2(p)$ and $J_W(p)$ denote the components that will contribute to Z_2 and Z_w , respectively. The physical amplitude can be written to $\mathcal{O}(p)$

$$J_q(p) = J_S(p=0) + ip \cdot \gamma [J_2(p=0) + \mathcal{A}J_W(p=0)] . \quad (\text{A.77})$$

The scalar coefficient is given by

$$J_S(p) = 16\pi^2 \int_{-\pi}^{\pi} \frac{d^d k}{(2\pi)^d} \frac{1}{4} \text{Tr}_D \left[\tilde{I}_{even}^-(ap, k) \right] \quad (\text{A.78})$$

$$= \int_{-\pi}^{\pi} \frac{d^d k}{(2\pi)^d} \frac{g_{\rho\sigma}(ap-k)}{(ap-k)^2 + \lambda^2} \left[\frac{r^2}{4} (\widehat{ap+k})_\rho (\widehat{ap+k})_\sigma \tilde{S}_- - g_{\rho\sigma} (\widetilde{ap+k})_\rho^2 \tilde{S}_+ + r (\widehat{ap+k})_\rho (\widetilde{ap+k})_\sigma \bar{k}_\sigma \tilde{\sigma}_V \right] . \quad (\text{A.79})$$

The $J_2(p)$ term in J_V^μ arises from \bar{I}_{odd}^+ , while the $J_W(p)$ component is generated by the $p \cdot \gamma \bar{I}_{even}^+ + \bar{I}_{even}^- p \cdot \gamma$ term. Thus, we have

$$\begin{aligned} J_2(p) &= 16\pi^2 \int_{-\pi}^{\pi} \frac{d^d k}{(2\pi)^d} \frac{1}{4} \text{Tr}_D \left[\frac{ip \cdot \gamma}{p^2} \bar{I}_{odd}^+(ap, k) \right] \\ \mathcal{A}J_W(p) &= 16\pi^2 \int_{-\pi}^{\pi} \frac{d^d k}{(2\pi)^d} \frac{1}{4} \text{Tr}_D \left[\frac{ip \cdot \gamma}{p^2} (-i\mathcal{A} (p \cdot \gamma \bar{I}_{even}^+(ap, k) + \bar{I}_{even}^-(ap, k) p \cdot \gamma)) \right] \\ &= 16\pi^2 \mathcal{A} \int_{-\pi}^{\pi} \frac{d^d k}{(2\pi)^d} \frac{1}{4} \text{Tr}_D \left[\bar{I}_{even}^+(ap, k) + \bar{I}_{even}^-(ap, k) \right] . \end{aligned} \quad (\text{A.80})$$

Evaluating these expressions, we obtain

$$J_2(p) = \int_{-\pi}^{\pi} \frac{d^d k}{(2\pi)^d} \frac{g_{\rho\sigma}(ap-k)}{(\widehat{ap-k})^2 + \lambda^2} \left\{ \frac{1}{p^2} \left(p \cdot \bar{k} \left[\frac{r^2}{4} (\widehat{ap+k})_{\rho} (\widehat{ap+k})_{\sigma} \bar{G}_+ + g_{\rho\sigma} (\widetilde{ap+k})_{\rho}^2 \bar{G}_- \right] \right. \right. \\ \left. \left. - 2(\widetilde{ap+k})_{\rho} (\widetilde{ap+k})_{\sigma} p_{\rho} \bar{k}_{\sigma} \bar{G}_- - r(\widehat{ap+k})_{\rho} (\widetilde{ap+k})_{\sigma} p_{\sigma} \bar{\sigma}_S \right) \right\} \quad (\text{A.81})$$

$$\mathcal{A}J_W(p) = \int_{-\pi}^{\pi} \frac{d^d k}{(2\pi)^d} \frac{g_{\rho\sigma}(ap-k)}{(\widehat{ap-k})^2 + \lambda^2} \left\{ 2\mathcal{A} \left(\left[\frac{r^2}{4} (\widehat{ap+k})_{\rho} (\widehat{ap+k})_{\sigma} - g_{\rho\sigma} (\widetilde{ap+k})_{\rho}^2 \right] \bar{\sigma}_S \right. \right. \\ \left. \left. + r(\widehat{ap+k})_{\rho} (\widetilde{ap+k})_{\sigma} \bar{k}_{\sigma} \bar{\sigma}_V \right) \right\}. \quad (\text{A.82})$$

In terms of parameters $\tilde{\Sigma}$ we then have

$$\tilde{\Sigma}_2 = J_2(p \rightarrow 0) \quad (\text{A.83})$$

$$\tilde{m} \tilde{\Sigma}_m = J_S(p \rightarrow 0) \quad (\text{A.84})$$

$$\tilde{\Sigma}_w = J_W(p \rightarrow 0). \quad (\text{A.85})$$

In addition to circumventing the need to obtain analytic expressions for the expansion of I_q in powers of p , the foregoing approach also facilitates the implementation of different IR regulators as may be most convenient for numerical integration.

A.3.1.3 IR singularities

Performing the loop integrals for the various $\tilde{\Sigma}$ requires care when treating the region in the vicinity of zero loop momentum. Similar issues arise in computing amplitudes for the twist-two and three operators, so we discuss them in detail for the self-energy graphs here. For terms that are IR singular in the limit of $\tilde{m}, p_{\mu} \rightarrow 0$, we regulate the IR divergences by keeping p_{μ} nonzero or by introducing a fictitious gluon mass λ . When $\tilde{m} = 0$ these integrals contain a $\ln pa$ singularity that we isolate numerically as discussed below. Keeping λ or p_{μ} nonzero also helps with the numerical integration.

In the case of IR-finite integrals, the use of naive integration can also lead to numerical divergences (or floating exceptions). When performed analytically, such integrals contain an explicit k^2 in the integration measure that cancels the $1/k^2$ appearing in the massless fermion propagator. Numerical integration, however, is performed using 4D Cartesian coordinates. The k^2 cancellation is not manifest and numerical divergences generally appear. To avoid

the latter, we keep both p_μ and \tilde{m} finite and observe the behavior of the result as a function of these parameters.

Once we know how to evaluate $J_q(p)$ for arbitrary p , there are several ways to extract the finite piece in the $p \rightarrow 0$ limit. For example, the general amplitude can be expanded in power series and rewritten in terms of $x = \ln p^2 a^2$ as

$$J(p) = \alpha + \gamma \ln p^2 a^2 + \sum_{n=1}^{\infty} c_n (p^2 a^2)^n, \quad (\text{A.86})$$

where γ is the anomalous dimension of the operator of interest. If we can keep p small enough to be able to neglect all $c_n (p^2 a^2)^n$ terms, we can fit the $J(p)$ curve to a straight line and read off coefficient α . Another (and usually faster) method is to identify an integral $K'(p)$ that can be evaluated analytically and that has the same logarithmic singularity as the integral of interest. Writing

$$K'(p) = \int_{-\pi}^{\pi} \frac{d^d k}{(2\pi)^d} K'(k, p) = \alpha' + \gamma \log p^2 a^2 + \mathcal{O}(p^2 a^2), \quad (\text{A.87})$$

we can subtract out the finite part to get just the logarithmic term:

$$K(p) = \int_{-\pi}^{\pi} \frac{d^d k}{(2\pi)^d} [K'(k, p) - \alpha'] = \int_{-\pi}^{\pi} \frac{d^d k}{(2\pi)^d} K(k, p) = \gamma \ln p^2 a^2 + \mathcal{O}(a^2 p^2). \quad (\text{A.88})$$

We can then add and subtract $K(p)$ from the integral of interest and end up with an expression which is IR finite and that one can easily evaluate numerically for small p :

$$[J(p) - K(p)] + K(p) = \log p^2 a^2 + \int_{-\pi}^{\pi} \frac{d^d k}{(2\pi)^d} [J(k, p) - K(k, p)]. \quad (\text{A.89})$$

For quantities (such as the self-energy) whose renormalization entails no mixing, this second procedure is usually the most efficient. For twist-two operators with several derivatives, however, the presence of mixing introduces complications that we discuss in more detail below.

A.3.1.4 Tadpole diagram

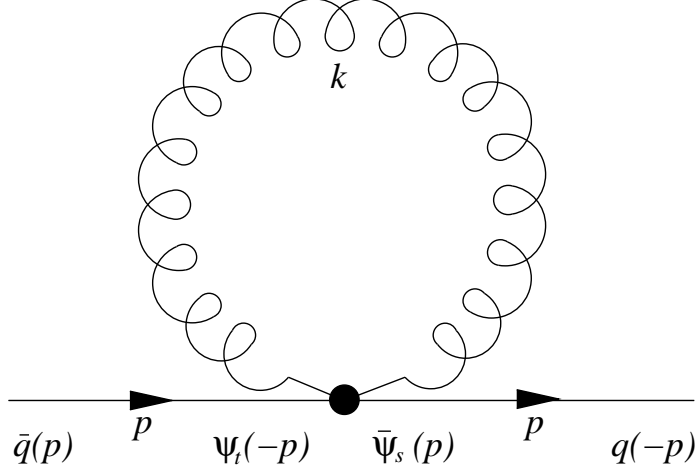


Figure A.2: Tadpole diagram for physical quarks. Solid and curly lines represent fermions and gluons, respectively.

Evaluation of the tadpole contribution is considerably more straightforward than for the sunset diagram, since we have no internal fermion lines. For the 5D self-energy, we have

$$\begin{aligned}
\Sigma_{st}(p) &= \frac{1}{2} \delta_{st} \int_{-\pi/a}^{\pi/a} \frac{d^d k}{(2\pi)^d} \sum_{\rho} G_{\lambda\rho}(k) V_{\rho\rho}^{aa}(p, p) = \int_{-\pi/a}^{\pi/a} \frac{d^d k}{(2\pi)^d} I_{st}(p, k) \\
&= \frac{\delta_{st}}{2} \int_{-\pi}^{\pi} \frac{d^d k}{(2\pi)^d} \sum_{\rho} (-ag_0^2 C_F) (r \cos ap_{\rho} - i\gamma_{\rho} \sin ap_{\rho}) a^2 \frac{g_{\rho\rho}(k)}{\hat{k}^2 + \lambda^2} \\
&= -\frac{\delta_{st} g_0^2 C_F}{2} \sum_{\rho} \left(r \frac{1}{a} - i\gamma_{\rho} p_{\rho} \right) \int_{-\pi}^{\pi} \frac{d^d k}{(2\pi)^d} \frac{g_{\rho\rho}(k)}{\hat{k}^2 + \lambda^2}. \tag{A.90}
\end{aligned}$$

The integral is the same for each ρ , so we get

$$I_{st} = -\frac{\delta_{st} g_0^2 C_F}{2} \left(r \frac{d}{a} - i\gamma \cdot p \right) \frac{g_{\rho\rho}(k)}{\hat{k}^2 + \lambda^2} \quad (\text{no summation over } \rho). \tag{A.91}$$

Since there are no fermion propagators here, the 5D sums are straightforward to evaluate:

$$\bar{I} \sim \sum_{s,t=1}^N w_0^{s-1} \delta_{st} w_0^{t-1} = \sum_{s=0}^{N-1} (w_0^2)^s = \frac{1 - w_0^{2N}}{1 - w_0^2} \rightarrow \frac{1}{1 - w_0^2} \quad (\text{A.92})$$

$$\tilde{I} \sim \sum_{s,t=1}^N w_0^{s-1} \delta_{st} w_0^{N-t} = \sum_{s=0}^{N-1} w_0^{N-1} = N w_0^{N-1} \rightarrow 0. \quad (\text{A.93})$$

so the physical amplitude equals

$$I_q(p) = \bar{S}_s^{OUT} I_{st} \bar{S}_t^{IN} \quad (\text{A.94})$$

$$= (-ip \cdot \gamma \mathcal{A}) \bar{I}_{odd}^- (-ip \cdot \gamma \mathcal{A}) + \bar{I}_{odd}^+ + (-ip \cdot \gamma \mathcal{A}) \bar{I}_{even}^+ + \bar{I}_{even}^- (-ip \cdot \gamma \mathcal{A}) \quad (\text{A.95})$$

$$= (1 - p^2 \mathcal{A}^2) \bar{I}_{odd} - ip \cdot \gamma \mathcal{A} \bar{I}_{even} \quad (\text{A.96})$$

$$= ip \cdot \gamma \frac{g_0^2 C_F}{2} \left(1 + 2r \mathcal{A} \frac{d}{a} \right) \frac{g_{\rho\rho}(k)}{\hat{k}^2 + \lambda^2}, \quad (\text{A.97})$$

which yields, after integration,

$$\tilde{\Sigma}_2 = 8\pi^2 T, \quad \Sigma_w = -\frac{4r}{a} (16\pi^2 T), \quad (\text{A.98})$$

where T is given by

$$T(\lambda^2) = \frac{1}{4} \int_{-\pi}^{\pi} \frac{d^d k}{(2\pi)^d} \sum_{\rho} \frac{g_{\rho\rho}}{\hat{k}^2 + \lambda^2}. \quad (\text{A.99})$$

Since T does not depend on external momentum and has no singularities, it is straightforward to evaluate.

A.3.1.5 Renormalization constants: Z_2 , Z_w , and Z_m

Combining Eqs. (A.50), (A.56), and (A.57) we have

$$\begin{aligned}
\hat{S}_q(p) &= \frac{1}{ip \cdot \gamma + \tilde{m}} \left(1 + \Sigma_q \frac{1}{ip \cdot \gamma + \tilde{m}} \right) = \frac{1}{ip \cdot \gamma + \tilde{m} - \Sigma_q} + \mathcal{O}(g_0^4) \\
&= \frac{1}{ip \cdot \gamma \left[1 - \frac{g_0^2 C_F}{16\pi^2} (\tilde{\Sigma}_2 - \mathcal{A}\tilde{\Sigma}_w) \right] + \tilde{m} \left(1 - \frac{g_0^2 C_F}{16\pi^2} \tilde{\Sigma}_m \right)} + \mathcal{O}(g_0^4) \\
&= \frac{\left[1 + \frac{g_0^2 C_F}{16\pi^2} (\tilde{\Sigma}_2 - \mathcal{A}\tilde{\Sigma}_w) \right]}{ip \cdot \gamma + \tilde{m} \left(1 - \frac{g_0^2 C_F}{16\pi^2} \Sigma_2 \right) \left[1 + \frac{g_0^2 C_F}{16\pi^2} (\tilde{\Sigma}_2 - \mathcal{A}\tilde{\Sigma}_w) \right]} + \mathcal{O}(g_0^4) \quad (\text{A.100}) \\
&= \frac{Z_w Z_2}{ip \cdot \gamma + \tilde{m} Z_w Z_m^{-1}} = \frac{Z_q}{ip \cdot \gamma + \tilde{m} Z_w Z_m^{-1}},
\end{aligned}$$

which allows us to read of the renormalization constants to order g^2 :

$$Z_w = 1 - \frac{2w_0}{1 - w_0^2} \frac{g^2 C_F}{16\pi^2} \tilde{\Sigma}_w, \quad (\text{A.101})$$

$$Z_2 = 1 + \frac{g^2 C_F}{16\pi^2} \tilde{\Sigma}_2, \quad (\text{A.102})$$

$$Z_m^{-1} = 1 - \frac{g^2 C_F}{16\pi^2} (\tilde{\Sigma}_m - \tilde{\Sigma}_2). \quad (\text{A.103})$$

Numerical values for the various $\tilde{\Sigma}_i$ are shown in Table A.2 and hint at rather poor convergence properties of the perturbative expansion for Z_w . In practice, we can sum the higher-order contributions by considering the ratio of matrix elements of two correlators. In particular, there exists an exactly conserved $5D$ axial current on the lattice,

$$\begin{aligned}
\mathcal{A}_\mu(x) &= \frac{1}{2} \sum_s \text{sign} \left(s - \frac{N-1}{2} \right) \left[\bar{\psi}_s(x + \hat{\mu})(1 + \gamma_\mu) U_\mu^\dagger(x) \psi_s(x) \right. \\
&\quad \left. - \bar{\psi}_s(x)(1 - \gamma_\mu) U_\mu(x) \psi_s(x + \hat{\mu}) \right], \quad (\text{A.104})
\end{aligned}$$

that is non-local and that has the same continuum limit as the local axial current on the lattice

$$A_\mu(x) = \bar{q}(x) \gamma_\mu \gamma_5 q(x). \quad (\text{A.105})$$

Since \mathcal{A}_μ is conserved on the lattice, it receives no renormalization. In contrast, A_μ is

renormalized by $Z_A^{-1}Z_q$. Thus, the ratio

$$R_A = \frac{\langle \mathcal{A}_\mu(x) \rangle}{\langle A_\mu(x) \rangle} = Z_A Z_q^{-1}. \quad (\text{A.106})$$

To the extent that the perturbative, one-loop computations of Z_A and Z_2 give good approximations to the non-perturbative values for these quantities, the ratio R_A in Eq. (A.106) that is computed non-perturbatively yields a non-perturbative value for Z_w^{-1} :

$$Z_w^{-1} = (Z_2)_{\text{pert}} (Z_A^{-1})_{\text{pert}} R_A, \quad (\text{A.107})$$

where the ‘‘pert’’ subscript indicates the value computed perturbatively. In practice, it turns out to be more tractable to consider the ratio of correlators

$$R_{AP} = \frac{\langle \mathcal{A}_\mu(x) \bar{q}(y) \gamma_5 q(y) \rangle}{\langle A_\mu(x) \bar{q}(y) \gamma_5 q(y) \rangle}. \quad (\text{A.108})$$

To the extent that x and y are sufficiently well separated in Euclidean spacetime, thereby avoiding additional short-distance singularities requiring operator product renormalization, one has $R_{AP} = Z_A Z_q^{-1}$ (the renormalization factors associated with the pseudoscalar current would cancel from R_{AP} in this case). In what follows, we will use R_{AP} to extract Z_w^{-1} .

It is also interesting to consider the physical origin of the non-perturbative nature of Z_w . At tree-level, Z_w just gives the overlap between the physical quark interpolating field $q(x)$ defined in Eq. (A.18) and the massless mode χ_0 of Eq. (A.17):

$$\left(Z_w^{1/2} \right)_{\text{tree}} = \langle q | \chi \rangle_{\text{tree}} = \sqrt{1 - w_0^2}. \quad (\text{A.109})$$

After renormalization, one might expect the bare massless mode χ_0 to have the same form as in Eq. (A.17) but with the $\psi_s \rightarrow \psi_{0s} = \sqrt{Z_2} \psi_s$ and w_0 being replaced by a suitably chosen parameter w (corresponding to a renormalized parameter M in the DW action). In this case, one would have

$$Z_w^{1/2} Z_2 = \langle q_0 | \chi_0 \rangle = Z_2 \sqrt{1 - w^2}. \quad (\text{A.110})$$

Letting $w = w_0 + \Delta w$ we would then have

$$Z_w = (1 - w_0^2) - 2w_0\Delta w + (\Delta w)^2 = (Z_w)_{\text{tree}} \left[1 - \frac{2w_0\Delta w}{1 - w_0^2} + \frac{(\Delta w)^2}{1 - w_0^2} \right]. \quad (\text{A.111})$$

Now observe that the overall $1 - w_0^2$ in Eq. (A.111) has been absorbed into a redefinition of the interpolating field q and that the second term in Eq. (A.111) has the same form as the second term in Eq. (A.101) with

$$\Delta w = \frac{g^2 C_F}{16\pi^2} \tilde{\Sigma}_w. \quad (\text{A.112})$$

Thus, we might expect the $\mathcal{O}(g^4)$ contribution to Z_w to have the opposite sign from the $\mathcal{O}(g^2)$ term and magnitude roughly $g^4 C_F^2 (4\pi)^{-4} (\tilde{\Sigma}_w)^2$. While this line of reasoning is somewhat heuristic, it is nonetheless suggestive that the large non-perturbative effects associated with Z_w arise from a finite renormalization of the physical zero mode that goes beyond the renormalization of the individual DW fields.

While at first, the separation of the piece in the expression for the self energy proportional to $ip \cdot \gamma$ may seem a bit arbitrary, the origin of two pieces is quite different. Let's take another look at the expression for the $5D$ self energy (A.62):

$$\Sigma_{st} = \int_{-\pi/a}^{\pi/a} \frac{d^d k}{(2\pi)^d} ([I_{\text{odd}}^\pm]_{st} P_\pm + [I_{\text{even}}^\pm]_{st} P_\pm). \quad (\text{A.113})$$

Terms I_{odd}^\pm contain one γ matrix and they give us the renormalization of the $5D$ wave function Z_2 . I_{even}^\pm terms have either no γ matrices or two γ matrices, so they yield the renormalization of the $5D$ mass parameter M , plus the term proportional to $\sigma_{\mu\nu}$ matrix which vanishes in the $p_\mu \rightarrow 0$ limit. Since the dynamics on the lattice is governed by the behavior of the zero mode

$$\begin{aligned} \chi_0(x) &= \sqrt{1 - w_0^2} \left(P_+ w_0^{s-1} \psi_s(x) + P_- w_0^{N-s} \psi_s(x) \right) \\ &= \sqrt{1 - w_0^2} [(P_+ \psi_1(x) + P_- \psi_N(x)) + \dots], \end{aligned} \quad (\text{A.114})$$

by choosing our “physical” field to be

$$q_0(x) = \frac{1}{\sqrt{1-w_0^2}} [(P_+\psi_1(x) + P_-\psi_N(x))] , \quad (\text{A.115})$$

it has an overlap of one with the zero mode

$$\langle q_0 | \chi_0 \rangle = 1 . \quad (\text{A.116})$$

In other words, we have created exactly one unit of the light $5D$ mode χ_0 , plus some amount of heavy $5D$ modes

$$q_0(x) = \chi_0(x) + \sum_{i>0} c_i \chi_i(x) , \quad (\text{A.117})$$

where $\chi_i(x)$ are the remaining heavy $5D$ modes on the lattice and c_i are some coefficients which we do not need to know. Symbolically, we can write the $5D$ quark propagator as a sum of terms coming from the light and heavy modes:

$$S_{st}(x) = |\chi_0\rangle \langle \chi_0| + \sum_{i>0} |\chi_i\rangle \langle \chi_i| . \quad (\text{A.118})$$

As the system evolves in time, all the heavy contributions die out and we are left only with the physics of the light chiral mode

$$S_{st}(x)|_{t \rightarrow \infty} = |\chi_0\rangle \langle \chi_0| . \quad (\text{A.119})$$

So by calculating the renormalized propagator, we are really getting the renormalization of the zero mode χ_0 :

$$\chi_0(x) = \sqrt{1-w_0^2} \left(P_+ w_0^{s-1} \psi_s(x) + P_- w_0^{N-s} \psi_s(x) \right) . \quad (\text{A.120})$$

Renormalization of this zero mode has two effects: $5D$ fields get renormalized by a factor Z_2 , but the $5D$ mass parameter also gets (additively) renormalized to $w = w_0 + \Delta w$, so the

new zero mode looks like

$$\begin{aligned}\chi(x) &= \sqrt{1-w^2} \left(P_+ Z_2^{1/2} \psi_1(x) + P_- Z_2^{1/2} \psi_N(x) \right) \\ &= \sqrt{\frac{1-w^2}{1-w_0^2}} Z_2^{1/2} \chi_0(x).\end{aligned}\tag{A.121}$$

As we can see, the renormalization of $q(x)$ has two pieces:

$$Z_q = Z_2 Z_W ,\tag{A.122}$$

where the first piece Z_2 describes the renormalization of the $5D$ wave function, and the second piece Z_W describes the renormalization of the $(1-w_0^2)^{1/2}$ factor. The factor $(1-w_0^2)^{1/2}$ comes from our requirement that the overlap of the tree-level light lattice mode χ_0 and the physical wave function $q_0(x)$ equals one; our renormalization condition ensures that the overlap stays one after the renormalization, so we think of the factor Z_W describing the effect of the shift of the light $5D$ lattice mode. To order g_0^2 we have

$$\frac{1-w^2}{1-w_0^2} = \frac{1 - \left(w_0 + \frac{g_0^2 C_F}{16\pi^2} \Sigma_3 \right)^2}{1-w_0^2} = 1 - \frac{2w_0}{1-w_0^2} \frac{g_0^2 C_F}{16\pi^2} \Sigma_3 + O(g_0^4) = Z_W + O(g_0^4).\tag{A.123}$$

Note that the one-loop result for Δw gives us order g_0^4 corrections for Z_W and therefore for Z_q as well.

operator	Wilson	DW M=1.6	DW M=1.7	M=1.8	M=1.9
$\Sigma_2^{MS} - \Sigma_2^{LATT}$	-16.644	-15.784	-15.896	-16.057	-16.29
$\tilde{\Sigma}_W$	0.	49.694	49.92	50.246	50.718
$Z_w(g_0^2)$	1.	1.787	2.157	2.886	5.057
$Z_w(g_0^4)$	1.	1.512	1.809	2.386	4.092
Z_q	1.141	1.713	2.051	2.709	4.655

Table A.2: *Results for Wilson and DW fermions, with no smearing.*

A.3.2 Vertex renormalization

We now build upon the methodology established for the self-energy renormalization to calculate the bilinear operators relevant to deep inelastic scattering. In this chapter we concentrate on local quark currents which have no derivative operators.

To evaluate the Feynman rule for the operator $\mathcal{O}_\Gamma = \bar{q}(x)\Gamma q(x)$, we need to evaluate the Fourier transform of the $a^4 \sum_x \bar{q}(x)\Gamma q(x)$

$$a^4 \sum_x \bar{q}(x)\Gamma q(x) = \int_{-\pi/a}^{\pi/a} \frac{d^d k}{(2\pi)^d} \bar{q}(k)\Gamma q(k), \quad (\text{A.124})$$

which says that the Feynman rule for the operator \mathcal{O}_Γ is simply the Γ matrix.

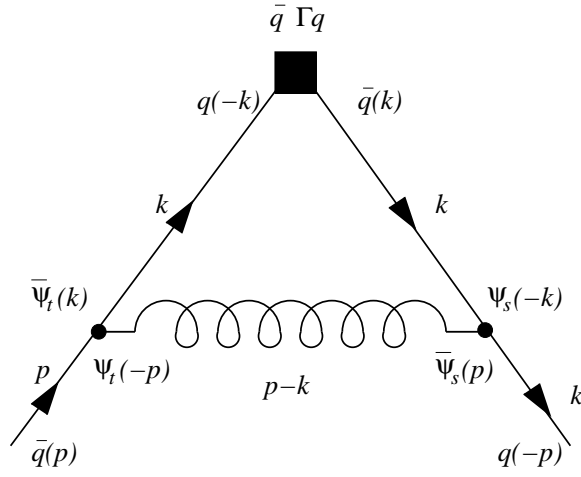


Figure A.3: Vertex diagram for quark bilinear operators (denoted by the box). Solid and curly lines represent fermions and gluons, respectively.

The 5D amplitude for the vertex diagram is given by

$$J_{st}(p) = \int_{-\pi/a}^{\pi/a} \frac{d^d k}{(2\pi)^d} V_\rho(p, k) S_s^{IN}(k) \mathcal{O}(k) S_t^{OUT}(k) V_\lambda(k, p) G_{\rho\lambda}(p - k) \quad (\text{A.125})$$

$$= \int_{-\pi/a}^{\pi/a} \frac{d^d k}{(2\pi)^d} I_{st}(p, k) \quad (\text{A.126})$$

where $\mathcal{O}(k)$ is the Feynman rule for the vertex operator $\bar{q}(k)\Gamma q(k)$ in which Γ is one of Dirac matrices $1, \gamma_5, \gamma_\mu, \gamma_\mu \gamma_5$, or $\sigma_{\mu\nu}$. Dirac algebra for this diagram is the same as for twist-two operators $\bar{q}\gamma_\mu D_\nu D_\alpha \dots q$, since each covariant derivative adds only a factor of four-momentum \bar{k}_μ . After rescaling the loop momentum $k_\mu \rightarrow k_\mu/a$, the amplitude is given

by

$$\begin{aligned}
I_{st}(ap, k) = & \left[\frac{\delta^{ab} g_{\rho\sigma}}{(\widehat{ap-k})^2 + \mu^2} \left[-g_0 T_{cd}^a \left(r \frac{a}{2} (\widehat{ap+k})_\rho + i\gamma_\rho (\widetilde{ap+k})_\rho \right) \right] \right. \\
& [(g_- P_+ + g_+ P_-)(-i\bar{k} \cdot \gamma) + (\sigma_- P_+ + \sigma_+ P_-)] [\Gamma] \\
& [(-i\bar{k} \cdot \gamma)(g_+ P_+ + g_- P_-) + (\sigma_+ P_+ + \sigma_- P_-)] \\
& \left. \left[-g_0 T_{dc}^b \left(r \frac{a}{2} (\widehat{ap+k})_\sigma + i\gamma_\rho (\widetilde{ap+k})_\sigma \right) \right] \right]. \tag{A.127}
\end{aligned}$$

A.3.2.1 Scalar and pseudoscalar currents

After performing the γ algebra and separating parts with even and odd numbers of γ matrices, we get

$$\begin{aligned}
I_{\pm}^{even} = & \frac{g_{\rho\sigma}}{(\widehat{ap-k})^2 + \mu^2} \left\{ \frac{r^2}{4} (\widehat{ap+k})_\rho (\widehat{ap+k})_\sigma ([\mp] \bar{k}^2 g_{\mp} g_{\pm} + \sigma_{\mp} \sigma_{\pm}) \right. \\
& + g_{\rho\sigma} (\widetilde{ap+k})_\rho^2 (\bar{k}^2 g_{\pm} g_{\mp} [\mp] \sigma_{\pm} \sigma_{\mp}) + \frac{r}{2} (\widehat{ap+k})_\rho (\widetilde{ap+k})_\sigma \\
& \left. \times (\gamma_\sigma \bar{k} \cdot \gamma (g_{\pm} \sigma_{\pm} [\pm] \sigma_{\pm} g_{\pm}) + \bar{k} \cdot \gamma \gamma_\sigma ([\pm] g_{\mp} \sigma_{\mp} + \sigma_{\mp} g_{\mp})) \right\} [\gamma_5] \tag{A.128}
\end{aligned}$$

and

$$\begin{aligned}
I_{\pm}^{odd} = & \frac{g_{\rho\sigma}}{(\widehat{ap-k})^2 + \mu^2} \left\{ -i\bar{k} \cdot \gamma \frac{r^2}{4} (\widehat{ap+k})_\rho (\widehat{ap+k})_\sigma (g_{\pm} \sigma_{\pm} [\pm] \sigma_{\pm} g_{\pm}) \right. \\
& - i\gamma_\mu \bar{k}_\nu \left[g_{\mu\nu} g_{\rho\sigma} (\widetilde{ap+k})_\rho^2 - 2g_{\rho\mu} g_{\sigma\nu} (\widetilde{ap+k})_\rho (\widetilde{ap+k})_\sigma \right] \\
& \times ([\pm] g_{\mp} \sigma_{\mp} + \sigma_{\mp} g_{\mp}) + \frac{r}{2} (\widehat{ap+k})_\rho (\widetilde{ap+k})_\sigma i\gamma_\sigma \\
& \left. [-\bar{k}^2 ([\pm] g_{\mp} g_{\pm} + g_{\pm} g_{\mp}) + (\sigma_{\mp} \sigma_{\pm} [\pm] \sigma_{\pm} \sigma_{\mp})] \right\} [\gamma_5]. \tag{A.129}
\end{aligned}$$

The physical amplitude is then obtained after summing in the 5th dimension

$$\begin{aligned}
I_q(ap, k) &= \bar{S}_s^{OUT} I_{st}(ap, k) \bar{S}_t^{IN} \\
&= \left[-ip \cdot \gamma \mathcal{A} \left(w_0^{N-s} P_- + w_0^{s-1} P_+ \right) + \left(w_0^{s-1} P_- + w_0^{N-s} P_+ \right) \right]_s [I_{st}^+ P_+ + I_{st}^- P_-] [\gamma_5] \\
&\quad \times \left[\left(w_0^{N-t} P_+ + w_0^{t-1} P_- \right) (-ip \cdot \gamma \mathcal{A}) + \left(w_0^{t-1} P_+ + w_0^{N-t} P_- \right) \right]_t \\
&= I_{phys}^{odd} + I_{phys}^{even}
\end{aligned} \tag{A.130}$$

$$\begin{aligned}
I_{phys}^{odd} &= (-ip \cdot \gamma \mathcal{A}) \bar{I}_{odd}^- [\gamma_5] (-ip \cdot \gamma \mathcal{A}) + \bar{I}_{odd}^+ [\gamma_5] \\
&\quad + (-ip \cdot \gamma \mathcal{A}) \tilde{I}_{odd}^- [\gamma_5] + \tilde{I}_{odd}^+ [\gamma_5] (-ip \cdot \gamma \mathcal{A})
\end{aligned} \tag{A.131}$$

$$\begin{aligned}
I_{phys}^{even} &= (-ip \cdot \gamma \mathcal{A}) \tilde{I}_{even}^+ [\gamma_5] (-ip \cdot \gamma \mathcal{A}) + \tilde{I}_{even}^- [\gamma_5] \\
&\quad + (-ip \cdot \gamma \mathcal{A}) \bar{I}_{even}^+ [\gamma_5] + \bar{I}_{even}^- [\gamma_5] (-ip \cdot \gamma \mathcal{A}),
\end{aligned} \tag{A.132}$$

where as before

$$\bar{I}^\pm \equiv (1 - w_0^2) \sum w_0^{s-1} I^\pm w_0^{t-1} \equiv (1 - w_0^2) \sum w_0^{N-s} I^\mp w_0^{N-t}, \tag{A.133}$$

$$\tilde{I}^\pm \equiv (1 - w_0^2) \sum w_0^{s-1} I^\pm w_0^{N-t} \equiv (1 - w_0^2) \sum w_0^{N-s} I^\mp w_0^{t-1}, \tag{A.134}$$

and we have used the fact

$$I_{odd} P_\pm = P_\mp I_{odd}, \quad I_{even} P_\pm = P_\pm I_{even}. \tag{A.135}$$

Performing the 5D sums, we get

$$\begin{aligned} \bar{I}_{\pm}^{even} &= \frac{g_{\rho\sigma}}{(\widehat{ap-k})^2 + \mu^2} \left[\frac{r^2}{4} (\widehat{ap+k})_{\rho} (\widehat{ap+k})_{\sigma} [\mp] g_{\rho\sigma} (\widehat{ap+k})_{\rho}^2 \right] \\ &\quad \times ([\mp] \bar{k}^2 \tilde{g}_{\mp} \tilde{g}_{\pm} + \tilde{\sigma}_{\mp} \tilde{\sigma}_{\pm}) [\gamma_5] \end{aligned} \quad (\text{A.136})$$

$$\begin{aligned} \tilde{I}_{\pm}^{even} &= \frac{g_{\rho\sigma}}{(\widehat{ap-k})^2 + \mu^2} \left\{ \frac{r^2}{4} (\widehat{ap+k})_{\rho} (\widehat{ap+k})_{\sigma} (\tilde{\sigma}_{\mp}^2 [\mp] \bar{k}^2 \tilde{g}_{\mp}^2) \right. \\ &\quad \left. + g_{\rho\sigma} (\widehat{ap+k})_{\rho}^2 (\bar{k}^2 \tilde{g}_{\pm}^2 [\mp] \tilde{\sigma}_{\pm}^2) \right. \\ &\quad \left. + r (\widehat{ap+k})_{\rho} (\widehat{ap+k})_{\sigma} \bar{k}_{\sigma} (\tilde{g}_{\pm} \tilde{\sigma}_{\mp} [\pm] \tilde{\sigma}_{\pm} \tilde{g}_{\mp}) \right\} [\gamma_5] \end{aligned} \quad (\text{A.137})$$

$$\begin{aligned} \bar{I}_{\pm}^{odd} &= \frac{g_{\rho\sigma}}{(\widehat{ap-k})^2 + \mu^2} \left\{ -i \bar{k} \cdot \gamma \frac{r^2}{4} (\widehat{ap+k})_{\rho} (\widehat{ap+k})_{\sigma} (\tilde{g}_{\pm} \tilde{\sigma}_{\pm} [\pm] \tilde{\sigma}_{\pm} \tilde{g}_{\pm}) \right. \\ &\quad \left. - i \gamma_{\mu} \bar{k}_{\nu} \left[g_{\mu\nu} g_{\rho\sigma} (\widehat{ap+k})_{\rho}^2 - 2 g_{\rho\mu} g_{\sigma\nu} (\widehat{ap+k})_{\rho} (\widehat{ap+k})_{\sigma} \right] \right. \\ &\quad \left. ([\pm] \tilde{g}_{\mp} \tilde{\sigma}_{\mp} + \tilde{\sigma}_{\mp} \tilde{g}_{\mp}) + i \gamma_{\sigma} \frac{r}{2} (\widehat{ap+k})_{\rho} (\widehat{ap+k})_{\sigma} \right. \\ &\quad \left. [-\bar{k}^2 ([\pm] \tilde{g}_{\mp} \tilde{g}_{\pm} + \tilde{g}_{\pm} \tilde{g}_{\mp}) + (\tilde{\sigma}_{\mp} \tilde{\sigma}_{\pm} [\pm] \tilde{\sigma}_{\pm} \tilde{\sigma}_{\mp})] \right\} [\gamma_5] \end{aligned} \quad (\text{A.138})$$

$$\begin{aligned} \tilde{I}_{\pm}^{odd} &= \frac{g_{\rho\sigma}}{(\widehat{ap-k})^2 + \mu^2} \left\{ -i \bar{k} \cdot \gamma \frac{r^2}{4} (\widehat{ap+k})_{\rho} (\widehat{ap+k})_{\sigma} (\tilde{g}_{\pm} \tilde{\sigma}_{\mp} [\pm] \tilde{\sigma}_{\pm} \tilde{g}_{\mp}) \right. \\ &\quad \left. - i \gamma_{\mu} \bar{k}_{\nu} \left[g_{\mu\nu} g_{\rho\sigma} (\widehat{ap+k})_{\rho}^2 - 2 g_{\rho\mu} g_{\sigma\nu} (\widehat{ap+k})_{\rho} (\widehat{ap+k})_{\sigma} \right] \right. \\ &\quad \left. ([\pm] \tilde{g}_{\mp} \tilde{\sigma}_{\pm} + \tilde{\sigma}_{\mp} \tilde{g}_{\pm}) + i \gamma_{\sigma} \frac{r}{2} (\widehat{ap+k})_{\rho} (\widehat{ap+k})_{\sigma} \right. \\ &\quad \left. [-\bar{k}^2 ([\pm] \tilde{g}_{\mp} \tilde{g}_{\mp} + \tilde{g}_{\pm} \tilde{g}_{\pm}) + (\tilde{\sigma}_{\mp} \tilde{\sigma}_{\mp} [\pm] \tilde{\sigma}_{\pm} \tilde{\sigma}_{\pm})] \right\} [\gamma_5]. \end{aligned} \quad (\text{A.139})$$

To get the physical amplitude, we evaluate this at $p = 0$ so we are left with

$$I_q = \bar{I}_{odd}^+ + \tilde{I}_{even}^-. \quad (\text{A.140})$$

It is easy to see that \bar{I}_{odd}^+ vanishes for $p \rightarrow 0$ since it is an odd function of k_{μ} , so the physical amplitude is given by

$$\begin{aligned} I_{S,P}(ap, k) &= \tilde{I}_{even}^- = \frac{g_{\rho\sigma}}{\hat{k}^2 + \mu^2} \left\{ \frac{r^2}{4} \hat{k}_{\rho} \hat{k}_{\sigma} (\tilde{\sigma}_{+}^2 [\mp] \bar{k}^2 \tilde{g}_{+}^2) + g_{\rho\sigma} \tilde{k}_{\rho}^2 (\bar{k}^2 \tilde{g}_{-}^2 [\mp] \tilde{\sigma}_{-}^2) \right. \\ &\quad \left. + r \hat{k}_{\rho} \tilde{k}_{\sigma} \bar{k}_{\sigma} (\tilde{g}_{-} \tilde{\sigma}_{+} [\pm] \tilde{\sigma}_{-} \tilde{g}_{+}) \right\} [\gamma_5]. \end{aligned} \quad (\text{A.141})$$

For DW fermions $\tilde{g}_{+}, \tilde{\sigma}_{-} \rightarrow 0$, we get

$$I_{S,P} = \frac{1}{\hat{k}^2 + \mu^2} \left\{ \frac{r^2}{4} \hat{k}^2 \tilde{\sigma}_{+}^2 + \tilde{k}^2 \bar{k}^2 \tilde{g}_{-}^2 + r \bar{k}^2 \tilde{g}_{-} \tilde{\sigma}_{+} \right\} [\gamma_5], \quad (\text{A.142})$$

which agrees with Eqs. (4.5) and (4.6) in [48].

A.3.2.2 Vector and axial vector currents

After doing the algebra, we get the result (which we again split into parts with odd and even number of γ -matrices)

$$\begin{aligned}
I_{st}^{odd} = & \frac{g_{\rho\sigma}}{(\widehat{ap-k})^2 + \mu^2} \left\{ \gamma_\alpha \left(g_{\rho\sigma} g_{\nu\alpha} (\widetilde{ap+k})_\rho^2 - 2g_{\rho\nu} g_{\sigma\alpha} (\widetilde{ap+k})_\rho (\widetilde{ap+k})_\sigma \right) \right. \\
& \left[(\bar{k}^2 g_{\mu\nu} - 2\bar{k}_\mu \bar{k}_\nu) g_\mp g_\mp \pm g_{\mu\nu} \sigma_\mp \sigma_\mp \right] \\
& + \gamma_\nu \frac{r^2}{4} (\widehat{ap+k})_\rho (\widehat{ap+k})_\sigma \left[\pm (\bar{k}^2 g_{\mu\nu} - 2\bar{k}_\mu \bar{k}_\nu) g_\pm g_\pm \pm g_{\mu\nu} \sigma_\pm \sigma_\pm \right] \\
& + \frac{r}{2} (\widehat{ap+k})_\rho (\widetilde{ap+k})_\sigma \left[\pm \gamma_\sigma \gamma_\mu \bar{k} \cdot \gamma \sigma_\mp g_\pm + \gamma_\sigma \bar{k} \cdot \gamma \gamma_\mu g_\mp \sigma_\pm \right. \\
& \left. + \gamma_\mu \bar{k} \cdot \gamma \gamma_\sigma \sigma_\pm g_\mp \pm \bar{k} \cdot \gamma \gamma_\mu \gamma_\sigma g_\pm \sigma_\mp \right] \left. \right\} [\gamma_5] \tag{A.143}
\end{aligned}$$

and

$$\begin{aligned}
I_{st}^{even} = & \frac{g_{\rho\sigma}}{(\widehat{ap-k})^2 + \mu^2} \left\{ i g_{\rho\sigma} (\widetilde{ap+k})_\rho^2 \left[\gamma_\mu \bar{k} \cdot \gamma \sigma_\pm g_\mp \pm \bar{k} \cdot \gamma \gamma_\mu g_\pm \sigma_\mp \right] \right. \\
& - 2i (\widetilde{ap+k})_\rho (\widetilde{ap+k})_\sigma \gamma_\rho (\gamma_\mu \bar{k}_\sigma - \bar{k} \cdot \gamma g_{\rho\sigma}) (\sigma_\pm g_\mp \mp g_\pm \sigma_\mp) \\
& - i \frac{r^2}{4} (\widehat{ap+k})_\rho (\widetilde{ap+k})_\sigma \left[\pm \gamma_\mu \bar{k} \cdot \gamma \sigma_\mp g_\pm \pm \bar{k} \cdot \gamma \gamma_\mu g_\mp \sigma_\pm \right] \\
& + i \frac{r}{2} (\widehat{ap+k})_\rho (\widetilde{ap+k})_\sigma \left[(\pm \gamma_\sigma \gamma_\nu g_\pm g_\pm + \gamma_\nu \gamma_\sigma g_\mp g_\mp) (\bar{k}^2 g_{\mu\nu} - 2\bar{k}_\mu \bar{k}_\nu) \right. \\
& \left. + \gamma_\sigma \gamma_\mu \sigma_\pm \sigma_\pm \pm \gamma_\mu \gamma_\sigma \sigma_\mp \sigma_\mp \right] \left. \right\} \tag{A.144}
\end{aligned}$$

where we have omitted indices s and t on functions g_\pm and σ_\pm with the understanding that the first always carries index s and the second t . For the amplitude for physical quarks we

get

$$\begin{aligned}
\bar{I}_{\pm}^{odd} &= \frac{g_{\rho\sigma}}{(\widehat{ap-k})^2 + \mu^2} \left\{ \gamma_{\alpha} \left(g_{\rho\sigma} g_{\nu\alpha} (\widehat{ap+k})_{\rho}^2 - 2g_{\rho\nu} g_{\sigma\alpha} (\widehat{ap+k})_{\rho} (\widehat{ap+k})_{\sigma} \right) \right. \\
&\quad \left[(\bar{k}^2 g_{\mu\nu} - 2\bar{k}_{\mu} \bar{k}_{\nu}) \tilde{g}_{\mp} \tilde{g}_{\mp} \pm g_{\mu\nu} \tilde{\sigma}_{\mp} \tilde{\sigma}_{\mp} \right] \\
&\quad + \gamma_{\nu} \frac{r^2}{4} (\widehat{ap+k})_{\rho} (\widehat{ap+k})_{\sigma} \left[\pm (\bar{k}^2 g_{\mu\nu} - 2\bar{k}_{\mu} \bar{k}_{\nu}) \tilde{g}_{\pm} \tilde{g}_{\pm} + g_{\mu\nu} \tilde{\sigma}_{\pm} \tilde{\sigma}_{\pm} \right] \\
&\quad + r (\widehat{ap+k})_{\rho} (\widehat{ap+k})_{\sigma} \left[\gamma_{\sigma} \bar{k}_{\mu} (\pm \tilde{\sigma}_{\mp} \tilde{g}_{\pm} + \tilde{g}_{\mp} \tilde{\sigma}_{\pm}) \right. \\
&\quad \left. + (\bar{k} \cdot \gamma g_{\sigma\mu} - \gamma_{\mu} \bar{k}_{\sigma}) (\pm \tilde{\sigma}_{\mp} \tilde{g}_{\pm} - \tilde{g}_{\mp} \tilde{\sigma}_{\pm}) \right] \left. \right\} [\gamma_5] \tag{A.145}
\end{aligned}$$

$$\begin{aligned}
\tilde{I}_{\pm}^{odd} &= \frac{g_{\rho\sigma}}{(\widehat{ap-k})^2 + \mu^2} \left\{ \gamma_{\alpha} \left(g_{\rho\sigma} g_{\nu\alpha} (\widehat{ap+k})_{\rho}^2 - 2g_{\rho\nu} g_{\sigma\alpha} (\widehat{ap+k})_{\rho} (\widehat{ap+k})_{\sigma} \right) \right. \\
&\quad \left[(\bar{k}^2 g_{\mu\nu} - 2\bar{k}_{\mu} \bar{k}_{\nu}) \tilde{g}_{\mp} \tilde{g}_{\pm} \pm g_{\mu\nu} \tilde{\sigma}_{\mp} \tilde{\sigma}_{\pm} \right] \\
&\quad + \gamma_{\nu} \frac{r^2}{4} (\widehat{ap+k})_{\rho} (\widehat{ap+k})_{\sigma} \left[\pm (\bar{k}^2 g_{\mu\nu} - 2\bar{k}_{\mu} \bar{k}_{\nu}) \tilde{g}_{\pm} \tilde{g}_{\mp} + g_{\mu\nu} \tilde{\sigma}_{\pm} \tilde{\sigma}_{\mp} \right] \\
&\quad + \frac{r}{2} (\widehat{ap+k})_{\rho} (\widehat{ap+k})_{\sigma} \left[\gamma_{\sigma} \tilde{\sigma}_{\mp} \tilde{g}_{\mp} (\bar{k} \cdot \gamma \gamma_{\mu} \pm \gamma_{\mu} \bar{k} \cdot \gamma) \right. \\
&\quad \left. + \tilde{\sigma}_{\pm} \tilde{g}_{\pm} (\bar{k} \cdot \gamma \gamma_{\mu} \pm \gamma_{\mu} \bar{k} \cdot \gamma) \gamma_{\sigma} \right] \left. \right\} [\gamma_5] \tag{A.146}
\end{aligned}$$

$$\begin{aligned}
\bar{I}_{\pm}^{even} &= \frac{g_{\rho\sigma}}{(\widehat{ap-k})^2 + \mu^2} \left\{ i g_{\rho\sigma} (\widehat{ap+k})_{\rho}^2 \left[\gamma_{\mu} \bar{k} \cdot \gamma \tilde{\sigma}_{\pm} \tilde{g}_{\mp} \pm \bar{k} \cdot \gamma \gamma_{\mu} \tilde{g}_{\pm} \tilde{\sigma}_{\mp} \right] \right. \\
&\quad - 2i (\widehat{ap+k})_{\rho} (\widehat{ap+k})_{\sigma} \gamma_{\rho} (\gamma_{\mu} \bar{k}_{\sigma} - \bar{k} \cdot \gamma g_{\sigma\mu}) (\tilde{\sigma}_{\pm} \tilde{g}_{\mp} \pm \tilde{g}_{\pm} \tilde{\sigma}_{\mp}) \\
&\quad - i \frac{r^2}{4} (\widehat{ap+k})_{\rho} (\widehat{ap+k})_{\sigma} (\pm \gamma_{\mu} \bar{k} \cdot \gamma \tilde{\sigma}_{\mp} \tilde{g}_{\pm} + \bar{k} \cdot \gamma \gamma_{\mu} \tilde{g}_{\mp} \tilde{\sigma}_{\pm}) \\
&\quad + i \frac{r}{2} (\widehat{ap+k})_{\rho} (\widehat{ap+k})_{\sigma} \left[(\pm \gamma_{\sigma} \gamma_{\nu} \tilde{g}_{\pm} \tilde{g}_{\pm} + \gamma_{\nu} \gamma_{\sigma} \tilde{g}_{\mp} \tilde{g}_{\mp}) (\bar{k}^2 g_{\mu\nu} - 2\bar{k}_{\mu} \bar{k}_{\nu}) \right. \\
&\quad \left. + \gamma_{\sigma} \gamma_{\mu} \tilde{\sigma}_{\pm} \tilde{\sigma}_{\pm} \pm \gamma_{\mu} \gamma_{\sigma} \tilde{\sigma}_{\mp} \tilde{\sigma}_{\mp} \right] \left. \right\} [\gamma_5] \tag{A.147}
\end{aligned}$$

$$\begin{aligned}
\tilde{I}_{\pm}^{even} &= \frac{g_{\rho\sigma}}{(\widehat{ap-k})^2 + \mu^2} \left\{ i g_{\rho\sigma} (\widehat{ap+k})_{\rho}^2 (\gamma_{\mu} \bar{k} \cdot \gamma \pm \bar{k} \cdot \gamma \gamma_{\mu}) \tilde{g}_{\pm} \tilde{\sigma}_{\pm} \right. \\
&\quad - 2i (\widehat{ap+k})_{\rho} (\widehat{ap+k})_{\sigma} \gamma_{\rho} (\gamma_{\mu} \bar{k}_{\sigma} - \bar{k} \cdot \gamma g_{\sigma\mu}) (\tilde{\sigma}_{\pm} \tilde{g}_{\pm} \pm \tilde{g}_{\pm} \tilde{\sigma}_{\pm}) \\
&\quad - i \frac{r^2}{4} (\widehat{ap+k})_{\rho} (\widehat{ap+k})_{\sigma} (\bar{k} \cdot \gamma \gamma_{\mu} \pm \gamma_{\mu} \bar{k} \cdot \gamma) \tilde{\sigma}_{\mp} \tilde{g}_{\mp} \\
&\quad + i \frac{r}{2} (\widehat{ap+k})_{\rho} (\widehat{ap+k})_{\sigma} (\gamma_{\nu} \gamma_{\sigma} \pm \gamma_{\sigma} \gamma_{\nu}) \left[\tilde{g}_{\pm} \tilde{g}_{\mp} (\bar{k}^2 g_{\mu\nu} - 2\bar{k}_{\mu} \bar{k}_{\nu}) \right. \\
&\quad \left. \pm g_{\mu\nu} \tilde{\sigma}_{\pm} \tilde{\sigma}_{\mp} \right] \left. \right\} [\gamma_5]. \tag{A.148}
\end{aligned}$$

To get the final expression for the amplitude for quark currents $\bar{g} \gamma_{\mu} [\gamma_5] q$, we evaluate the amplitude at zero external momentum to get

$$I_q = \bar{I}_{odd}^+ + \tilde{I}_{even}^- . \tag{A.149}$$

Again, it's easy to see that \tilde{I}_{even}^- vanishes after integration for $p \rightarrow 0$ since it's an odd function of k_μ . After projecting out the component proportional to γ_μ we get

$$\begin{aligned}
I_{V,A}(ap, k) &= \frac{1}{d} \text{Tr}_D \left\{ \tilde{I}_+^{odd} [\gamma_5] \gamma_\mu \right\} \\
&= \frac{g_{\rho\sigma}}{(\widehat{ap-k})^2 + \mu^2} \left\{ g_{\mu\alpha} \left(g_{\rho\sigma} g_{\nu\alpha} (\widetilde{ap+k})_\rho^2 - 2g_{\rho\nu} g_{\sigma\alpha} (\widetilde{ap+k})_\rho (\widetilde{ap+k})_\sigma \right) \right. \\
&\quad \left[(\bar{k}^2 g_{\mu\nu} - 2\bar{k}_\mu \bar{k}_\nu) \tilde{g}_-^2 \pm g_{\mu\nu} \tilde{\sigma}_-^2 \right] \\
&\quad + g_{\mu\nu} \frac{r^2}{4} (\widehat{ap+k})_\rho (\widehat{ap+k})_\sigma \left[\pm (\bar{k}^2 g_{\mu\nu} - 2\bar{k}_\mu \bar{k}_\nu) \tilde{g}_+^2 + g_{\mu\nu} \tilde{\sigma}_+^2 \right] \\
&\quad + r (\widehat{ap+k})_\rho (\widetilde{ap+k})_\sigma \left[g_{\sigma\mu} \bar{k}_\mu (\pm \tilde{\sigma}_- \tilde{g}_+ + \tilde{g}_- \tilde{\sigma}_+) \right. \\
&\quad \left. + (\bar{k}_\mu g_{\sigma\mu} - g_{\mu\mu} \bar{k}_\sigma) (\pm \tilde{\sigma}_- \tilde{g}_+ - \tilde{g}_- \tilde{\sigma}_+) \right] \left. \right\} [\gamma_5] \\
&= \frac{1}{(\widehat{ap-k})^2 + \mu^2} \left\{ g_{\rho\sigma} g_{\rho\sigma} (\widetilde{ap+k})_\rho^2 \left[(\bar{k}^2 - 2\bar{k}_\mu^2) \tilde{g}_-^2 \pm \tilde{\sigma}_-^2 \right] \right. \\
&\quad - 2g_{\mu\mu} (\widetilde{ap+k})_\mu^2 \left[\bar{k}^2 \tilde{g}_-^2 \pm \tilde{\sigma}_-^2 \right] + 4g_{\rho\mu} (\widetilde{ap+k})_\rho (\widetilde{ap+k})_\mu \bar{k}_\rho \bar{k}_\mu \tilde{g}_-^2 \\
&\quad + \frac{r^2}{4} g_{\rho\sigma} (\widehat{ap+k})_\rho (\widehat{ap+k})_\sigma \left[\tilde{\sigma}_+^2 \pm (\bar{k}^2 - 2\bar{k}_\mu^2) \tilde{g}_+^2 \right] \\
&\quad + r (\widehat{ap+k})_\rho \left(g_{\rho\mu} (\widetilde{ap+k})_\mu \bar{k}_\mu (\pm 2g_+ \sigma_-) \right. \\
&\quad \left. + g_{\rho\sigma} (\widetilde{ap+k})_\sigma \bar{k}_\sigma (g_- \sigma_+ \mp g_+ \sigma_-) \right) \left. \right\} [\gamma_5]. \tag{A.150}
\end{aligned}$$

Simplifying further, we get

$$I_{V,A}^{DW,NOS} = \frac{\gamma_\mu}{\hat{k}^2 + \mu^2} \left\{ \frac{4}{d} \sum_\rho \tilde{k}_\rho^2 \bar{k}_\rho^2 \tilde{g}_-^2 + \frac{r^2}{4} \hat{k}^2 \tilde{\sigma}_+^2 + r \bar{k}^2 \tilde{g}_- \tilde{\sigma}_+ \right\} [\gamma_5], \tag{A.151}$$

which agrees with Eqs. (4.5) and (4.6) in [48].

A.3.2.3 Tensor current

Procedure for the tensor current is exactly the same as before (except for the γ algebra), so the amplitude is again given by $I_q = \bar{I}_{odd}^+ + \tilde{I}_{even}^-$, with the term \bar{I}_{odd}^+ vanishing after the integration over k_μ since it's an odd function. That leaves us with the physical amplitude

given by \tilde{I}_-^{even}

$$\begin{aligned}
I_{\mu\nu}^T &= \frac{g_{\rho\sigma}}{(\widehat{ap-k})^2 + \mu^2} \left\{ \frac{r^2}{4} (\widehat{ap+k})_\rho (\widehat{ap+k})_\sigma (\sigma_{\mu\nu} \tilde{\sigma}_+^2 [\mp] [\bar{k}^2 \sigma_{\mu\nu} - 2\bar{k}_\mu \sigma_{k\nu} + 2\bar{k}_\nu \sigma_{k\mu}] \tilde{g}_+^2) \right. \\
&\quad + \left[g_{\rho\sigma} (\widetilde{ap+k})_\rho^2 \sigma_{\mu\nu} + 2(\widetilde{ap+k})_\rho (\widetilde{ap+k})_\sigma (g_{\rho\nu} \sigma_{\sigma\mu} - g_{\rho\mu} \sigma_{\sigma\nu}) \right] (\bar{k}^2 \tilde{g}_-^2 [\mp] \tilde{\sigma}_-^2) \\
&\quad + 2 \left(g_{\rho\sigma} (\widetilde{ap+k})_\rho^2 (\bar{k}_\nu \sigma_{k\mu} - \bar{k}_\mu \sigma_{k\nu}) + 2(\widetilde{ap+k})_\rho (\widetilde{ap+k})_\sigma \right. \\
&\quad \quad \times [\sigma_{\sigma k} (\bar{k}_\nu g_{\rho\mu} - \bar{k}_\mu g_{\rho\nu}) - \bar{k}_\rho (\bar{k}_\nu \sigma_{\sigma\mu} - \bar{k}_\mu \sigma_{\sigma\nu})] \tilde{g}_-^2 \\
&\quad \quad \left. + r(\widetilde{ap+k})_\rho (\widetilde{ap+k})_\sigma [(\tilde{g}_- \tilde{\sigma}_+ [\pm] g_+ \sigma_-) (\bar{k}_\sigma \sigma_{\mu\nu} + g_{\sigma\nu} \sigma_{k\mu} - g_{\sigma\mu} \sigma_{k\nu}) \right. \\
&\quad \quad \left. + (\tilde{g}_- \tilde{\sigma}_+ [\mp] g_+ \sigma_-) (\bar{k}_\mu \sigma_{\sigma\nu} - \bar{k}_\nu \sigma_{\sigma\mu}) \right] \} [\gamma_5], \tag{A.152}
\end{aligned}$$

where we have used the notation

$$\sigma_{k\mu} \equiv \sum_\alpha \bar{k}_\alpha \sigma_{\alpha\mu}. \tag{A.153}$$

To extract the $\sigma_{\alpha\beta}$ component, we multiply by $\sigma_{\alpha\beta}$ and take a trace; the result is then obtained by using the fact that

$$\frac{1}{d} \text{Tr}_D [\sigma_{\mu\nu} \sigma_{\alpha\beta}] = g_{\mu\alpha} g_{\nu\beta} - g_{\mu\beta} g_{\nu\alpha}. \tag{A.154}$$

The final formula is then obtained by replacing $\sigma_{xy} \rightarrow g_{x\alpha} g_{y\beta} - g_{x\beta} g_{y\alpha}$ for all x, y in formula (A.152) and will be omitted here. To simplify, we again take the $p \rightarrow 0$ limit and use the fact that due to parity

$$\int \bar{k}_\mu \bar{k}_\nu f(k^2) = \int \bar{k}^2 g_{\mu\nu} f(k^2) \tag{A.155}$$

and that for domain-wall fermions, $\tilde{g}_+, \tilde{\sigma}_- \rightarrow 0$ to get the result

$$I_T = \frac{\sigma_{\mu\nu}}{\hat{k}^2 + \mu^2} \left\{ \frac{r^2}{4} \hat{k}^2 \tilde{\sigma}_+^2 + \left[4(\bar{k}_\mu^2 \tilde{k}_\mu^2 + \bar{k}_\nu^2 \tilde{k}_\nu^2) + 4(\bar{k}_\mu^2 \tilde{k}_\nu^2 + \bar{k}_\nu^2 \tilde{k}_\mu^2) \right] \tilde{g}_-^2 + r \bar{k}^2 \tilde{g}_- \tilde{\sigma}_+ \right\}. \tag{A.156}$$

Since $\mu \neq \nu$, all integrals with $\bar{k}_\mu^2 \tilde{k}_\nu^2$ are the same, so we can use the identity

$$\bar{k}^2 \tilde{k}^2 = \sum_{\alpha\beta} \bar{k}_\alpha^2 \tilde{k}_\beta^2 = \sum_\alpha \bar{k}_\alpha^2 \tilde{k}_\alpha^2 + \sum_{\alpha \neq \beta} \bar{k}_\alpha^2 \tilde{k}_\beta^2 \tag{A.157}$$

to simplify the coefficient of \tilde{g}_-^2 to get

$$I_T = \frac{\sigma_{\mu\nu}}{\hat{k}^2 + \mu^2} \left\{ \frac{r^2}{4} \hat{k}^2 \tilde{\sigma}_+^2 + r \bar{k}^2 \tilde{g}_- \tilde{\sigma}_+ + \frac{\tilde{g}_-^2}{3} \left[4 \sum_{\rho} \bar{k}_{\rho}^2 \tilde{k}_{\rho}^2 - \bar{k}^2 \tilde{k}^2 \right] \right\}. \quad (\text{A.158})$$

which agrees with Eqs. (4.5) and (4.6) in [48].

A.4 Twist-Two Operators

Here we build upon previous two chapters for current and self energy renormalization to calculate renormalization coefficients for twist-two operators with one derivative. Specifically, we will be looking at the operator $\bar{q}(x)\gamma_{\{\mu}D_{\nu\}}q(x)$. The renormalization of twist-two operators relevant to the analysis of deep inelastic scattering introduces many new elements that are not present for the renormalization of quark self-energies and bilinear operators, such as new Feynman rules associated with the derivatives in the operators and additional graphs. For example, while the vertex diagram with this operator insertion is very similar to the vertex diagram for local currents, a new feature that appears here are the ‘‘sails’’ diagrams.

However, before we evaluate the twist-two amplitudes, we need to evaluate the Feynman rules for twist-two operators. The derivative operator D_{ν} on the lattice contains all powers of the gluon field A_{μ} , so we expand it in powers of g_0 . For one-loop corrections we need only terms up to order g_0^2

$$\mathcal{O}_{\mu\nu} = \mathcal{O}_{\mu\nu}^{(0)} + g_0 \mathcal{O}_{\mu\nu}^{(1)} + g_0^2 \mathcal{O}_{\mu\nu}^{(2)}. \quad (\text{A.159})$$

We then perform the Fourier transform to momentum space (the details of the expansion can be found in [51]). The result for the Feynman rules is then given by

$$\mathcal{O}_{\mu\nu}^{(0)}(p, k) = i\gamma_{\mu}\bar{k}_{\nu} \quad (\text{A.160})$$

$$\mathcal{O}_{\mu\nu}^{(1)}(p, k) = T^a i\gamma_{\mu} \cos \frac{(ap + k)_{\nu}}{2} \quad (\text{A.161})$$

$$\mathcal{O}_{\mu\nu}^{(2)}(p, k) = -\frac{a^2}{2} \{T^a, T^b\} \bar{p}_{\nu} \rightarrow -\frac{a^2}{2} C_F \gamma_{\mu} \bar{p}_{\nu}, \quad (\text{A.162})$$

where in the last step we have performed the summation over the group index

$$\text{Tr} \sum_a \delta^{ab} \{T^a, T^b\} = \frac{N_c^2 - 1}{2N_c} = C_F. \quad (\text{A.163})$$

The zeroth-order $\mathcal{O}_{\mu\nu}^{(0)}$ contributes to the vertex diagram, the first-order contributes to the sails diagrams, and the second order contributes to the tadpole diagram.

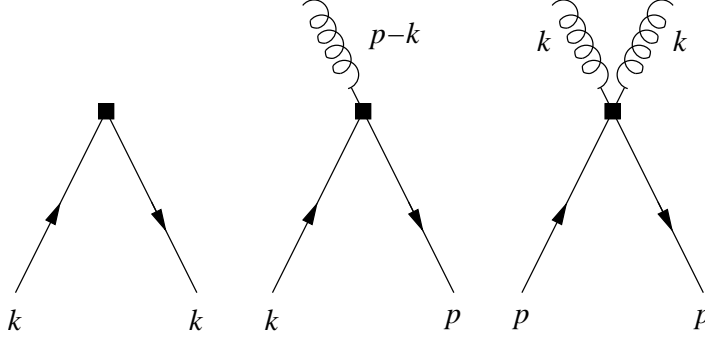


Figure A.4: *Momentum conventions for the twist-two operator $\bar{q}(x)\Gamma D_\nu \bar{q}$ (denoted by the box). Solid and curly lines represent fermions and gluons, respectively.*

The next step is to consider the Lorentz-index structure of the amplitude. The general structure of a particular one-loop diagram for a twist-two operator is [49]

$$J_{\mu\nu}(p) = \langle q(p) | \gamma_\mu D_\nu | q(p) \rangle = c_1 \gamma_\mu p_\nu + c_2 \gamma_\nu p_\mu + c_3 g_{\mu\nu} \gamma_\mu p_\mu + c_4 g_{\mu\nu} p \cdot \gamma + c_5 \frac{p_\mu p_\nu}{p^2} p \cdot \gamma. \quad (\text{A.164})$$

For operators in the $\mathbf{6}_3^+$ representation, $\mu \neq \nu$, so only terms c_1 and c_2 contribute

$$\langle q(p) | \gamma_1 D_4 | q(p) \rangle = (c_1 + c_2) \frac{\gamma_1 p_4 + \gamma_4 p_1}{2}. \quad (\text{A.165})$$

On the other hand, for the $\mathbf{3}_1^+$ representation, c_3 will contribute as well

$$\begin{aligned} & \left\langle q(p) \left| \left[\gamma_4 D_4 - \frac{1}{3} (\gamma_1 D_1 + \gamma_2 D_2 + \gamma_3 D_3) \right] \right| q(p) \right\rangle \\ &= (c_1 + c_2 + c_3) \left[\gamma_4 p_4 - \frac{1}{3} (\gamma_1 p_1 + \gamma_2 p_2 + \gamma_3 p_3) \right]. \end{aligned} \quad (\text{A.166})$$

We can see that the term proportional to $p \cdot \gamma g_{\mu\nu}$ does not contribute, so we want to eliminate it. To extract coefficients c_i in the case $\mu \neq \nu$, we multiply the amplitude with γ_α and take

a trace to get

$$\frac{1}{d}\text{Tr}[J_{\mu\nu}\gamma_\alpha] = c_1 g_{\mu\alpha} p_\nu + c_2 g_{\nu\alpha} p_\mu + c_3 g_{\mu\nu} g_{\mu\alpha} p_\mu + c_4 g_{\mu\nu} p_\alpha. \quad (\text{A.167})$$

For the $\mathbf{6}_3^+$ representation, we choose $\alpha = \mu, \nu$ and add them up

$$\frac{1}{p_4} \frac{1}{d} \text{Tr}[J_{14}\gamma_1] = c_1 \quad (\text{A.168})$$

$$\frac{1}{p_1} \frac{1}{d} \text{Tr}[J_{14}\gamma_4] = c_2. \quad (\text{A.169})$$

Alternatively, we can take the symmetrized combination $J_{\mu\nu} + J_{\nu\mu}$ to get⁶

$$\frac{1}{p_4} \frac{1}{d} \text{Tr}[(J_{14} + J_{41})\gamma_1] = c_1 + c_2 \quad (\text{A.170})$$

For the $\mathbf{3}_1^+$ representation, we first choose $\mu = \nu = \alpha$ to get

$$\frac{1}{d} \text{Tr}[J_{\mu\mu}\gamma_\mu] = (c_1 + c_2 + c_3 + c_4)p_\mu. \quad (\text{A.171})$$

To eliminate the c_4 term, note that if we choose $\mu = \nu \neq \alpha$ (for definiteness, let's pick $\mu = 4$ and $\alpha = 3$), we get

$$\frac{1}{d} \text{Tr}[J_{44}\gamma_3] = c_1 g_{43} p_4 + c_2 g_{43} p_4 + c_3 g_{44} g_{43} p_4 + c_4 g_{44} p_3 = c_4 p_3 \quad (\text{A.172})$$

so dividing by p_α will give us the c_4 coefficient

$$\frac{1}{p_\alpha} \frac{1}{d} \text{Tr}[J_{\mu\mu}\gamma_\alpha] = c_4. \quad (\text{A.173})$$

So, for the $\mathbf{3}_1^+$ representation the final result is

$$c_1 + c_2 + c_3 = \frac{1}{p_\mu} \frac{1}{d} \text{Tr}[J_{\mu\mu}(\gamma_\mu - \gamma_\alpha)], \quad (\text{A.174})$$

where we have chosen $\mu \neq \alpha$ and the vector p such that the components p_μ and p_α are

⁶Here we choose the momentum p_μ to have only the p_4 component nonzero, so the term $p_\mu p_\nu / p^2 p \cdot \gamma$ does not contribute. If our 4-momentum had both components p_1 and p_4 nonzero, we would have to subtract $-2\text{Tr}[J_{14}\gamma_\alpha]$ with $\alpha \neq 1, 4$ to cancel the extra contribution.

numerically equal. For the example above it would be

$$p_\mu = \left\{ 0, 0, \sqrt{\frac{p^2}{2}}, \sqrt{\frac{p^2}{2}} \right\}. \quad (\text{A.175})$$

For the operator $\bar{q}\gamma_\mu\gamma_5 D_\nu q$ we multiply by $\gamma_5\gamma_\alpha$ instead of γ_α . With all this done, we can now consider individual diagrams.

A.4.1 Vertex diagram

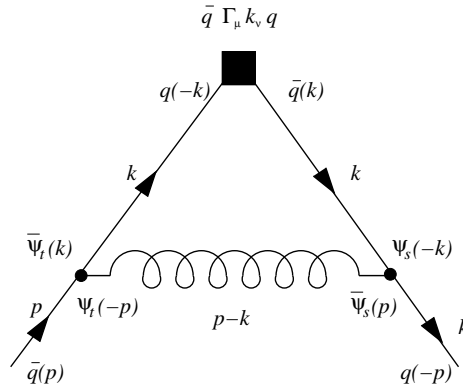


Figure A.5: Vertex diagram for twist-two operators (denoted by the box). Solid and curly lines represent fermions and gluons, respectively.

The only difference between amplitude expressions for the vertex diagram for current and twist-two operators is the different Feynman rule for the operator \mathcal{O} :

$$\begin{aligned} \mathcal{O} &= \bar{q}(x)\Gamma q(x) && \implies \Gamma \\ \mathcal{O} &= \bar{q}(x)\Gamma D_\nu q(x) && \implies \Gamma i\bar{k}_\nu. \end{aligned} \quad (\text{A.176})$$

This means that the integrand $I_{\mu\nu}(ap, k)$ for the amplitude $J_{\mu\nu}(ap)$ for the twist-two operator $\mathcal{O}_{\mu\nu} = \bar{q}(x)\gamma_\mu D_\nu q(x)$ can be written in terms of an integrand $I_\mu(ap, k)$ for amplitude for the current $\mathcal{O}_{\mu\nu} = \bar{q}(x)\gamma_\mu q(x)$ given in Eq. (A.148) as

$$J_{\mu\nu}(ap) = \int_{-\pi}^{\pi} \frac{d^d k}{(2\pi)^d} I_{\mu\nu}(ap, k) = \int_{-\pi}^{\pi} \frac{d^d k}{(2\pi)^d} I_\mu(ap, k) i\bar{k}_\nu. \quad (\text{A.177})$$

All that remains to be done is symmetrization in indices and projecting out the desired part as discussed in the previous subsection. As before, the physical amplitude is the sum of odd

and even terms in Eq. A.130, but now, since we are expanding to first order in p_μ , we have to keep terms with $p \cdot \gamma$ as well. Terms \tilde{I}_{odd}^\pm and \bar{I}_{even}^\pm are evaluated to 0^{th} order in p ; \tilde{I}_{odd}^\pm vanishes since it's odd in k_μ . The term $\tilde{I}_{even}^-(p \rightarrow 0)$ is even in k_μ which means $\partial \tilde{I}_{even}^- / \partial p_\mu$ will be odd and won't contribute. $\bar{I}_{odd}^+(p \rightarrow 0)$ is odd so it vanishes as well. Hence, we are left with

$$I_q(p) = p_\alpha \frac{\partial \bar{I}_{odd}^+}{\partial p_\alpha}[\gamma_5] + (-ip \cdot \gamma \mathcal{A}) \bar{I}_{even}^+[\gamma_5] + \bar{I}_{even}^-[\gamma_5] (-ip \cdot \gamma \mathcal{A}). \quad (\text{A.178})$$

Since we are evaluating \bar{I}_{even}^\pm at zero momentum, after symmetrizing in μ and ν , it must be proportional to

$$\bar{I}_{even}^\pm \sim g_{\mu\nu} \times const. \quad \implies \quad (-ip \cdot \gamma \mathcal{A}) \bar{I}_{even}^+[\gamma_5] + \bar{I}_{even}^-[\gamma_5] (-ip \cdot \gamma \mathcal{A}) \sim p \cdot \gamma g_{\mu\nu} \quad (\text{A.179})$$

so it does not contribute in either representation we are interested in. We are now left with

$$I_q(p) = p_\alpha \frac{\partial \bar{I}_{odd}^+}{\partial p_\alpha}[\gamma_5]. \quad (\text{A.180})$$

Instead of expanding the amplitude, to get the finite piece we can use the numerical method discussed in the self energy section.

A.4.2 Sails diagrams

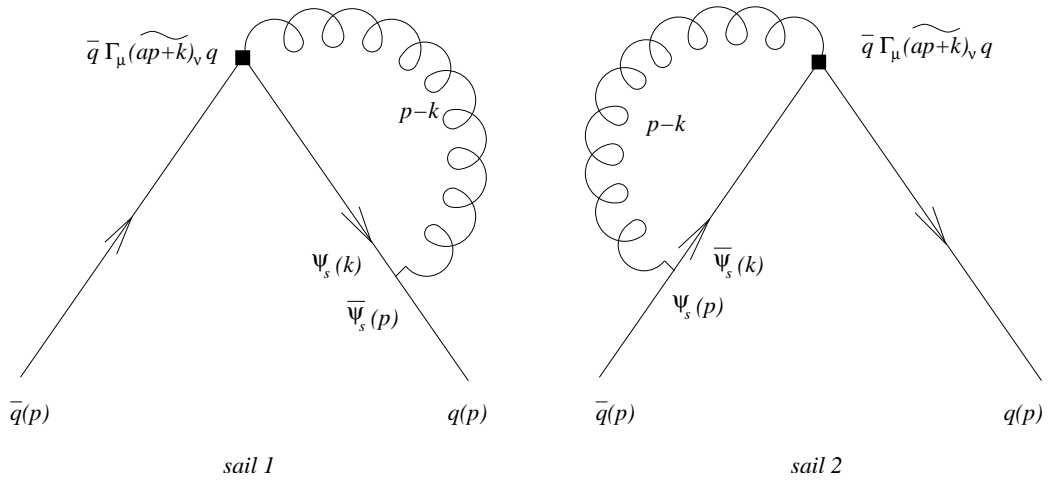


Figure A.6: *Sails diagram for twist-two operators (denoted by the box). Solid and curly lines represent fermions and gluons, respectively.*

Since the amplitudes for the two sails diagrams are related, we will evaluate them together. They are given by

$$I_s^{(1)} = G_{\nu\rho}(p-k)V_\rho(p,k)S_s^{IN}\mathcal{O}_{\mu\nu} \quad (\text{A.181})$$

$$I_s^{(2)} = G_{\nu\rho}(p-k)\mathcal{O}_{\mu\nu}S_s^{OUT}V_\rho(k,p). \quad (\text{A.182})$$

Physical amplitudes are then obtained by adding the 5D-to-physical propagator and amputating the external leg

$$I_1 = \bar{S}_s^{OUT}I_s^{(1)} = \bar{S}_s^{OUT}V_\rho(p,k)S_s^{IN}\mathcal{O}_{\mu\nu}G_{\nu\rho}(p-k) \quad (\text{A.183})$$

$$I_2 = I_s^{(2)}\bar{S}_s^{IN} = \mathcal{O}_{\mu\nu}S_s^{OUT}V_\rho(k,p)G_{\nu\rho}(p-k)\bar{S}_s^{IN}. \quad (\text{A.184})$$

As in the case of vertex diagram, part of \bar{S}_s^{OUT} and \bar{S}_s^{IN} proportional to $p \cdot \gamma$ will give us a contribution proportional to $p \cdot \gamma g_{\mu\nu}$ so we can neglect it from the start. Contracting with $\bar{S}_{IN,OUT}$, adding them up, and simplifying the γ algebra, we get

$$\begin{aligned} I_{\mu\nu} = & \frac{g_0^2 C_F g_{\nu\rho} (\widehat{ap+k})_\nu}{(\widehat{ap-k})^2 + \mu^2} \left\{ -2\gamma_\mu \frac{r}{2} (\widehat{ap+k})_\rho \tilde{\sigma}_+ \right. \\ & - 2 \left(\bar{k}_\mu \gamma_\rho (\widehat{ap+k})_\rho - \bar{k} \cdot \gamma g_{\rho\mu} (\widehat{ap+k})_\mu + \gamma_\mu \bar{k}_\rho (\widehat{ap+k})_\rho \right) \tilde{g}_- \\ & \left. + \frac{r}{2} i (\widehat{ap+k})_\rho [\bar{k} \cdot \gamma, \gamma_\mu]_\pm \tilde{g}_+ + i (\widehat{ap+k})_\rho [\gamma_\rho, \gamma_\mu]_\pm \tilde{\sigma}_- \right\} [\gamma_5], \quad (\text{A.185}) \end{aligned}$$

where $[\dots, \dots]_\pm$ is the commutator/anticommutator of γ matrices. For $p \rightarrow 0$, the first two lines are odd while the third one is even, so to order p^1 the third line vanishes due to parity⁷. That gives us the final result

$$\begin{aligned} I_{\mu\nu} = & \frac{g_0^2 C_F g_{\nu\rho} (\widehat{ap+k})_\nu}{(\widehat{ap-k})^2 + \mu^2} \left\{ \gamma_\mu (-r) (\widehat{ap+k})_\rho \tilde{\sigma}_+ \right. \\ & \left. - 2 \left(\bar{k}_\mu \gamma_\rho (\widehat{ap+k})_\rho - \bar{k} \cdot \gamma g_{\rho\mu} (\widehat{ap+k})_\mu + \gamma_\mu \bar{k}_\rho (\widehat{ap+k})_\rho \right) \tilde{g}_- \right\}. \quad (\text{A.186}) \end{aligned}$$

⁷To zeroth-order in p_μ it gives a finite contribution proportional to either $g_{\mu\nu}$ or $\sigma_{\mu\nu}$. The $\sigma_{\mu\nu}$ contribution is killed by symmetrization, while $g_{\mu\nu}$ does not contribute to either representation we are considering.

The amplitude for the $\mathbf{6}_3^+$ representation is then

$$\begin{aligned}
I_q &= \frac{1}{d} \text{Tr}_D [(\bar{I}_{\mu\nu} + \bar{I}_{\nu\mu})\gamma_\mu] \frac{1}{p_\nu} \\
&= \frac{1}{p_\nu} \frac{g_0^2 C_F}{(\widehat{ap-k})^2 + \mu^2} \left\{ \sum_\rho g_{\nu\rho}(\widehat{ap+k})_\nu \left[-r(\widehat{ap+k})_\rho \tilde{\sigma}_+ - 2\tilde{g}_- \bar{k}_\rho(\widehat{ap+k})_\rho \right] \right. \\
&\quad \left. - 2\tilde{g}_-(\widehat{ap+k})_\mu \left[g_{\mu\mu}(\widehat{ap+k})_\mu \bar{k}_\nu - g_{\mu\nu}(\widehat{ap+k})_\nu \bar{k}_\mu \right] \right\}. \tag{A.187}
\end{aligned}$$

After simplifying, this becomes

$$\begin{aligned}
I_q &= \frac{1}{p_\nu} \frac{g_0^2 C_F}{(\widehat{ap-k})^2 + \mu^2} \left\{ -r(\widehat{ap+k})_\nu \tilde{\sigma}_+ \right. \\
&\quad \left. - 2 \left(\bar{k}_\nu(\widehat{ap+k})_\mu^2 + \bar{k}_\nu(\widehat{ap+k})_\nu^2 \right) \tilde{g}_- \right\}. \tag{A.188}
\end{aligned}$$

and after expansion in p_μ to first order this yields

$$\begin{aligned}
I_q &= g_0^2 C_F \left\{ \frac{1}{\hat{k}^2 + \mu^2} \left[-2r \cos k_\nu \tilde{\sigma}_+ + \bar{k}_\nu^2 \tilde{g}_- \right] \right. \\
&\quad \left. - \frac{1}{(\hat{k}^2 + \mu^2)^2} \left[r \bar{k}_\nu^2 \tilde{\sigma}_+ + 4\tilde{g}_- \bar{k}_\nu^2 (\tilde{k}_\nu^2 + \tilde{k}_\mu^2) \right] \right\}. \tag{A.189}
\end{aligned}$$

For Wilson fermions, this agrees with Capitani's formula (15.102) In the $\mathbf{3}_1^+$ representation we have $\mu = \nu$. Using formulas from the previous section, we get

$$I_q = \frac{1}{p_\mu} \frac{1}{d} \text{Tr} [I_{\mu\mu}(\gamma_\mu - \gamma_\alpha)], \tag{A.190}$$

where $\mu \neq \alpha$ and the four-vector p has components p_μ and p_α numerically equal. This yields

$$\begin{aligned}
I_q &= \frac{1}{p_\mu} \frac{g_0^2 C_F}{(\widehat{ap-k})^2 + \mu^2} \left\{ g_{\mu\rho}(\widehat{ap+k})_\mu \left[-r(\widehat{ap+k})_\rho \tilde{\sigma}_+ - 2\tilde{g}_- \bar{k}_\rho(\widehat{ap+k})_\rho \right] \right. \\
&\quad \left. - 2\tilde{g}_-(\widehat{ap+k})_\mu \left[g_{\mu\mu} \bar{k}_\alpha(\widehat{ap+k})_\mu - g_{\mu\alpha} \bar{k}_\mu(\widehat{ap+k})_\alpha \right] \right\}. \tag{A.191}
\end{aligned}$$

This becomes

$$I_q = \frac{1}{p_\mu} \frac{g_0^2 C_F}{(\widehat{ap-k})^2 + \mu^2} \left\{ -r(\widehat{ap+k})_\mu \tilde{\sigma}_+ - 2\tilde{g}_-(\widehat{ap+k})_\mu^2 [\bar{k}_\mu + \bar{k}_\alpha] \right\}, \tag{A.192}$$

which after expansion in p_μ yields

$$I_q = g_0^2 C_F \left\{ \frac{1}{\hat{k}^2 + \mu^2} [\cos k_\mu \tilde{\sigma}_+ + \bar{k}_\mu^2 \tilde{g}_-] - \frac{1}{(\hat{k}^2 + \mu^2)^2} [r \bar{k}_\mu^2 \tilde{\sigma}_+ + 4\tilde{g}_- \tilde{k}_\mu^2 (\bar{k}_\mu^2 + \bar{k}_\alpha^2)] \right\}. \quad (\text{A.193})$$

This is numerically the same as expression (A.189) since indices μ and α can be exchanged in term with $\tilde{k}_\mu^2 \bar{k}_\alpha^2$. Another way to see this is to observe that the amplitude $I_{\mu\nu}$ has no parts proportional to $g_{\mu\nu} \gamma_\mu p_\mu$, which causes the difference between the two representations:

$$I_{\mu\nu} = \frac{g_0^2 C_F}{(\widehat{ap - k})^2 + \mu^2} \left\{ \frac{r}{2} (\overline{ap + k})_\nu \tilde{\sigma}_+ - 2 \left(\bar{k}_\mu \gamma_\nu (\widetilde{ap + k})_\nu^2 - \bar{k} \cdot \gamma (\widetilde{ap + k})_\mu (\widetilde{ap + k})_\nu + \gamma_\mu \bar{k}_\nu (\widetilde{ap + k})_\rho^2 \right) \tilde{g}_- \right\}. \quad (\text{A.194})$$

which, after expansion in p_μ to first order, yields

$$I_{\mu\nu} = \frac{g_0^2 C_F \gamma_\mu p_\nu}{\hat{k}^2 + \mu^2} \{ \cos k_\nu \tilde{\sigma}_+ + \bar{k}_\nu^2 \tilde{g}_- \} - \frac{g_0^2 C_F}{(\hat{k}^2 + \mu^2)^2} \left\{ \gamma_\mu p_\nu r \bar{k}_\nu^2 \tilde{\sigma}_+ + 4\tilde{g}_- \left(\gamma_\mu p_\nu \bar{k}_\nu^2 \tilde{k}_\nu^2 + \gamma_\nu p_\mu \bar{k}_\mu^2 \tilde{k}_\nu^2 \right) \right\}. \quad (\text{A.195})$$

After symmetrization in μ and ν we get expressions (A.189) and (A.193).

A.4.3 Tadpole diagram

The amplitude for the tadpole diagram is given by

$$J_q(p) = \int_{-\pi/a}^{\pi/a} \frac{d^d k}{(2\pi)^d} G_{\nu\nu}(k) \mathcal{O}_{\mu\nu}^{aa}(p, p). \quad (\text{A.196})$$

The operator vertex expanded to second order in g_0

$$\mathcal{O}_{\mu\nu}^{(2)} = -\frac{a^2}{2} \{T^a, T^b\} \bar{p}_\nu \rightarrow -\frac{a^2}{2} C_F \gamma_\mu \bar{p}_\nu \quad (\text{A.197})$$

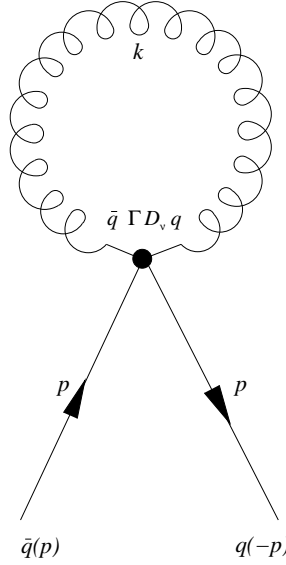


Figure A.7: *Tadpole diagram for twist-two operators (denoted by the box). Solid and curly lines represent fermions and gluons, respectively.*

is independent of the loop momentum so (after rescaling the loop momentum) we are left with the amplitude

$$J_q(p) = -\frac{1}{2}g_0^2 C_F i\gamma_\mu p_\nu T = -\frac{g_0^2 C_F}{16\pi^2} i\gamma_\mu p_\nu (8\pi^2 T) = i\gamma_\mu p_\nu \frac{g_0^2 C_F}{16\pi^2} \Sigma^{OPtad} \quad (\text{A.198})$$

where T is the tadpole integral

$$T = \lim_{\mu^2 \rightarrow 0} T(\mu^2) = \lim_{\mu^2 \rightarrow 0} \frac{1}{d} \int_{-\pi}^{\pi} \frac{d^d k}{(2\pi)^d} \sum_{\rho} \frac{g_{\rho\rho}}{\hat{k}^2 + \mu^2} \quad (\text{A.199})$$

and

$$\Sigma^{OPtad} = -8\pi^2 T \quad (\text{A.200})$$

has already been encountered in the self-energy renormalization. Note that the tadpole contribution does not depend on the γ structure of the operator.

A.5 Conclusions

In this appendix we calculated renormalization factors for twist-two operators in domain-wall QCD at one-loop in perturbation theory, with no smearing. The main results of our work are numerical values for the \bar{Z}_{jk} for matrix elements of operators (listed in Table A.3).

Operator	$H(4)$	Wilson	DW M=1.6	DW M=1.7	M=1.8	M=1.9	\overline{MS}
$\bar{q}q$	1_1^-	6.101	16.401	17.313	18.425	19.875	6
$\bar{q}\gamma_5q$	1_1^+	15.743	16.401	17.313	18.425	19.875	6
$\bar{q}\gamma_\mu q$	4_4^-	8.765	6.422	6.436	6.452	6.471	1
$\bar{q}\gamma_\mu\gamma_5q$	4_4^+	3.944	6.422	6.436	6.452	6.471	1
$\bar{q}\sigma_{\mu\nu}q$	6_1^-	4.166	2.428	2.142	1.793	1.334	0
$\bar{q}\gamma_{\{\mu}D_{\nu\}}q$	6_3^+	-15.016	-14.868	-14.771	-14.653	-14.499	-31/9
$\bar{q}\gamma_{\{\mu}D_{\nu\}}q$	3_1^+	-13.734	-13.92	-13.758	-13.568	-13.334	-31/9

Table A.3: *Final results for Wilson and DW fermions, with no smearing.*

To provide as many cross checks as possible, we have compared our results in various limits with those obtained in [47], [48], and [51], and find perfect agreement. The introductory nature of this appendix, and the following Appendix B, can also serve to establish the basics of perturbative renormalization with DW quarks.

Appendix B

Domain-Wall Propagators

It is simplest to begin with a fifth dimension of infinite extent, and subsequently consider the corrections associated with the boundaries for the semi-infinite and finite cases. It is easiest to first compute the inverse of $\Omega_{s,s'}^0(p) \equiv [D^0(D^0)^\dagger]_{s,s'}$. Then, one has

$$[(D^0)^{-1}]_{s,s'} = [(D^0)^\dagger G^0]_{s,s'} \quad G_{s,s'}^0(p) \equiv [\Omega^0(p)^{-1}]_{s,s'}. \quad (\text{B.1})$$

Explicitly, one has

$$\Omega_{s,s'}^0 = \left(\frac{1}{a_5^2} + W^2(p) + \bar{p}^2 \right) \delta_{s,s'} - \frac{W(p)}{a_5} (\delta_{s,s'+1} + \delta_{s,s'-1}). \quad (\text{B.2})$$

We now define $\alpha(p)$ via

$$\cosh \alpha(p) = \frac{\frac{1}{a_5^2} + W^2(p) + \bar{p}^2}{2|W(p)|/a_5}. \quad (\text{B.3})$$

It is then straightforward to show that

$$G_{s,s'}^0 = A_0 e^{-\alpha|s-s'|}, \quad (\text{B.4})$$

$$A_0^{-1} \equiv 2 \frac{W(p)}{a_5} \sinh \alpha. \quad (\text{B.5})$$

The resulting propagator is given by

$$[(D^0)^{-1}]_{s,s'} = S_{s,s'}^+ P_+ + S_{s,s'}^- P_- \quad (\text{B.6})$$

$$S_{s,s'}^\pm = \left(\frac{1}{2W \sinh \alpha} \right) \left[e^{-\alpha|s-s' \mp 1|} - a_5(i\bar{p} \cdot \gamma + W) e^{-\alpha|s-s'|} \right]. \quad (\text{B.7})$$

We now proceed to compute the propagator for the semi-infinite fifth dimension, for

which the Dirac operator is given by

$$D_{s,s'}(p) = \theta(s-1)\theta(s'-1)D_{s,s'}^0(p). \quad (\text{B.8})$$

Again, we first find the inverse of $\Omega_{s,s'} = [DD^\dagger]_{s,s'}$. In carrying out the matrix multiplication to obtain an explicit expression for $\Omega_{s,s'}$, one must take care to restrict the sum over intermediate values of s to the positive integers. Doing so leads to

$$\Omega_{s,s'} = \Omega_{s,s'}^0 - \frac{1}{a_5^2} P_- \delta_{s,1} \delta_{s',1} \quad (\text{B.9})$$

$$\equiv \Omega_{s,s'}^+ P_+ + \Omega_{s,s'}^- P_- \quad (\text{B.10})$$

$$\Omega_{s,s'}^+ = \Omega_{s,s'}^0 \quad (\text{B.11})$$

$$\Omega_{s,s'}^- = \Omega_{s,s'}^0 - \frac{1}{a_5^2} \delta_{s,1} \delta_{s',1}. \quad (\text{B.12})$$

The inverse, G , of Ω has a similar decomposition:

$$G_{s,s'} = G_{s,s'}^+ P_+ + G_{s,s'}^- P_- \quad \text{with} \quad G_{s,t}^\pm \Omega_{t,s'}^\pm = \delta_{s,s'}. \quad (\text{B.13})$$

For large values of s, s' , one expects boundary effects to be suppressed and $G^\pm \approx G^0$. Thus, a reasonable *ansatz* is

$$G_{s,s'}^\pm = G_{s,s'}^0 + A_\pm e^{-\alpha(s+s'-2)}. \quad (\text{B.14})$$

Expressions for the A_\pm are obtained by requiring $[\Omega^\pm G^\pm]_{s,s'} = \delta_{s,s'}$. Notice that for all $s > 1$, $\Omega_{s,t}^\pm G_{t,s'}^0 = \delta_{s,s'}$ and $\Omega_{s,t}^\pm e^{-\alpha t} = 0$. We must therefore pay special attention to the behavior of $[\Omega^\pm G^\pm]_{s,s'}$ at the boundary $s = 1$. After considerable algebra one obtains

$$\begin{aligned} [\Omega^- G^-]_{s,s'} &= \delta_{s,s'} = \sum_{t \geq 1} \Omega_{s,t}^- G_{t,s'}^0 + \sum_{t \geq 1} \Omega_{s,t}^- A_- e^{-\alpha(t+s'-2)} \\ &= \delta_{s,s'} + \frac{W a_5 - e^\alpha}{2W a_5 \sinh \alpha} e^{-\alpha s'} \delta_{1,s'} + A_- e^{-\alpha(s'-2)} \left(\frac{W}{a_5} - \frac{e^{-\alpha}}{a_5^2} \right) \delta_{1,s'} \end{aligned} \quad (\text{B.15})$$

$$\begin{aligned} [\Omega^+ G^+]_{s,s'} &= \delta_{s,s'} = \sum_{t \geq 1} \Omega_{s,t}^+ G_{t,s'}^0 + \sum_{t \geq 1} \Omega_{s,t}^+ A_+ e^{-\alpha(t+s'-2)} \\ &= \delta_{s,s'} + \frac{1}{2 \sinh \alpha} e^{-\alpha s'} \delta_{1,s'} + A_+ e^{-\alpha(s'-2)} \left(\frac{W}{a_5} \right) \delta_{1,s'}. \end{aligned} \quad (\text{B.16})$$

From these equations we get the constraints

$$\begin{aligned} A_-(W a_5 e^\alpha - 1)e^\alpha &= -A_0(W a_5 - e^\alpha) \\ A_+ \frac{W}{a_5} e^{2\alpha} &= -A_0 \frac{W}{a_5}, \end{aligned} \quad (\text{B.17})$$

with solutions

$$A_- = -A_0 \frac{1 - W a_5 e^{-\alpha}}{1 - W a_5 e^\alpha}, \quad A_+ = -A_0 e^{-2\alpha}. \quad (\text{B.18})$$

The resulting expression for the propagator is

$$[D^{-1}]_{s,s'} = S_{s,s'}^+ P_+ + S_{s,s'}^- P_- \quad (\text{B.19})$$

$$S_{s,s'}^+ = -(i\bar{p} \cdot \gamma + W) \left(G_{s,s'}^0 + A_+ e^{-\alpha|s+s'|} \right) \quad (\text{B.20})$$

$$+ \frac{1}{a_5} \left(G_{s-1,s'}^0 + A_+ e^{-\alpha|s+s'-1|} \right) (1 - \delta_{1,s'}) \quad (\text{B.21})$$

$$S_{s,s'}^- = -(i\bar{p} \cdot \gamma + W) \left(G_{s,s'}^0 + A_- e^{-\alpha|s+s'|} \right) \quad (\text{B.22})$$

$$+ \frac{1}{a_5} \left(G_{s+1,s'}^0 + A_- e^{-\alpha|s+s'+1|} \right). \quad (\text{B.23})$$

The derivation of the propagator for the finite fifth dimension case proceeds along similar lines. Starting with

$$\hat{D}_{s,s'}(p) = \theta(s-1)\theta(s'-1)\theta(N-s)\theta(N-s')D_{s,s'}^0(p), \quad (\text{B.24})$$

where s, s' are now restricted to the range $1 \leq s, s' \leq N$, leads to $\hat{\Omega}_{s,s'} = \hat{\Omega}_{s,s'}^+ P_+ + \hat{\Omega}_{s,s'}^- P_-$ with

$$\hat{\Omega}_{s,s'}^+ = \Omega_{s,s'}^0 - \frac{1}{a_5^2} \delta_{s,N} \delta_{s',N} \quad (\text{B.25})$$

$$\hat{\Omega}_{s,s'}^- = \Omega_{s,s'}^0 - \frac{1}{a_5^2} \delta_{s,1} \delta_{s',1}. \quad (\text{B.26})$$

From these expressions, one notes that

$$\hat{\Omega}_{s,s'}^\pm = \hat{\Omega}_{N-(s-1),N-(s'-1)}^\mp. \quad (\text{B.27})$$

It is then straightforward to show that if $\hat{\Omega}_{s,t}^- \hat{G}_{t,s'}^- = \delta_{s,s'}$, one has $\hat{\Omega}_{s,t}^+ \hat{G}_{N-(t-1),N-(s'-1)}^- = \delta_{s,s'}$, or $\hat{G}_{s,s'}^+ = \hat{G}_{N-(s-1),N-(s'-1)}^-$. Hence, it suffices to determine $\hat{G}_{s,s'}^-$ or $\hat{G}_{s,s'}^+$.

We again make the reasonable *ansatz*

$$\hat{G}_{s,s'}^{\pm} = G_{s,s'}^0 + \hat{A}_{\pm} e^{-\alpha(s+s'-2)} + \hat{A}_{\mp} e^{-\alpha(2N-s-s')} \quad (\text{B.28})$$

and solve for the \hat{A}_{\pm} by considering $\hat{\Omega}_{s,t}^- \hat{G}_{t,s'}^- = \delta_{s,s'}$ at $s = 1$ and $s = N$. Doing so leads to

$$A_- = A_0 \frac{W a_5 e^{-\alpha} - 1}{f_N} \quad (\text{B.29})$$

$$A_+ = A_0 \frac{W a_5 e^{\alpha} - 1}{f_N} e^{-2\alpha} \quad (\text{B.30})$$

$$f_N = 1 - W a_5 e^{\alpha} - e^{-2\alpha N} (1 - W a_5 e^{-\alpha}) . \quad (\text{B.31})$$

Note that in the $N \rightarrow \infty$ limit, one recovers the expressions in Eqs. (B.18) and (B.14).

In practical calculations, one always works with quarks having non-zero mass, m . Since the physical quarks are defined as linear combinations of the quarks living at $s = 1$ and $s = N$, we add mass terms on the boundaries to the Dirac operator in Eq. (B.24):

$$\hat{D}_{s,s'}(m) = \theta(s-1)\theta(s'-1)\theta(N-s)\theta(N-s')D_{s,s'}^0 + mP_- \delta_{s,1} \delta_{s',N} + mP_+ \delta_{s,N} \delta_{s',1} \quad (\text{B.32})$$

which leads to

$$\hat{\Omega}_{s,s'}^+ = \Omega_{s,s'}^0 - mW(p)[\delta_{s,1} \delta_{s',N} + \delta_{s,N} \delta_{s',1}] - \left(\frac{1}{a_5^2} - m^2 \right) \delta_{s,N} \delta_{s',N} \quad (\text{B.33})$$

$$\hat{\Omega}_{s,s'}^- = \Omega_{s,s'}^0 - mW(p)[\delta_{s,1} \delta_{s',N} + \delta_{s,N} \delta_{s',1}] - \left(\frac{1}{a_5^2} - m^2 \right) \delta_{s,1} \delta_{s',1} . \quad (\text{B.34})$$

The symmetry condition $\hat{\Omega}_{s,s'}^{\pm} = \hat{\Omega}_{N-(s-1),N-(s'-1)}^{\mp}$ is unchanged by the presence of the terms proportional to m , so it again suffices to determine either $\hat{G}_{s,s'}^-$ or $\hat{G}_{s,s'}^+$. We take

$$\hat{G}_{s,s'}^{\pm} = G_{s,s'}^0 + \hat{A}_{\pm} e^{-\alpha(s+s'-2)} + \hat{A}_{\mp} e^{-\alpha(2N-s-s')} + \hat{A}_m \left(e^{-\alpha(N-s+s')} + e^{-\alpha(N+s-s')} \right) , \quad (\text{B.35})$$

and solve for \hat{A}_\pm and \hat{A}_m , as before. Doing so yields

$$\hat{A}_- = A_0 \frac{(1 - a_5^2 m^2) (W a_5 e^{-\alpha} - 1)}{f_N} \quad (\text{B.36})$$

$$\hat{A}_+ = A_0 \frac{(1 - a_5^2 m^2) (W a_5 e^\alpha - 1)}{f_N} e^{-2\alpha} \quad (\text{B.37})$$

$$\begin{aligned} \hat{A}_m &= A_0 \frac{1}{f_N} [e^{-\alpha N} \{a_5^2 m^2 (W a_5 e^\alpha - 1) - (W a_5 e^{-\alpha} - 1)\} \\ &\quad - 2m W a_5^2 \sinh \alpha] \end{aligned} \quad (\text{B.38})$$

$$\begin{aligned} f_N(m) &= [1 - W a_5 e^\alpha - a_5^2 m^2 (1 - W a_5 e^{-\alpha})] \\ &\quad - e^{-2\alpha N} [1 - W a_5 e^{-\alpha} - a_5^2 m^2 (1 - W a_5 e^\alpha)] + 4m W a_5^2 e^{-\alpha N} \sinh \alpha. \end{aligned} \quad (\text{B.39})$$

Letting

$$\Lambda_{s,t}^+ = -(i\bar{p} \cdot \gamma + W) \delta_{s,t} + \frac{1}{a_5} \delta_{s,t+1} + m \delta_{s,1} \delta_{t,N} \quad (\text{B.40})$$

$$\Lambda_{s,t}^- = -(i\bar{p} \cdot \gamma + W) \delta_{s,t} + \frac{1}{a_5} \delta_{s,t-1} + m \delta_{s,N} \delta_{t,1} \quad (\text{B.41})$$

we have $[\hat{D}^{-1}]_{s,s'} = \hat{S}_{s,s'}^+ P_+ + \hat{S}_{s,s'}^- P_-$ with $\hat{S}_{s,s'}^\pm = [\Lambda^\pm \hat{G}^\pm]_{s,s'}$.

Bibliography

- [1] B. Kayser, F. Gibrat-Debu, and F. Frederic Perrier, *The Physics of Massive Neutrinos*, World Scientific Publishing, 1989.
- [2] Y. Kuno and Y. Okada, *Rev. Mod. Phys.* **73**, 151 (2001) [arXiv:hep-ph/9909265].
- [3] J. F. Donoghue, E. Golowich, and B. R. Holstein, *Dynamics of the Standard Model*, Cambridge University Press, 1992, p. 138.
- [4] R. Engfer and H. K. Walter, *Ann. Rev. Nucl. Part. Sci.* **36**, 327 (1986).
- [5] G. D. Morris, *Muonium Formation and Diffusion in Cryocrystals*, Ph.D. Thesis, University of British Columbia, 1997.
- [6] R. S. Henderson et al., *Nucl. Instrum. Meth. A* **548**, 306 (2005) [arXiv:hep-ex/0409066].
- [7] J. R. Musser [TWIST Collaboration], *Phys. Rev. Lett.* **94**, 101805 (2005) [arXiv:hep-ex/0409063].
- [8] A. Gaponenko et al. [TWIST Collaboration], *Phys. Rev. D* **71**, 071101 (2005) [arXiv:hep-ex/0410045].
- [9] B. Jamieson et al. [TWIST Collaboration], *Phys. Rev. D* **74**, 072007 (2006) [arXiv:hep-ex/0605100].
- [10] L. Michel, *Proc. Roy. Soc. Lond.* **A63**, 514 (1950); C. Bouchiat and L. Michel, *Phys. Rev.* **106**, 170 (1957).
- [11] T. Kinoshita and A. Sirlin, *Phys. Rev.* **108**, 844 (1957).
- [12] N. Danneberg et al., *Phys. Rev. Lett.* **94**, 021802 (2005).

- [13] R. Tribble and G. Marshall, private communication. See also J. Hu in the proceedings of the PANIC05 conference, Sante Fe, N.M., 2005.
- [14] F. Scheck, *Electroweak and Strong Interactions: An Introduction to Theoretical Particle Physics*, Springer Verlag, 1996, p. 282.
- [15] C. A. Gagliardi, R. E. Tribble, and N. J. Williams, *Phys. Rev. D* **72**, 073002 (2005) [arXiv:hep-ph/0509069].
- [16] G. Prezeau and A. Kurylov, *Phys. Rev. Lett.* **95**, 101802 (2005) [arXiv:hep-ph/0409193].
- [17] N. F. Bell, V. Cirigliano, M. J. Ramsey-Musolf, P. Vogel, and M. B. Wise, *Phys. Rev. Lett.* **95**, 151802 (2005) [arXiv:hep-ph/0504134].
- [18] S. Davidson, M. Gorbahn, and A. Santamaria, *Phys. Lett. B* **626**, 151 (2005) [arXiv:hep-ph/0506085].
- [19] N. F. Bell, M. Gorchtein, M. J. Ramsey-Musolf, P. Vogel, and P. Wang, *Phys. Lett. B* **642**, 377 (2006) [arXiv:hep-ph/0606248].
- [20] J. Giedt, G. L. Kane, P. Langacker, and B. D. Nelson, *Phys. Rev. D* **71**, 115013 (2005) [arXiv:hep-th/0502032].
- [21] P. Langacker and B. D. Nelson, *Phys. Rev. D* **72**, 053013 (2005) [arXiv:hep-ph/0507063].
- [22] C. Aalseth et al., [arXiv:hep-ph/0412300].
- [23] S. R. Elliott and P. Vogel, *Ann. Rev. Nucl. Part. Sci.* **52**, 115 (2002) [arXiv:hep-ph/0202264].
- [24] M. Doi, T. Kotani, and H. Nishiura, *Prog. Theor. Phys.* **114**, 845 (2005) [arXiv:hep-ph/0502136].
- [25] C. P. Burgess and D. London, *Phys. Rev. D* **48**, 4337 (1993) [arXiv:hep-ph/9203216].
- [26] S. A. Frolov and A. A. Slavnov, *Phys. Lett. B* **309**, 344 (1993).
- [27] L. F. Abbott, *Nucl. Phys. B* **185**, 189 (1981).

- [28] V. M. Lobashev et al., *Phys. Lett. B* **460**, 227 (1999).
- [29] C. Weinheimer et al., *Phys. Lett. B* **460**, 219 (1999).
- [30] LEP Electroweak Working Group [<http://lepewwg.web.cern.ch/LEPEWWG/>].
- [31] J. F. Beacom and P. Vogel, *Phys. Rev. Lett.* **83**, 5222 (1999) [arXiv:hep-ph/9907383].
- [32] D. W. Liu et al. [Super-Kamiokande Collaboration], *Phys. Rev. Lett.* **93**, 021802 (2004) [arXiv:hep-ex/0402015].
- [33] Z. Daraktchieva et al. [MUNU Collaboration], *Phys. Lett. B* **615**, 153 (2005) [arXiv:hep-ex/0502037].
- [34] B. Xin et al. [TEXONO Collaboration], *Phys. Rev. D* **72**, 012006 (2005) [arXiv:hep-ex/0502001].
- [35] G. G. Raffelt, *Phys. Rept.* **320**, 319 (1999).
- [36] T. M. Ito and G. Prezeau, *Phys. Rev. Lett.* **94**, 161802 (2005) [arXiv:hep-ph/0410254].
- [37] R. J. Erwin, J. Kile, M. J. Ramsey-Musolf, and P. Wang, *Phys. Rev. D* **75**, 033005 (2007) [arXiv:hep-ph/0602240].
- [38] K. S. Babu and C. N. Leung, *Nucl. Phys. B* **619**, 667 (2001) [arXiv:hep-ph/0106054].
- [39] J. F. Nieves and P. B. Pal, *Am. J. Phys.* **72**, 1100 (2004) [arXiv:hep-ph/0306087].
- [40] S. Willenbrock [arXiv:hep-ph/0410370].
- [41] A. de Gouvea [arXiv:hep-ph/0411274].
- [42] A. Denner, H. Eck, O. Hahn, and J. Kublbeck, *Nucl. Phys. B* **387**, 467 (1992).
- [43] J. Gluza and M. Zralek, *Phys. Rev. D* **45**, 1693 (1992).
- [44] D. B. Kaplan, *Phys. Lett. B* **288**, 342 (1992) [arXiv:hep-lat/9206013].
- [45] Y. Shamir, *Nucl. Phys. B* **406**, 90 (1993) [arXiv:hep-lat/9303005].
- [46] T. Blum and A. Soni, *Phys. Rev. D* **56**, 174 (1997) [arXiv:hep-lat/9611030].
- [47] S. Aoki and Y. Taniguchi, *Phys. Rev. D* **59**, 054510 (1999) [arXiv:hep-lat/9711004].

- [48] S. Aoki, T. Izubuchi, Y. Kuramashi, and Y. Taniguchi, *Phys. Rev. D* **59**, 094505 (1999) [arXiv:hep-lat/9810020].
- [49] M. Gockeler, R. Horsley, E. M. Ilgenfritz, H. Perlt, P. Rakow, G. Schierholz, and A. Schiller, *Nucl. Phys. B* **472**, 309 (1996) [arXiv:hep-lat/9603006].
- [50] S. Capitani, *Nucl. Phys. B* **597**, 313 (2001) [arXiv:hep-lat/0009018].
- [51] S. Capitani, *Phys. Rept.* **382**, 113 (2003) [arXiv:hep-lat/0211036].